Progress in Materials Science 107 (2020) 100590

Contents lists available at ScienceDirect

Progress in Materials Science

journal homepage: www.elsevier.com/locate/pmatsci

Revisiting fundamental welding concepts to improve additive manufacturing: From theory to practice

J.P. Oliveira*, T.G. Santos, R.M. Miranda

UNIDEMI, Department of Mechanical and Industrial Engineering, NOVA School of Science and Technology, NOVA University of Lisbon, 2829-516 Caparica, Portugal

ARTICLE INFO

Keywords:
Additive manufacturing
Arc welding
Electron beam additive manufacturing
Laser additive manufacturing
Energy density
Microstructure

ABSTRACT

Additive manufacturing technologies based on melting and solidification have considerable similarities with fusion-based welding technologies, either by electric arc or high-power beams. However, several concepts are being introduced in additive manufacturing which have been extensively used in multipass arc welding with filler material. Therefore, clarification of fundamental definitions is important to establish a common background between welding and additive manufacturing research communities. This paper aims to review these concepts, highlighting the distinctive characteristics of fusion welding that can be embraced by additive manufacturing, namely the nature of rapid thermal cycles associated to small size and localized heat sources, the non-equilibrium nature of rapid solidification and its effects on: internal defects formation, phase transformations, residual stresses and distortions. Concerning process optimization, distinct criteria are proposed based on geometric, energetic and thermal considerations, allowing to determine an upper bound limit for the optimum hatch distance during additive manufacturing. Finally, a unified equation to compute the energy density is proposed. This equation enables to compare works performed with distinct equipment and experimental conditions, covering the major process parameters: power, travel speed, heat source dimension, hatch distance, deposited layer thickness and material grain size.

1. Introduction

Additive manufacturing allows structures fabrication in a layer-by-layer deposition process and is revolutionizing the manufacturing industry due to its ability to obtain near-net shape products, in a short time span, with almost no material waste.

An upmost key feature of additive manufacturing based on melting and solidification, is the use of fundamental knowledge generated by decades of research on welding metallurgy and technologies, based on electric arc and high-energy density beams (laser and electron beam). This experience in welding can be used to better understand the additive manufacturing process and the implications on the microstructural features of the produced parts, including the origin of internal defects (type, morphology, location and quantity).

Most prevailing industrial applications of additive manufacturing use laser beam systems which, under appropriate process control, produce parts with good dimensional precision and surface finish [1–3]. However, electron beam-based systems tend to deliver sound parts with better mechanical properties, since the process is developed in a vacuum chamber at a uniform high temperature, which decreases residual stresses that build-up during layer deposition. Both electron and laser systems require high

* Corresponding author.
E-mail address: jp.oliveira@fct.unl.pt (J.P. Oliveira).

https://doi.org/10.1016/j.pmatsci.2019.100590
Received 24 July 2018; Received in revised form 7 June 2019; Accepted 23 July 2019
Available online 01 August 2019

Nomenclature

BD	Building Direction
CAD	Computer Aided Design
CMT	Cold Metal Transfer
DR	Deposition Rate
E	Energy
EBSD	Electron Backscattered Diffraction
HI	Heat Input
HIP	Hot Isostatic Pressing
LHI	Linear Heat Input
MAG	Metal Active Gas
MIG	Metal Inert Gas
PDD	Powder Deposition Rate
TIG	Tungsten Inert Gas
WAAM	Wire and Arc Additive Manufacturing
WPS	Welding Procedure Specification
C_p	heat capacity
d_{Laser}	laser beam diameter
$d_{HeatSource}$	diameter of the heat source
d_t	track width
E	energy
E_d	energy density
E_{eff}	effective energy per unit of area
F	volumetric fluency
h	hatch spacing/distance
$Heat_{fusion}$	latent heat of fusion
I	current intensity
m	mass of material
K	thermal conductivity
K_0	modified Bessel function of the second kind and zero order
L	travelled length
T	temperature
T_0	initial temperature of the base material
t_{int}	laser/material interaction time
o	overlap distance between two consecutive points in the same hatch
P	welding power
R	radial distance
R_m	melted radius
R_{powder}	powder feed rate
v	welding speed
V	voltage
x	distance travelled by the heat source
w	layer width
α	thermal diffusivity
β	dimensionless parameter defined by the grain size to heat source diameter ratio
ρ	density of the material
ρ_{bed}	relative density of the powder-bed
η	heat source efficiency
φ	wire diameter
ΔT	variation of temperature

investment costs. Thus, additive manufacturing with electric arc and plasma are dedicated to large parts manufacturing.

Alternatively to high-power beams, electric arc heat sources can be used in additive manufacturing where the production rate is a major requirement [4]. Nevertheless, laser or electron beam sources are preferred for parts with fine features or requiring high dimensional tolerances, due to their small size heat source.

Additive manufacturing techniques based on melting and solidification induce complex thermal profiles throughout the material [5,6]. Whether, the added material is powder or wire, the first layer is melted and solidified onto a substrate. When a second layer is deposited on the previous, the introduced heat must completely melt this second layer and partially re-melt the one underneath. Moreover, a heat affected zone is created in the first deposited layer, which, depending on the material, may promote additional solid-state transformations. This process is repeated over and over until the part is complete. Therefore, the heat introduced to deposit each layer generates successive heat affected zones on previously deposited layers, in a process similar to multipass fusion welding [7–10]. As in welding, additive manufactured parts experience non-equilibrium solidification [11–13], due to fast cooling rates observed. The effect of multiple thermal cycles over these non-equilibrium structures may promote the formation of new phases and precipitates if the permanence time at a specific temperature for the solid-state transformation to occur is reached.

As additive manufacturing technologies based on electric arc or high-power beams are still being matured, well-established knowledge from welding metallurgy can be transferred to better understand and improve additive manufacturing techniques.

Currently, the processing parameters used by the additive manufacturing community lack comparability and, thus, a comprehensive effort to encompass the vast generated knowledge over the past years is necessary to foster the development of additive manufacturing techniques into new applications.

Recently, a very comprehensive revision on additive manufacturing was published by DebRoy et al. [1]. The present paper aims to revise fusion welding concepts applicable to additive manufacturing of metals, highlighting the similarities between both technologies and the procedures used in welding that can be directly applicable in additive manufacturing. Specifically, this paper focus on strategies to control the microstructure of the fusion zone in welds in terms of heat source manipulation, optimization of operating procedures and correction of microstructure, to improve mechanical performance and avoid internal defects in additively manufactured parts. In fact, most of existing literature on additive manufacturing is built on welding technology and welding metallurgy. Therefore, this paper intends to evidence how the welding and additive manufacturing communities can establish a synergetic relationship. Concerning additive manufacturing process optimization, distinct criteria (geometric, energetic and thermal) are proposed to determine an upper bound limit for the hatch distance. Finally, an equation to compare energy densities used with different additive manufacturing equipment and varying the most relevant process parameters (power, travel speed, hatch distance, layer thickness, grain size and diameter of the heat source) is proposed.

2. Welding

The need to produce complex parts constituted a major driving force for the development of welding technologies. In fact, welding dates back from 8000 bC, namely brazing, where a molten metallic alloy with a low melting temperature was poured between two solid materials promoting joining [14]. However, it was just in beginning of the 20th century, that welding became a reality in industry, after major scientific and technological breakthroughs. Some of these developments included mastering of the electrical arc, discovered in the 1800′s and easier access to electricity after World War I. However, it was after World War II that major developments were achieved, both in the technology itself and in materials behavior. Because of such technological conquests, welding disseminated rapidly and was finally embraced by the industry for mass production of complex structures.

One of the most important developments was the invention of Tungsten Inert Gas (TIG) process in 1942 [15], where a non-consumable tungsten rod was used to initiate the electric arc under the protection of an inert gas. TIG is commonly used to join a wide variety of materials including steels [16], Ni-based [17], Ti-based [18] and Aluminum alloys [19], for example. The fact it does not use a filler material limits its use to thin plates or tubes.

Further developments encompassed the use of a continuous wire feed, which significantly increased production rates in an automatized process. Metal Inert/Active Gas (MIG/MAG) was developed late in the 40́s of the 20th century. In this process, an electric arc is established between a consumable electrode and the base material, under a shielding gas atmosphere. The gas can be inert (He or Ar) or active (mostly CO_2 or other gas mixtures) [20,21]. Melting of both electrode and base materials to join is promoted by the heat generated in the electrical arc. This process is one of the most used in industry, in either manual or in robotized welding cells.

Melting of the consumable rod originates the formation of drops that are directed to the molten pool through a combination of forces due to: electromagnetic effects (F_{em}), gravity (F_g), surface tension (F_{ts}) and vaporization (F_v). Fig. 1 depicts the contribution of each acting force either to push or to pull a drop out of the consumable rod. The gas type, rod diameter, feeding rate and stick-out affect the acting forces and, thus, the drop detachment form. Depending on the current voltage and intensity, three main regimes for drop detachment from the tip of the wire can occur and these are: short circuit, spray and globular. Nevertheless, far more modes have been identified by researchers and recognized by the International Institute of Welding.

Short circuit occurs at both low voltage and current intensity leading to small drop size, being easy to control the deposited metal [22]. However, the deposition rate is low and in cases where productivity is a major requirement, globular transfer is desirable despite the large quantity of fumes and particles emitted.

The need for increased productivity and better weld quality pushed for the development of several variants of MIG/MAG. Synergic MIG is an alternative technique developed in the early 1980′s which is now widely used in industry. This welding source allows to vary the wire feed rate, together with the power, while the voltage slightly varies with the current intensity. It measures the arc voltage and compares this value to a reference one so that, when necessary, the feed rate is corrected to have a continuous and regular molten pool. The source is electronically controlled.

More recently, another variant of MIG/MAG welding was developed that permits to control the molten pool at high welding speeds. Cold Metal Transfer (CMT) uses a push and pull electro-mechanical system acting on the consumable rod allowing to have regular small drop size at low heat input. Some authors find it interesting for additive manufacturing using electric arc, though the deposition rate is low [23].

The use of high-power beams applied in welding dates from the 1960′s and is now recurrent in industry [24]. Both laser and electron beam share common features which include: small beam size, precise control of beam shape and position, and very high energy density. The extension of the thermal affected areas is narrow with consequent low residual stresses and almost no distortions

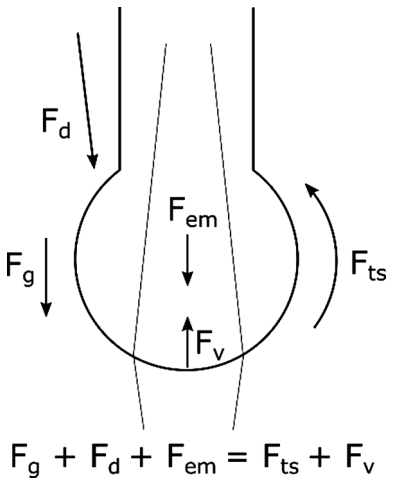

Fig. 1. Forces acting on a drop hanging from a wire during welding: F_g – gravity; F_d – plasma jet; F_{em} – electromagnetic forces/Pitch effect; F_{ts} – surface tension; F_v – vaporization.

[25,26]. Additionally, both processes can be used for dissimilar welding [27–34].

In electron beam welding, a beam of electrons is produced in the cathode and accelerated onto the materials to be joined, which act as the anode. In the interaction area, the kinetic energy of the electrons is converted into heat, melting the base materials and promoting joining. This is a very efficient energy process, since up to 95% of the kinetic energy is converted into heat [34].

In laser welding, a monochromatic beam of light radiation, coherent and with virtually no divergence, is used to heat the material. Depending on the laser beam wavelength and the absorptivity of the materials to be joined, the efficiency of the process varies. For metallic alloys the absorptivity increases when decreasing the laser beam wavelength, which partially explains the weldability improvements observed when transitioning from CO_2 lasers (with a beam radiation wavelength of 10.6 μm) to Nd:YAG and fiber ones (with 1.06 μm of wavelength) [35,36]. Both electron and laser beam welding are commonly referred as high-density energy welding processes, owing to the ability to decrease the beam spot significantly.

Electron beam welding was first developed but required a vacuum chamber [37,38]. However, it does not need consumables, such as gases, to protect the molten pool and adjacent zones from oxidation, during the process. Currently, pumping systems enable high production rates, with significant benefits to industry.

Laser welding appeared after electron beam welding and became rapidly popular since no vacuum chamber was needed (the process could run in open air atmosphere) with less equipment investment. Currently, a wide range of laser welding systems exist and the most used are Nd:YAG, fiber and CO_2.

Similarly to electron beam welding, the high versatility of laser welding makes it a unique technique capable of performing both similar and dissimilar materials joining [39–42]. During laser welding, shielding gases are necessary to protect the fusion and heat affected zones from oxidation and/or incorporation of undesired gases and particles [43,44].

The high energy density of both processes originates a keyhole welding mode when the heat is transferred in depth and the weld width is narrow [45]. When keyhole mode is observed the welds tend to have an aspect ratio, defined by the depth to width ratio, larger than 1. If the energy density is reduced, conduction welding mode is observed and the depth to width ratio in the fusion zone is well below 1. Though in deep welding keyhole mode is desirable, for thin sheets and dissimilar materials welding, conduction mode is preferred. A mixed mode of keyhole and conduction welding can also be observed at intermediate values of energy density [46,47].

Besides the technological aspects of welding processes, extensive and detailed studies were performed on welding metallurgy. The processes and their effects on materials were also subjected to tremendous research efforts to understand the connection and interaction between processing, microstructure and mechanical properties. For accurate metallurgical understanding and description of the underlying phenomena, new tools for materials analysis, such as dilatometry [48,49], scanning electron microscopy [39,50–53], transmission electron microscopy [54–56], X-ray diffraction [57–59] and software for thermodynamics, thermal and mechanical behavior [60], have been developed and are now extensively used by both academia and industry.

Associated to any fusion-based welding process there are four major aspects to consider and these are of thermal, chemical, metallurgical and mechanical domains. The thermal effect due to high temperature cycle is, eventually, the most important since it affects the thermal distribution and the metallurgical behavior of the materials to be joined, as well as, its mechanical performance, so these are discussed separately.

2.1. Thermal aspects

The quantity of heat introduced during welding, the thermal conductivity and specific heat of the base material(s) are fundamental to determine the cooling rate, and this is of paramount importance to control solid-state transformations upon cooling that may occur in the heat affected and fusion zones.

Rosenthal, in 1941, developed the theory for the thermal cycle description and presented two equations that are still the basis of analytical and numerical mathematical modelling of heat transfer in welding [61]. Despite its extensive use, it is worth to mention that these equations have some limiting assumptions, such as: it considers punctual heat sources, heat dissipation simply by conduction under equilibrium conditions, disregarding convection losses in the dynamic molten pool and surface radiation. Additionally, it does not consider phase transformation enthalpy, including melting, and the variability of thermal properties with temperature. The developed solutions for bi and three-dimensional heat flow, observed in thin and thick plates, respectively, are described by Eqs. (1) and (2), allow the calculation of the peak temperature T in [K] at any point distant, x, from the heat source:

$$T - T_0 = \frac{P}{2\,\pi\,K} e^{v\,x/2\alpha} K_0\left(\frac{v\,R}{2\alpha}\right) \tag{1}$$

$$T - T_0 = \frac{P}{2\,\pi\,K\,R} e^{-v(R-x)/2\alpha} \tag{2}$$

Where:

- T [K], is the temperature at a given position;
- T_0 [K], is the initial temperature of the base material;
- P [W], is the welding power;
- K [$W\ m^{-1}\ K^{-1}$], is the thermal conductivity of the material;
- K_0 is a modified Bessel function of the second kind and zero order;
- α [$m^2\ s^{-1}$], is the thermal diffusivity of the material;

– R [m], is the radial distance from the weld centerline, that is, $R = (x^2 + y^2)^{1/2}$ or $R = (x^2 + y^2 + z^2)^{1/2}$ for 2D and 3D heat flow, respectively;
– v [m s^{-1}], is the welding speed;
– x [m], is the distance from the heat source.

The heat input, HI in [W s mm^{-1}] or [J mm^{-1}], is a fundamental parameter in welding, controlling the quantity of heat introduced into the material, and is defined as the welding power (Q) [W] to welding speed (v) [m s^{-1}] ratio, according to Eq. (3):

$$HI = \eta \frac{Q}{v} \tag{3}$$

With η [%] being the efficiency of power transferred, that is, the ratio between the power delivered and the one effectively introduced into the material.

The physical meaning of the heat input is, thus, the energy [J] introduced by unit of length [m]. So, Eq. (3) is equivalent to Eq. (4), considering that the power is the energy per unit of time, E/t, while the travel speed is the distance covered per unit of time. So, Eq. (4) establishes the final definition of heat input in one dimension, that is:

$$HI = \eta \frac{Q}{v} = \eta \frac{\frac{E}{t}}{\frac{L}{t}} = \eta \frac{E}{L} \tag{4}$$

where E is the energy [J] and L [m] the distance travelled by the heat source.

For arc welding, the heat input is defined by:

$$HI = \eta \frac{V\ I}{v} = \eta \frac{V\ I\ t}{L} = \eta \frac{E}{L} \tag{5}$$

where I [A] and V [V] are the electric current intensity and voltage, respectively, and v [m s^{-1}] is the travel speed of the heat source. The energy efficiency, η, depends on the welding process and can vary from about 95% for electron beam [34] and up to 80% for laser [62], while it is lower for gas metal arc welding (30–50%) [63]. This parameter considers the energy losses for gas ionization, to surrounding environment and to the filler material, if any.

The heat input is fundamental in welding, since it affects the volume and shape of the molten material, the extension of both heat affected and fusion zones and the cooling rate in these regions. In high-power density processes, such as electron beam and laser welding, another important parameter is the energy density, which controls the welding mode (keyhole, conduction or mixed mode). The energy density is the energy deposited per unit of interaction area and has units of [J mm^{-2}] and is also referred to as the power density [W mm^{-2}].

The concept of power density is not considered in arc welding since the arc/material interaction area is difficult to quantify as it varies during welding, even when automated.

Since the heat is deposited locally on the material surface through a moving heat source, a three-dimensional distribution of temperature, which identifies the peak temperature at any point of a weld and allows to determine the cooling rate, can be computed. Both the maximum temperature and the cooling rate control the microstructural modifications and the residual stresses (magnitude and pattern), along the welded joint. Fig. 2 depicts the peak temperature evolution along a butt weld, in the so-called thermal solid, as well as, the isothermal lines created by the heat source.

2.2. Chemical and microstructural aspects

In the melted region, due to high temperatures, different chemical reactions can occur: (1) within the liquid; (2) between the liquid and the solid filler material, if any; (3) between the liquid and the surrounding atmosphere. The main consequences of each type of reaction are: (1) volatilization of low vapor pressure elements with corresponding modification of the chemical composition of the molten metal; (2) pores and lack of fusion; (3) oxide inclusions. Loss of elements generally leads to poor mechanical properties, as well as, to the formation of defects.

Solidification occurs by epitaxial grain growth, that is, it starts on non-melted solid grains from the heat affected zone, which is

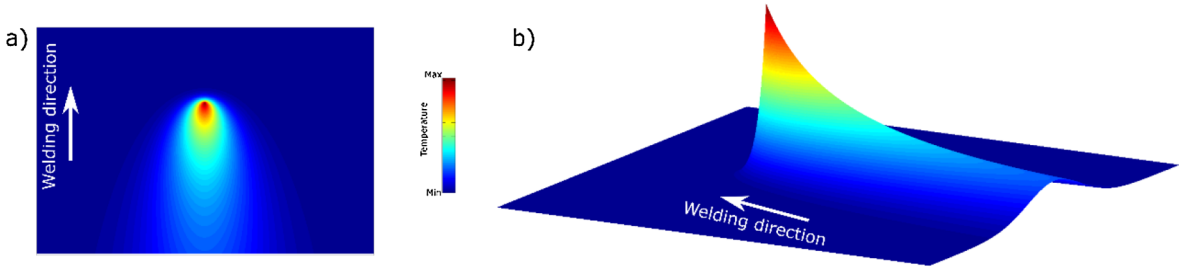

Fig. 2. Schematic representation of: (a) isothermal lines and (b) of the thermal solid (temperature evolution along the material) for a welded joint.

favored by grains with a crystallographic orientation parallel to the heat flow direction. This is a feature of welding solidification that is also observed in casting, though at smaller scale. The microstructures in the fusion zone can have different morphologies, such as, planar, cellular and dendritic and these are controlled by: temperature gradient (T), grain growth rate (R), undercooling (ΔT) and chemical composition. While the morphology is controlled by the grain growth rate to temperature gradient ratio (G/T), the crystal growth is governed by the G.R product as shown in Fig. 3. With increasing constitutional undercooling, the microstructure may shift from planar to cellular and from this to dendritic or exhibit a combination of these. The first grains solidify as dendrites since the underneath base material is much cooler than the molten metal and, so, the thermal gradient is predominant relative to crystal growth. However, after some time the supercooling effect decreases, and solidification tends to be planar, in an epitaxial grain growth mode, where the new grains form over the previous ones, and growth along more compact crystallographic directions perpendicular to isothermal lines, in a competitive grain growth process.

2.3. Mechanical aspects

Since there is always a thermal gradient along a weld, expansion and contraction upon heating and cooling, respectively, are not uniform and thus, the material undergoes differential deformation. This creates permanent plastic deformations, distortions and residual stresses [64–66]. The pattern of these stresses depend on the joint configuration, material thermo-physical properties (thermal conductivity and coefficient of thermal expansion) and mechanical properties (elastic modulus, yield strength and Poisson ratio). Fig. 4 depicts a common residual stress pattern observed in a butt welded joint of a thin plate.

Since there is a sharp temperature gradient near the weld, the material experiences distinct rates of expansion and contraction in adjacent sections. As the temperature increases, expansion of an area is constrained by the adjacent one, further away from the heat source, which is cooler. As a result, tensile and compressive stresses are generated in the fusion and heat affected zones, as schematically shown in Fig. 4. If the flow stress is surpassed, causing the material to yield locally, the residual stresses decrease. As the temperature lowers, adjacent hotter material reverses this plastic strain and tensile stresses form. Depending on the rigidity of the structure residual stresses may equal or exceed the yield stress of the material. If these residual stresses and residual strains imposed at high temperatures overcome the yield strength of the material distortions occur, as schematically shown in Fig. 5.

Another important contribution to the formation and magnitude of residual stresses are the solid-state transformations. As an example, in high strength steels, the martensitic transformation can be followed by nearly 4% dilation, or about 1.4% linear strain. Other factors such as grain size, affects the magnitude of volume changes and therefore may impact the developed residual stresses. Pre- and/or post-heating are typically used to reduce residual stresses, since the thermal cycle is smoother and the cooling rate decreases. However, other strategies can be used, such as deposition sequence and weld length, besides the control of the heat input, and the use of post-weld heat treatments.

2.4. Multipass welding

In multipass or multi-run welds, microstructural refinement is observed with improvements of weld toughness and reduction of residual stresses [67]. The main reasons are:

- each subsequent thermal cycle refines or “normalizes” the grains of the previous weld metal;
- the previous pass has an effect of pre-heating the material and, so, the cooling rate decreases;
- subsequent thermal cycles tend to anneal out residual stresses caused by previous passes.

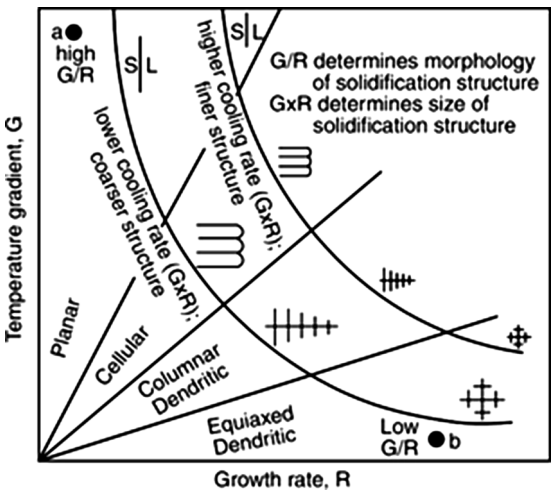

Fig. 3. Schematic representation of the effect of temperature gradient and growth rate on the solidification microstructures (from [1]).

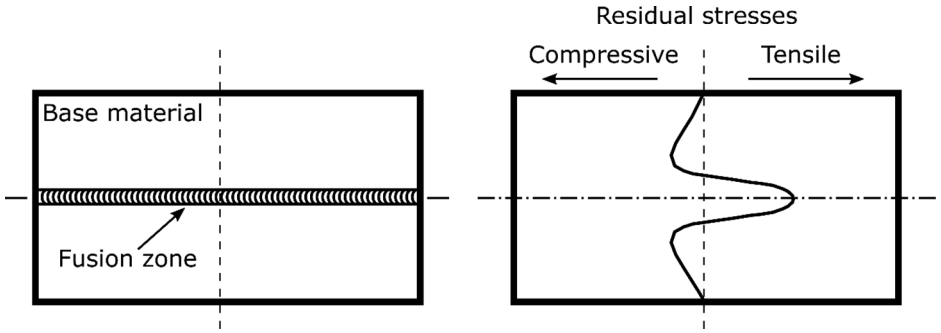

Fig. 4. Schematic of a butt welded joint showing a residual stress pattern.

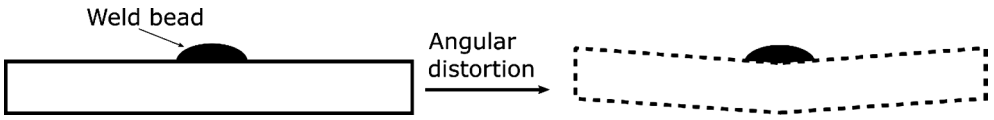

Fig. 5. Example of angular distortion due to a weld deposited bead.

Thus, successive thermal cycles affect the microstructure of both as-solidified material and heat affected zones. The subsequent pass partially remelts the previous one and, if there are no solid-state phase transformations, grains grow by epitaxy. Nevertheless, the dislocation density of the previously solidified weld metal can hinder excessive grain growth and cause recrystallization to occur.

A schematic representation of a multipass weld is depicted in Fig. 6. It is observed that different regions of the weld metal may be reheated multiple times during deposition of subsequent beads. For example, region A is only reheated once due to deposition of weld bead number 2. In opposition, region B is reheated twice due to weld beads number 2 and 3. Therefore, it is expected that the resulting microstructure is different in regions A and B. This behavior can be even more complex depending on the deposition sequence and the heat input of each weld bead, which influence the cooling rate of subsequent passes. Therefore, a graded microstructure is often observed along deposited beads, with characteristics and morphologies that depend on the material solid-state transformations.

In multipass welding, there is no guidance or consensus on how to analyze the heat input. However, a common procedure adopted in design and in welding procedure specifications (WPS) is to record the heat input for each single pass and calculate an average value that is later used in process qualification.

During multipass welding, only a small part of the reheated heat affected zone is subjected to high temperature peaks during a subsequent pass (Fig. 7). Thus, the heat affected zone of previous passes experiences a mild post-weld heat treatment.

As previously stated, welding microstructures largely depend on the material behavior under a thermal cycle and so, precipitation or formation of new phases can be observed depending on the peak temperature and the cooling time that each region experienced during welding. However, it must be noticed that some materials, such as steels or aluminum alloys, undergo reheat cracking.

3. Additive manufacturing

Several technologies of fusion-based additive manufacturing are currently under development. They all have two common features: (1) the use of computer aided design (CAD) tools to create parts and (2) the part is manufactured in a layer-by-layer deposition strategy. The most important advantage of this new way of manufacturing relies in the freedom to produce, virtually, any shape and geometry, in any material or combination of distinct materials. Other advantages emerge, such as: material savings, independence of

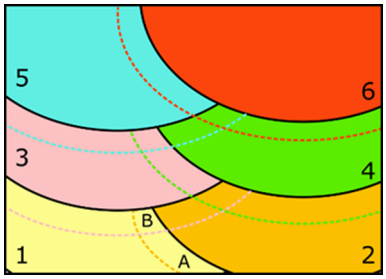

Fig. 6. Schematic representation of a multipass weld. Numbers 1 to 6 represent the sequence of passes. Dotted lines correspond to the heat affected zones created by each pass. Zone A is reheated once (by weld pass 2), whereas zone B is reheated twice (by weld passes 2 and 3) (adapted from [68]).

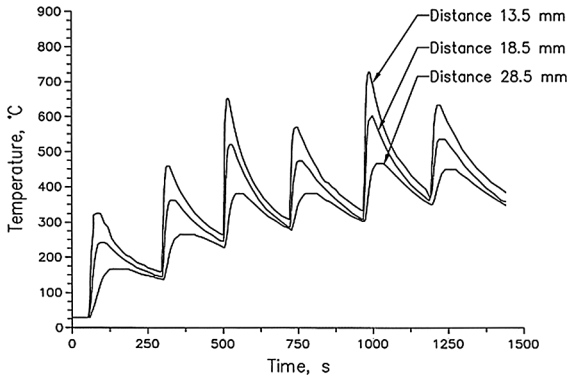

Fig. 7. Effect of multipass welding on the temperature profile in the heat affected zone of a low carbon steel (from [67]).

human interaction and short production times in line with new manufacturing and costumer delivering approaches [69].

Though solid-state manufacturing technologies are being investigated, fusion-based ones are still the most interesting due to productivity issues. As far as heat sources are concerned, laser beam, electron beam, electric arc and plasma are the ones under use, while materials to melt can be in the form of powder or wire.

The thermal effects of successive melted layers deposited on top, or aside, of each other are of paramount importance to prevent defect formation, microstructural features and mechanical performance of the produced parts [70] and, thus, the next section is devoted to analyze the specific effects of multiple thermal cycles.

3.1. Thermal aspects

While in welding, the heat input concept is well established and it has a linear dimension, in additive manufacturing this largely varies between research groups, especially those using laser-based systems. Firstly, an in-volume energy density concept, ED [J mm^{-3}], was introduced. This energy density, captured from welding, was adjusted by introducing new parameters, namely, the hatch distance, h [mm], which is the lateral distance between two consecutive passes, and the layer thickness [71–74] (or track width [75]), d [mm], as described by Eq. (6), with P [W] and v [m s^{-1}] being, respectively, the power and the travel speed of the heat source.

$$ED = \frac{P}{v\ h\ d} \tag{6}$$

Haberland et al. [75] further extended the concept of energy density depicted in Eq. (6) (using the track width term instead of layer thickness) by introducing Eqs. (7) and (8), depending if the track width (d_t) exceeded the hatch (h) distance or not, and inserting new variables, such as the laser beam diameter, d_{Laser} [mm], and the relative density of the powder-bed, ρ_{bed}, with arbitrary units. Despite the units presented in Haberland's work [75] are inappropriate, dimensional analysis using correct units ensure that both Eqs. (7) and (8) exhibit units of [J mm^{-3}], that is, in-volume energy density.

$$ED = \frac{P}{\rho_{bed}\ d_{Laser}\ h\ d}, \quad \text{for } h \geq d_t \tag{7}$$

$$ED = \frac{P}{\rho_{bed}\ d_{Laser}\ h\ d}\left(2 - \frac{h}{d_t}\right), \quad \text{for } 0 < h < d_t \tag{8}$$

Another term that is widely used in additive manufacturing is the linear heat input (LHI) [J mm^{-1}] [76–80] which is defined by Eq. (9) as:

$$LHI = \frac{P}{v} \tag{9}$$

Other authors [81] have also defined an effective energy per unit of area (E_{eff}) [J mm^{-2}] as in Eq. (10), and for powder fed systems, a powder deposition density (PDD) [g mm^{-2}] as in Eq. (11), where R_{powder} is the powder feed rate in [g min^{-1}].

$$E_{eff} = \frac{P}{v\ d_{Laser}} \tag{10}$$

$$PDD = \frac{R_{powder}}{v\ d_{Laser}} \tag{11}$$

Finally, a volumetric fluence, F [J mm^{-3}], was also defined in [82] for laser additive manufacturing based on pulsed wave heat sources, by introducing the laser beam/material interaction time, t_{int} [s], instead of the travel speed. This last one is replaced by an overlap distance between two consecutive laser pulses within the same track, o [mm], so that:

$$F = \frac{t_{int}\ P}{h\ d\ o} \tag{12}$$

Currently, there is no consensual definition on how to quantify the heat introduced in each deposited layer, which is fundamental to control solidification and molten metal transfer, in case of wire feed systems. In fact, all these equations are empirical without phenomenological physical demonstration. Table 1 resumes the most used physical quantities considered in additive manufacturing.

The deposition rate, DR [kg h^{-1}], is a parameter of critical importance, when productivity is a major concern, and this is calculated using the layer thickness (d) and width (w), and the density of the powder material (ρ), following Eq. (13) for powder-bed systems. In case of wire feed systems, Eq. (14) can be used to determine the deposition rate, considering the wire diameter, ϕ.

$$DR = d{\cdot}w{\cdot}60{\cdot}\rho \tag{13}$$

$$DR = \phi^2{\cdot}60{\cdot}\rho \tag{14}$$

Mathematical modelling of additive manufacturing is not a simple task, particularly if other than thermal analysis is envisaged, as material transfer and structural analysis [83]. Several research efforts are ongoing, attempting to predict component characteristics that could accomplish process certification [1]. This is a very important area that will allow researchers to have a deeper understanding on the peculiarities of the process, in order to improve it and complete parts with optimized microstructures and enhanced mechanical and functional properties.

3.2. Thermal analysis of additive manufacturing in light of welding technology

The well-established concept of heat input used in fusion welding can be generalized to additive manufacturing, if a proper interpretation of linear, or 1D heat input, is used. That is, the physical quantity of heat input based on “energy per length” must be used instead of “power per velocity”.

Therefore, a simple thermodynamic analysis, based on the identification of: (i) a control volume and (ii) an energy balance, leads to conclude that, the 3D equivalent of heat input for additive manufacturing is “Energy per Volume” and is given in Table 2.

The demonstration of the previous equation regarding the equivalent 3D heat input (or in-volume heat input), HI_{3D}, for additive manufacturing consists of:

- Defining a 3D control volume, $\Delta x \times \Delta y \times \Delta z$, encompassing all the melted material (Fig. 8);
- Quantifying the summation of the energy input, due to multiple passes, spaced by a lateral displacement (hatch distance, h). It is important to notice that both end passes (1 and 4 in Fig. 8) contribute with just one half each to the energy balance;
- Dividing this energy input summation by the volume of melted material encompassed in the control volume (Eq. (15)).

$$HI_{3D} = \frac{\text{Energy}}{\text{Volume}} = \frac{\text{Number of passes} \times \text{Energy per pass}}{\Delta x \times \Delta y \times \Delta z}, \tag{15}$$

Since the number of passes that fully contributes to the energy input is Δx divided by h, and noticing that the energy per pass is the power (Q) multiplied by time (t), the previous equation can be rewritten according to Eq. (16) as:

$$HI_{3D} = \frac{\frac{\Delta x}{h}{\cdot}Q{\cdot}t}{\Delta x{\cdot}\Delta y{\cdot}\Delta z}, \tag{16}$$

The time (t) that each pass is under the control volume corresponds to the length (Δy) divided by the linear travel speed (v), and, therefore Eq. (16) can be rearranged into Eq. (17):

$$HI_{3D} = \frac{\frac{\Delta x{\cdot}Q{\cdot}\Delta y}{h{\cdot}v}}{\Delta x{\cdot}\Delta y{\cdot}\Delta z}, \tag{17}$$

Table 1
Summary of the main equations for energy/power calculations in additive manufacturing found in the literature.

Designation	Equation	Source
Linear heat input [J mm^{-1}]	$LHI = \frac{P}{v}$	[76–80]
Effective energy per unit of area [J mm^{-2}]	$E_{eff} = \frac{P}{v\ d_{Laser}}$	[81]
Energy density or volumetric fluency [J mm^{-3}]	$F = \frac{t_{int}\ P}{h\ d\ o}$	[82]
Energy density [J mm^{-3}]	$ED = \frac{P}{v\ h\ d}$	[71–74]
Energy density [J mm^{-3}]	$ED = \frac{P}{\rho_{bed}\ d_{Laser}\ h\ d}$	[75]
Energy density [J mm^{-3}]	$ED = \frac{P}{\rho_{bed}\ d_{Laser}\ h\ d}\left(2 - \frac{h}{d_t}\right)$	[75]
Powder deposition density [g mm^{-2}]	$PDD = \frac{R}{v\ d_{Laser}}$	[81]

Table 2
Heat input calculation for welding (1D) and for additive manufacturing (3D).

Heat Input for welding (1D)	Heat Input for Additive Manufacturing (3D)
$HI_{1D} = \frac{Q}{v} = \frac{Energy}{Length}$	$HI_{3D} = \frac{Energy}{Volume} = \frac{Q}{v \cdot h \cdot \Delta z}$

Where: Q [W] is the heat source power, v [m s^{-1}] is the travel speed, h [mm] is the hatch distance and Δz [mm] is the thickness of the melted layer. This equation is applicable in wire and arc additive manufacturing (WAAM), since this process is very similar to multiple welds overlapped (fully or in part) and in laser or electron beam-based additive manufacturing where fusion occurs.

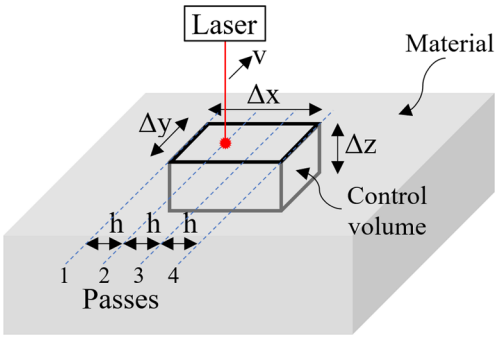

Fig. 8. Control volume used to determine the in-volume heat input (or energy density) during additive manufacturing.

This equation can be simplified resulting in Eq. (18), which provides the 3D generalization of heat input in additive manufacturing, referred as energy density (ED):

$$HI_{3D} = \frac{Q}{v \cdot h \cdot \Delta z} = ED, \tag{18}$$

3.3. Microstructural effects in fusion-based additive manufacturing

The energy density highly affects the amount of heat deposited in a certain point, and so the heat transfer conditions. This is critical since the energy density governs the deposition rate and the productivity, but it cannot be seen separately from the material solid-state transformations and its effect on the mechanical performance. Basically, metallic alloys have one or more of the three basic types of solid-state transformations: (1) those leading to precipitation, as most aluminum alloys, which can either produce strain hardening or material softening; (2) the inexistence of solid-state transformations, as in ferritic and austenitic stainless steels; (3) the formation of predicted phases after the equilibrium phase diagrams or metastable ones in rapid cooling conditions.

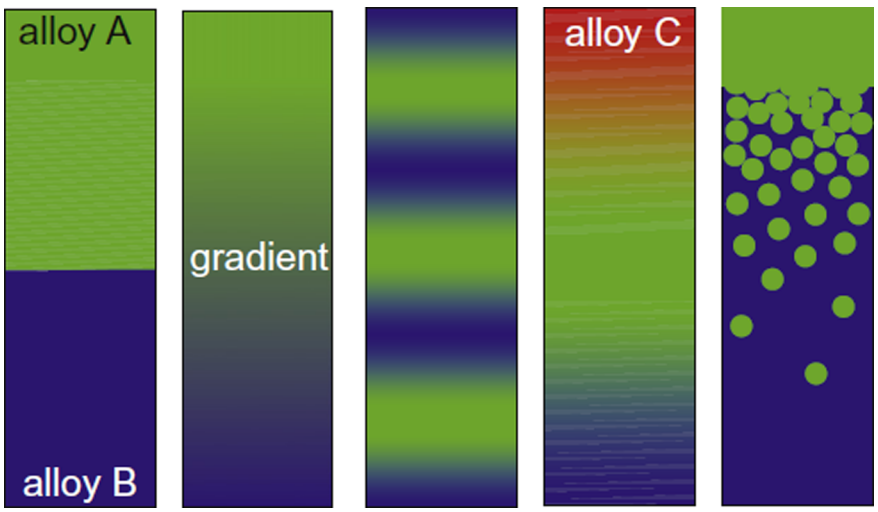

Fig. 9. Schematic representation of different gradient structures which can be created by additive manufacturing (from [91]).

An interesting feature of fusion-based additive manufacturing is its potential to obtain very small grain size due to the high cooling rates observed. For most metallic engineering alloys, this increases strength [84–86], though other materials behave differently [87–89]. However, the thermal cycle experienced by the as-built part may favor grain growth if there is sufficient residence time at critical temperatures for grain coarsening. Therefore, the building sequence can be optimized to minimize such potential undesirable effects.

With additive manufacturing technologies it is possible to develop chemically graded structures as exemplified in [90–92], and schematically shown in Fig. 9. In dissimilar welding, there are materials pairs with a vast potential of applications, if successful joined. Examples include: austenitic to ferritic steels joining [93], Ni-based alloys to steels [50,94], and Ni- to Ti-based alloys [29,95]. In all cases, successful joining is defined by a sound weld joint with mechanical properties adequate for the envisaged application. This is not an easy task due to limited control of chemistry in the fusion zone which can lead to the formation of detrimental intermetallic phases and therefore to a significant decrease in the mechanical properties. In fact, a smooth transition between one base material into the other would be a more desirable scenario during dissimilar welding. In additive manufacturing, this can be accomplished through a precise control of process parameters [90,96]. Furthermore, by controlling the chemical composition throughout the part, it is possible to avoid chemical composition ranges where undesirable phases are formed thus circumventing them.

Another interesting feature, in parts manufactured by additive manufacturing, is the capability to control texture along the part. For example, recent works have shown that by changing the scan strategy it is possible to modify the grain characteristics along the part [5,97–99]. Texture control in fusion welding is significantly more difficult. Because of this capability, new and more functional applications can be obtained in parts fabricated by additive manufacturing, provided that the control of the microstructure yields interesting structural and/or functional properties.

From the examples highlighted above, it is clear that the microstructural control that can be achieved in additive manufacturing is an important characteristic, since it can overcome some of the most intricate problems observed in conventional manufacturing processes. To this sense, the potential to create functionally graded structures, either by controlling the composition and/or the grain structure, is a clear advantage when compared to other technologies, such as welding.

Defects may occur in both welding and additive manufacturing processes, but basically, they have the same origin. Typical welding defects include: porosities, spatters, hot and/or cold cracking, lack of fusion and distortions caused by thermal/residual stresses. The origins and potential remedies of welding defects are well-known by now after decades of dedicated study of welding metallurgy, where extensive experimental and modelling work has been performed to understand how different welding parameters can influence them.

The main defects that may occur in additive manufacturing and the (simplified) reasons for their appearance are as follows: porosity is caused by entrapped gases resulting from decomposition of oxides at high temperatures; lack of fusion is caused by incomplete melting between subsequent depositions; hot cracking is due to the formation of low temperature eutectic films; cold cracking results from the formation of hard and brittle phases; delamination occurs by residual stresses build-up in between adjacent deposited layers.

The presence of porosity in parts fabricated by additive manufacturing may be intentional, when it is aimed to obtain porous structures [100,101], or unintentional, when the process is not controlled and undesired pores remain in the part [102]. Porosity or gas voids resulting from entrapped gases are typically observed in powder-bed systems [103]. To decrease the number of such defects, hot isostatic pressing (HIP) is typically performed after the part is build [104]. However, this strategy increases time and costs, thus its elimination (by obtaining fully dense parts after additive manufacturing) would significantly increase the widespread of additive manufacturing technologies. Another common feature in powder-bed systems, where a laser is used as the heat source, is the requirement for stress relieve heat treatments after production [105]. Both shielding gas type and flow rate are critical in porosity formation/control. For example, hydrogen is responsible for the formation of pores in fusion welding, due to the development of small blow holes [106]. In laser-based additive manufacturing, protection of the molten pool and adjacent material is usually performed by the gas atmosphere that fills the working envelope, which is less effective than in laser welding, where shielding gas is more localized and better oriented towards the molten pool. Therefore, the incorporation of strange elements into the molten pool during additive manufacturing is easier to occur than in laser welding [107], thus intensifying potential detrimental effects created by such elements.

Delamination is another defect that is identified during additive manufacturing, but not in welding. Since for powder-bed systems it is necessary to selectively solidify the top powder layer, the energy is non-uniformly introduced into the material. Selective heating of the powder origins steep thermal gradients and, therefore, residual stresses are generated between layers. Once the residual stress magnitude is higher than the bonding between two consecutive layers, delamination occurs. To overcome such problems, it has been reported that the scan strategy is of critical importance [108].

Residual stresses, evaluated by either modelling or experimental approaches, also attracts significant interest by the additive manufacturing community [6,78,109,110] since controlling the residual stress distribution across the parts is critical to optimize mechanical properties and prevent distortions, or incorrect geometries and dimensions.

Recent works have clarified the cracking mechanisms that occur in additively manufactured parts in materials that are known for their poor weldability, mainly Ni-based alloys [111–115]. These works provide useful information on the fundamental mechanisms, namely the formation of undesired phases and liquid films that drive crack formation and propagation during part production and can be used to obtain general guidelines that enable to obtain crack-free parts.

Defect-free parts are critical in structural applications under dynamic loads. For example, the presence of internal defects such as porosity, lack of fusion and micro-cracks will have a detrimental impact on the fatigue resistance of the as-built components. Since

these defects can vary from one part to another even within the same build it is expected that the fatigue life scattering is larger than in materials processed by conventional manufacturing technologies. On the other hand, under static load solicitations no significant scattering of mechanical properties is expected provided that the process parameters are well controlled. Moreover, with the ability to obtain very fine microstructures, owing to the fast cooling rates experienced, an increase in the overall mechanical properties of additive manufactured parts, when compared to more conventional manufacturing processes, can be expected.

Even though tight process control and understanding is necessary to obtain defect-free parts, the use of non-destructive techniques is crucial for faster and more significant implementation of additive manufacturing in a wide range of industries, especially in those where fabricated parts are used as structural materials.

Unlike subtractive manufacturing technologies, in additive manufacturing the use of in-situ process monitoring is not a standard yet [116]. This means that any discontinuities generated during the process will be detected just after the part is build. This may represent a significant setback owing to the high production costs and, therefore, there is a significant interest in the development of in-situ non-destructive techniques that can monitor the production and alert operators once a defect is detected. This will decrease production time and material waste with obvious economic advantages for the industry.

However, the use of non-destructive techniques in additive manufacturing requires significant adaptations to what is currently performed in welding inspection. Welding inspection typically involves ultrasounds and X-rays for detection of internal defects, as well as, dye penetrants and magnetic particles for surface and sub-surface defects detection. This inspection is usually performed offline, that is, after welding. However, when it comes to additive manufacturing, online inspection is mostly wanted, since a layer-by-layer monitoring is most appropriate to detect defects earlier in production of the parts, allowing its correction and the adjustment of the process parameters [117]. Also, due to the complex shape of the parts, inspection of the finished product can be very difficult to perform, and this is critical for structural parts. Therefore, conventional non-destructive testing methods as ultrasound, X-ray, dye penetrants and magnetic particles have several drawbacks regarding inspection of parts fabricated by additive manufacturing.

This leads to a new inspection paradigm that implies major adjustments and customization of traditional non-destructive methods, as well as, the use of new ones [116,118]. Other non-destructive techniques, such as eddy currents, can be used for online monitoring of the process, and eventually for microstructural characterization [119]. Mapping of heterogeneities along the material by electrical current 2D scanning [120], proved to detect defects but also microstructural changes. Other in-situ monitoring techniques currently used in additive manufacturing encompass the use of high-speed cameras to control the size of the melt pool and its temperature.

4. Strategies to improve weld fusion zone microstructures and its application to additive manufacturing

One of the critical issues in fusion-based welding is the development of coarse columnar grains in the fusion zone [61], which, according to the Hall-Petch equation [86], decreases the yield stress of the deposited material and, thus, its mechanical resistance. Additionally, for some materials, such as duplex stainless steels, the existence of large grains in the fusion zone is sufficient to promote a higher amount of austenite upon cooling, thus disrupting the nearly equal proportion of austenite and ferrite required for these materials [121]. Aside from the large grain size observed in the fusion zone, the columnar structure promotes a preferential texture, leading to anisotropic properties that can cause premature failure during service, especially in multiaxial loading conditions.

So, the need to control the microstructure, especially in the fusion zone, is crucial to increase the mechanical properties. For certain alloys, such as Mg alloys, the existence of a fine grained fusion zone can greatly improve the solidification-cracking resistance [122]. Several techniques exist to control the microstructure and dilution with the parent base material is, eventually, the simplest one. However, other operating techniques have been developed for alloys without solid state transformations to improve their mechanical resistance.

This section describes the most important techniques, how they impact the microstructure and mechanical properties of the fusion zone, and how additive manufacturing can use them to improve the microstructure control in as-built 3D parts.

Microstructural control during fusion-based welding can be achieved through: (i) manipulation of the heat source, which includes, amongst others, control of the pulse shape [123], by arc pulsation [124] or oscillation [125]; (ii) control the chemical composition of the fusion zone by the introduction of nucleation particles into the melt pool [126]; (iii) adjustment of welding parameters (welding power, welding speed, shielding gas type and flow) [21,47,127]; (iv) through the use of external electromagnetic [128,129] and ultrasonic stimuli [130]. Due to the distinct nature of each technique for grain refinement, each one is discussed separately supported by the existing knowledge in welding and discussing some of the approaches that can be incorporated in additive manufacturing.

4.1. Heat source manipulation

In either welding or additive manufacturing techniques based on melting, the heat source plays a fundamental role in the heat transfer, developed microstructures and residual stresses. Therefore, the control and manipulation of the heat source is of major importance and this is typically performed by modulation of the pulse current (for arc or high-power beam sources) or by oscillation of the welding arc induced by a magnetic oscillator (for arc-based heat sources). Because manipulation of the heat source can be performed in distinct ways, this section is divided in Sections 4.1.1 and 4.1.2.

4.1.1. Modulation of the heat source

Modulation of the pulse current has been widely exemplified in both arc-based welding [131–133], and laser and electron beam

welding [134]. The most important parameters during pulse shaping include the peak and base current values and their duration. For arc welding, when joining materials with high thermal and electrical conductivity there is a need to increase the heat input so that the temperature of the material can increase until melting occurs. This procedure can impair the microstructure and resulting mechanical properties of the joints due to the excessive heat introduced during welding. Even if the material to be joined is not a good thermal nor an electrical conductor, high heat inputs, which can be used to improve deposition rate, can be detrimental for certain classes of engineering alloys, such as high strength low alloy steels [135,136]. Therefore, pulse modulation during arc-based welding can be used to achieve spray transfer mode, known for enabling high productivity, using an average welding current lower than that required to achieve the same transfer mode when constant voltage is used. Further productivity increase can be attained by using high frequency pulsing. With such high frequency pulses, it is possible to decrease the arc length, thus providing a tighter control of the fusion zone width and depth, reducing remelting of previous passes and increasing the deposited material quantity.

Pulse control during arc welding is also effective, for some alloys, in promoting grain refinement [137,138]. The grain refinement effect obtained during pulsed arc welding (in opposition to continuous current) arises from the complex effect between the continuously changing thermal cycle and can be explained as follows: the use of a pulse welding current leads to periodic significant temperature fluctuations within the fusion zone, which affects the solidification process. When the current is decaying, the solid/liquid interface advances towards the electric arc and any minor external influence can drastically modify the solidification mode. As a result of this decay and subsequent raise of the welding current, the temperature gradient, cooling rates and microstructure can vary within the fusion zone. When continuous welding current is used, the high temperature of the molten pool is approximately constant during the process. As such, any heterogeneous nuclei formed ahead of the solid/liquid interface can be dissolved and do not perform as grain refiners. In opposition, for a pulsed welding current, there is a temperature decay as a result of the current decay, and any heterogeneous nuclei ahead of the solidification front can develop since they are in a liquid at a lower temperature due to the supercooling effect. These heterogeneous nuclei can then promote a grain refinement effect in the fusion zone.

While using pulsed welding current, there is a continuous change of the melt pool geometry, as such the direction of maximum thermal gradient changes accordingly. Since it is known that during solidification processes there are preferential growth directions, the continuous change in the direction of maximum thermal gradient restricts grain growth, thus favoring the formation of a refined grain structure, in comparison to joints obtained using continuous welding current.

Another consequence from the use of pulsed welding current is the variation of the arc force during arc welding, which, in turn, enhances fluid flow, thus lowering the temperature at the solidification front. This increased fluid flow can promote the detachment of the already solidified grains and, if these particles are not redissolved by the molten pool, can actively contribute as nucleation agents within the fusion zone.

An example of source manipulation can be found during gas tungsten arc welding of Al alloys, where alternated current (AC) is used to break the Al_2O_3 brittle oxide that forms on the material surface due to the fast oxidation reaction [139].

So far, to the best of the authors' knowledge, no systematic comparisons between the use of continuous or pulsed welding current during arc-based additive manufacturing can be found to the exception of [140,141]. In these works, the same group of authors studied, separately, the effect of using continuous or pulsed welding current during plasma-based additive manufacturing. Indeed, as expected from the previously derived welding knowledge, the samples manufactured with pulsed current exhibited higher ultimate tensile strength than those obtained with continuous current. Though the authors do not discuss these results in terms of the operating procedure, it is certain that the mechanism that promotes this increase in mechanical strength arise from the refined grain structure obtained when using a pulsed welding current. Both [140,141] are examples of welding knowledge transferred to additive manufacturing technologies.

Guo et al. [142] fabricated Mg samples by wire and arc additive manufacturing and modulated the heat source by adjusting the pulse frequency. Of special interest in this research work is the fact that the selected pulse frequency has a significant impact on the developed microstructure: lower pulse frequencies actually refines the grain structure, while when the pulse frequency is above 10 Hz grain coarsening is observed as a result of a lower cooling rate.

Though manipulation of the heat source is made often during arc-based welding, it has a more substantial effect during welding with high-power beams, since it can be used not only for microstructural modification of the fusion zone, by promoting grain refinement [88,134,143,144], but also to decrease or suppress porosity formation [145].

The microstructural refinement obtained by pulse modification during laser and electron beam welding have another key aspect: as a result of the very low heat input in high-power beam processes compared to arc-based ones, the cooling rate and thermal gradients are steeper. Therefore, solidification occurs faster, and this can be enough to, not only restrict excessive grain growth, but also to prevent excessive elemental segregation which can lead to the formation of undesired phases.

Potentially, one of the most interesting capability for heat source modulation when using high-power beams during additive manufacturing comes from its capabilities to reduce pore formation. Avoiding such type of defect is fundamental in structural applications, especially those subjected to dynamic loadings. Porosity is often found in powder-bed additively manufactured parts [102,146–148]. Though porosity can be formed due to the evaporation of light elements, often the existence of space in between the raw feedstock powders causes pore formation.

One way to mitigate keyhole instability during high-power beam welding is through power modulation during the process. If this modulation is performed at the same frequency of the melt pool oscillation, then porosity can be significantly decreased [145]. However, the selected frequency of modulation must be carefully controlled: if high frequency is used (> 100 Hz) a resonant effect occurs, and keyhole instability is exacerbated. When keyhole mode is achieved during powder-bed additive manufacturing [149–151] these instabilities can contribute to increase the probability for pore formation.

Ni-based superalloys, mainly Inconel alloys, are one of the most investigated materials in the area of additive manufacturing

[152–158]. One of the problems associated to the solidification of Inconel is the segregation of Nb, which promotes the formation of brittle Laves phase. Aside from Laves formation depletes the surrounding matrix of alloying elements, this phase is known to assist crack initiation and subsequent propagation. Xiao et al. [156] showed that trough heat source manipulation during selective laser melting it is possible to decrease Nb segregation and therefore the amount of Laves phase in the as-built parts. By using a quasi-continuous wave laser source, it was possible to significantly increase the cooling rate, resulting in a microstructure composed of equiaxed dendrites and with reduced Nb segregation and Laves. In opposition, the use of continuous wave laser heat source, caused lower cooling rates, which lead to significant Nb segregation and preferential formation of Laves. Due to the decrease of Nb segregation and reduced grain size when a quasi-continuous wave source was used, the mechanical properties greatly increased.

Up to know, modulation of the heat source during laser or electron beam additive manufacturing has not focused in decreasing porosity in the as-build parts. However, some exciting developments have been presented recently and these are discussed now.

One concerns texture control, i.e. control of grain orientation, within a built part. Increasing the functionally of the as-built parts often requires changing the grain morphology and orientation in site-specific locations, which primarily depend on the solidification conditions. The control of the grain morphology was demonstrated for both laser [83] and electron beam [99,159] powder-bed additive manufacturing. Though different in nature, these works rationalized the grain size and morphology evolution based on the combined effect of the thermal gradient and solidification rate, which, similar to fusion-based welding [61], dictate the grain size and morphology in the fusion zone.

By modulating the laser intensity [83], or by modifying the scan strategy [99,159] the solidification conditions experienced by the melt pool during the building process were modified, giving origin to distinct grain structures. In particular, Raghavan et al. [99] were able to determine the columnar-to-equiaxed transition as function of the thermal gradient and solidification rate, as depicted in Fig. 10.

Aside from controlling the grain size and morphology, manipulation of the heat source can be used to texture the material in different regions of interest. As exemplified in Fig. 11 [160], it is possible to locally change the grain orientation at precise locations in the as-built part. The manipulation of the heat source enabled to create specific scan strategies, which allowed to consider the heat source as a point or a line, as desired. As a result, the thermal gradient in the melt pool as well as the liquid/solid interface stability change, grains grown with preferential orientation. The innovative aspect of this work was the intentional modification of the grain orientation is specific locations of the part.

4.1.2. Heat source control via magnetic oscillation

Another way to manipulate the heat source is trough magnetic oscillation and this can be only applied in arc-based processes. Basically, a magnetic oscillator will cause the electrical arc to move in the transverse, circular or longitudinal direction relatively to the welding direction, as schematically shown in Fig. 12. As it will be shown, the type of movement enabled by the magnetic oscillation will impact differently in the generated microstructures of the fusion zone.

Magnetic arc oscillation for microstructural refinement of the fusion zone was nicely exemplified by the works of Kou's group [122,125,161] in gas tungsten arc welding of Al and Mg alloys. Parameters of interest during magnetic arc oscillation include the amplitude of oscillation, whose maximum is typically equal to the arc length, and frequency of oscillation. Oscillation of the arc during welding is effective in modifying the grain orientation in the fusion zone [125]. This is especially important for alloys that are prone to solidification cracking: because it is intergranular, the existence of multiple grain orientations within the fusion zone cause the crack to deflect periodically, thus its propagation is hampered. It must be noticed however, that the combination of the oscillation movement and frequency has a critical role in decreasing solidification cracking in fusion welds: for the transverse and circular arc movements at low frequency ($\approx$ 1 Hz) grain refinement and reduction of solidification cracking phenomena occurred; whereas for the longitudinal arc movement, only at high frequency ($>$ 25 Hz) the same effect was noticed.

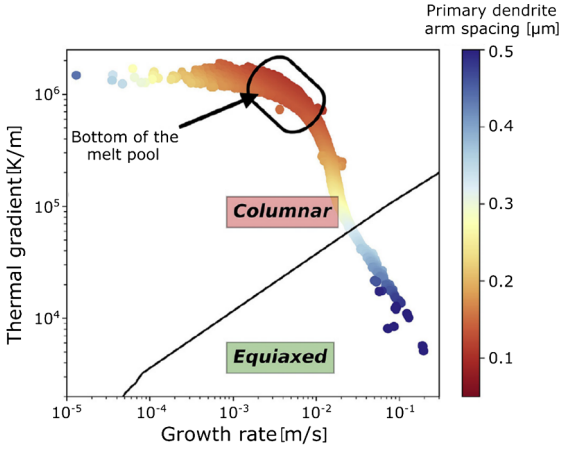

Fig. 10. Effect of thermal gradient and solidification rate on the columnar-to-equiaxed transition during laser-based additive manufacturing (adapted from [99]).

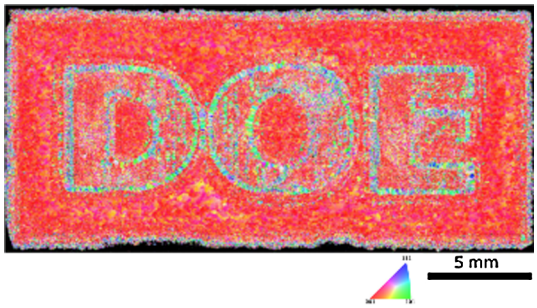

Fig. 11. Inverse pole figure orientation maps on the cross-section of a Ni-based superalloy fabricated using powder-bed electron beam additive manufacturing (from [160]).

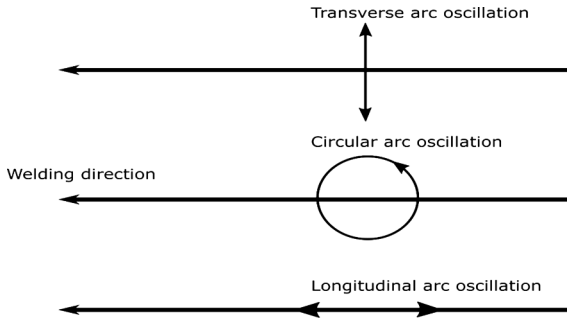

Fig. 12. Different types of movements enabled using a magnetic oscillator.

Though arc oscillation can effectively promote grain refinement in the fusion zone its effect is dependent on the alloy composition, since some alloys are known to be more prone to form columnar than equiaxed grains. For example, in AZ31 Mg alloys, it has been shown that equiaxed grains can grow into columnar ones, while such has not been observed for AZ91 Mg alloys [122]. This tendency for the grains to growth into columnar or equiaxed morphologies can be further manipulated by the controlled addition of alloying elements that can provide extra constitutional supercooling. For Mg alloys, the controlled addition of Al increases constitutional supercooling, allowing that small solid particles that exist within the fusion zone are not remelted and grow into an equiaxed structure.

It must be noticed that despite most of the works that use arc oscillation require an external magnetic oscillator, a similar arc movement can also be achieved using mechanical oscillators [162]. Similar refinement effect can be achieved, provided that the oscillation amplitude and frequency operate within a suitable range.

The use of magnetic arc oscillation during additive manufacturing can be highly effective in promoting grain refinement, though it has not been used yet. It is likely that the most effective arc movements during arc-based additive manufacturing are transverse and circular oscillation, following the observations made during arc-welding of Mg and Al alloys by Kou et al. [122,125]. The relevance of using either transverse or circular arc movements arise from three different effects: (i) it can ensure that during subsequent material depositions there is an actual overlap between adjacent beads, which can prevent defects such as lack of fusion and pores; (ii) it can provide lower cooling rates, which mitigate residual stresses, though the formation of non-desired precipitates may occur; (iii) because of the non-continuous movement of the arc, it is possible to promote detachment of previously solidified material from the partially melted zone (solid + liquid domain in a phase diagram), which, combined with the fluid flow enhanced by the arc movement, can promote grain refinement via dendrite fragmentation [42,54,122]. Dendrite fragmentation occurs due to the annular flow in the liquid metal along the solidification front. The solid fragments, are not melted again in the melt pool, will provide extra nucleation points, thus promoting grain refinement. However, arc oscillation during arc-based additive manufacturing may not be used for building single walls, unless longitudinal oscillation is used. This is related to the fact that arc-based additive manufacturing processes have poor dimensional accuracy and the use of circular or transverse arc oscillation will increase the width of each deposited layer.

4.2. Adjustment of operating procedures

4.2.1. In welding

The adjustment of operating procedures during welding, namely the control of the arc voltage, current intensity and type (AC/DC and/or pulsed/continuous), welding power, welding speed and protective gas are fundamental not only to modify the microstructure of the fusion zone but also its geometry, that is, width and depth of the molten pool. Furthermore, the control of these parameters can be used to gain better process stability.

In welding, the ratio between the welding power and the welding speed defines the heat input. The heat input is eventually the most important parameter during fusion welding since it gives a qualitative estimate on the cooling rate and extension of the fusion zone. For example, fixing the welding process and the material to be joined, it is known that higher heat input leads to lower cooling rates and to a higher extension of the fusion zone.

Additionally, the heat input introduced during welding impacts distortions due to the large volume of material melted and that shrinks during solidification. In particular, arc-based welding techniques have associated higher heat input than those in high power beam (laser and electron beam) techniques. This is one of the reasons why laser or electron beam welding are less prone to distortion during welding.

The cooling rate is of special importance during fusion-based welding since it controls the solidification mechanisms, solid-state transformations and residual stresses. Therefore, the control of the heat input during welding is of major importance as referred in Section 2 and in multiple research works [62,163–170].

During gas tungsten arc welding of 304 stainless steel, Kumar et al. [171] reported that the heat input selection had all the aforementioned consequences: higher heat input lead to a greater extension of the fusion and heat affected zones. Additionally, the average dendrite length and interdendritic spacing, which give an indication of the solidification conditions, increased with increasing heat input due to a lower cooling rate experienced by the material. Another research work on arc welding of 304 stainless steel [172], reported that increasing heat input resulted in a higher volume fraction of ferrite in the fusion zone, pointing the need to carefully control the heat input to promote or avoid solid-state transformations upon cooling.

The selection of the heat input, and therefore of the cooling rate, indirectly controls the segregation phenomena in the weld pool, and, since it facilitates the formation of liquid films of low melting point along the grain boundaries it can affected cracking susceptibility. Therefore, control of the heat input is fundamental in materials that experience hot cracking, such as Ni alloys and austenitic stainless steels.

One important difference that exists between welding and additive manufacturing is that in the former mechanical constraints are typically used. As a result of these mechanical constraints, the material is not able to freely expand and contract during the weld thermal cycle and significant residual stresses, and distortions, can occur. The effect of mechanical constraints during welding has been studied by [173]. When no mechanical constrains were used a decrease in both the transverse and longitudinal residual stresses was measured. During additive manufacturing the absence of highly restrictive mechanical constrains can allow for the material to better accommodate the thermal stresses during multiple thermal cycles experienced. However, up to now no significant detailed studies of the development of residual stresses during fusion-based additive manufacturing are available. It must be noticed however, that the constant heat and cooling experienced during sample build-up and the prolonged times at higher temperatures during wire and arc additive manufacturing can act to promote an in-situ stress relieve heat treatment which can lower previously developed residual stresses. However, in large parts built by wire and arc additive manufacturing, mechanical constraints are usually imposed and residual stresses are added up, so distortions can be significant and post-production heat treatment may be required.

The control of the heat input is also of major importance for alloys that are prone to liquation cracking. This defect occurs in the partially melted zone when the liquated material solidifies. Such type of cracking can occur in both welding and additive manufacturing where fusion occurs, since the thermal cycle experienced by the material in both cases will promote partial liquation at the fusion boundary. For example, Aluminum alloys with high freezing temperature range, such as AA 7075, are prone to liquation cracking. By increasing the heat input the amount of liquated material is higher and the probability for liquation cracking to occur drastically increases as exemplified in [174,175]. For this reason, decrease of the heat input, which can be performed by multipass arc-welding or by high power beam welding, is of paramount importance.

During multipass welding of steels, temper bead welding is often used to control the microstructure and toughness of the deposited material and its surroundings. When temper bead welding is correctly applied it is possible to temper the already solidified material by controlling the heat input [176]. Parameters of interest to control the temper bead technique include the heat input, which will control the thermal cycle but also the bead overlap. Depending of the steel that is to be welded, thickness and hardness tolerance for the desired application, the heat input selection and bead overlap can greatly differ between different arc welding techniques [177]. The final deposited material will have a higher hardness than that previously deposited, since this last welding pass does not experience any tempering [178].

Temper bead technique can be useful for the creation of large parts via arc-based additive manufacturing, though this has not yet reported. One potential issue that may arise from using temper bead during additive manufacturing is related to the bead overlap, or hatch distance as commonly referred in additive manufacturing. Typically, the required bead overlap for successful temper bead is above 50%, which can be detrimental to the process productivity. On the other hand, arc-based techniques have high production rates. Hence, it is possible that the ability for in-situ microstructural control enabled by temper bead technique during arc-based additive manufacturing can surpass the lower production times associated with the high bead overlap required.

The control of the interpass temperature during multipass welding is another welding operating procedure that needs to be carefully controlled to optimize the microstructure and mechanical properties of welded joints. This is common in multipass welding of steels [179]. Residual stresses are known to develop as a result of the weld thermal cycle. In steels, martensite can easily fracture as a result of these thermal residual stresses. However, if each welding pass is performed so that the temperature of the already deposited material is above the martensitic start transformation temperature, then the weld deposit will be composed of austenite and/or ferrite, which can sustain higher residual stresses without the development of cracks. Once the weld is completely performed, post-weld heat treatments can be applied to decrease the residual stress and improve the joint mechanical properties. It must be noticed that the interpass temperature directly depends on the thickness of materials to be deposited, heat input, environmental conditions and heat transfer.

Control of the interpass temperature can be performed for a wide range of alloys systems such as Ni-based super alloys [180], high strength steels [181] and aluminum alloys [182], for example.

Another important operating variable during fusion welding is the protection gas. All fusion-based welding techniques, except electron beam welding, submerged arc welding and shielded metal arc welding, require a protective atmosphere whose primary function it to protect the fusion zone and its surrounding from oxidation [183]. However, according to their physical characteristics, namely ionization energy and thermal conductivity it can affect the weld geometry.

Welding shielding gases also have other roles during welding. During laser welding, the process high energy density easily generates a high amount of plasma. However, with proper shielding gas optimization, that is, by careful selection of the shielding gas type and flow, it is possible to remove the plasma plume and control the weld penetration [184,185].

The metal transfer modes during arc-based welding can also be influenced by the type of shielding gas [186]. For example, Zhao et al. [186] showed that during metal active gas welding of carbon steel changing the gas mixture can modify metal transfer mode. In this case, a mixture of Ar, CO_2 and O_2 was used. When only Ar and CO_2 were used significant spatter occurred. However, the introduction of O_2 to the gas mixture greatly decrease spatter generation. With increasing CO_2 content (and maintaining the O_2 concentration) the transfer mode changed from streaming to pulsed. Additionally, the introduction of CO_2 in the shielding gas mixture was seen to increase the width and penetration of the fusion zone. This effect is of significant importance for both welding and additive manufacturing: if a selected shielding gas promotes an increase in both width and penetration of the weld metal, then low heat inputs can be used, potentially decreasing the risk of distortion.

Some operating parameters in arc-based welding, as the welding voltage and intensity, are also intimately related to the selected shielding gas. Pires et al. [187] highlighted that during metal active gas welding of a low carbon steel using an Ar-CO_2 mixture as shielding gas, an increase in CO_2 required an increase of the welding voltage and current to obtain a stable arc. As such, the increase in CO_2 content required an increase of the heat input, which, depending on the alloy system, may be detrimental to the joint microstructure and mechanical properties.

4.2.2. In additive manufacturing

As described above, there are multiple operating parameters that can be modified to control the microstructure, mechanical properties and defect generation during fusion-based welding. The most important ones include the welding voltage and intensity, which alongside with the travel speed control the heat input, and the shielding gases. Fortunately, some of the fundamental knowledge developed for decades by the welding community for adjusting the operating procedures is now being used in additive manufacturing.

The vast majority of the research in fusion-based additive manufacturing focus in selective laser melting. In these works, most of the focus is given to the creation of fully dense parts. To that sense, researchers often focus on determining the optimum hatch distance, vector length and scanning strategy [73,74,112,113,188–191]. Because these aspects are addressed in Section 5 of the paper, we refrain from developing the topic here. Instead, we focus on how changes in power and travel speed affect the microstructure and mechanical properties of additively manufactured parts, starting with powder-bed techniques and moving to arc-based techniques.

Aluminum alloys are probably one of the alloy systems more prone to defects during fusion-based additive manufacturing. Their cracking susceptibility and low evaporation temperature of some alloying elements are part of the distinct features that promote solidification cracking and pore formation during additive manufacturing. In the work of Qi et al. [150], on selective laser melting of AA 7050 alloy, for a wide range of scanning speeds (from 150 to 750 mm/s) cracking was always observed, even though the range of scanning speeds used allowed to transition from conduction to keyhole. Nie et al. [192] showed that very low scanning speeds ($\approx$ 80 mm/s) could be used to achieve crack-free parts in AA 2024 alloys. Eventually, the scanning speed could be increased up to $\approx$ 580 mm/s, though the addition of Zr was required to promote grain refinement and decrease cracking susceptibility.

Often, researchers in both the welding and additive manufacturing fields, focus on the microstructural changes induced by using different values of heat input. This approach simplifies the analysis, since otherwise it would be required to analyze, individually, the effect of power and travel speed. Therefore, it is not a surprise that several works on additive manufacturing correlate the selected heat input with the developed microstructures and mechanical properties.

Bi et al. [193] showed that during laser assisted additive manufacturing of Inconel 100 control of the heat input is fundamental to obtain crack-free parts. By reducing the heat input, the thermal stresses decrease, preventing crack initiation. Although this was not discussed by the authors, decreasing the heat input results in lower shrinkage upon cooling, which further justifies why the use of low heat input is helpful during additive manufacturing of materials with high cracking susceptibility, such as Inconel. The results of Bi et al. [193] are further corroborated in [194], where laser-assisted additive manufacturing was used for the repair of a Ni-based turbine: by decreasing the process heat input, the cracking susceptibility decreased.

The effect of heat input during laser-based additive manufacturing of 304L stainless was evaluated in [76]. As expected, by decreasing the heat input a fine grain structure was obtained, and, consequently an increase in the mechanical properties was observed. Similar to what occurs during fusion welding, the heat input controls the amount of deposited material during the process. Though a decrease of the heat input may be beneficial from a microstructural point of view, a trade-off between the selected heat input, which controls the microstructure and mechanical properties, and production time is critical. This trade-off aims at finding the heat input that balances an acceptable microstructure for the targeted application, with appropriate built up times.

Though it is observed that decreasing the heat input usually decreases the cracking susceptibility, it has been reported that during powder-bed manufacturing of a titanium aluminides using an electron beam as the heat source an increase in the heat input was beneficial to avoid the development of cracks in the as-built parts [195]. This may be justified by the fact that titanium aluminides are

more prone to cold cracking than to hot cracking. So, a longer time to cool benefits its internal arrangements and decreases the stresses associated with liquid to solid transformation. As a rule of thumb, materials with liquation susceptibility must be processes with low heat input, while for those prone to cold cracking the opposite is required.

A less used experimental variation during additive manufacturing using high power sources is related with the incident angle between the heat source and the substrate. The angle of incidence can impact the heat extraction and therefore the solidification conditions, resulting in potentially different microstructures. Chen et al. [196] studied the effect of different incident angles during laser melting of Inconel 718. Through a systematic analysis of the incident angle it was observed that an increase of the incident angle lead to an increase on the lateral temperature gradient. As a result, growth of secondary dendrites was fostered which, in turn, enhanced the interdendritic bonding. Due to a better interdendritic bonding, for higher incident angles liquation cracking, a common phenomenon observed in Inconel alloys, was suppressed.

The same authors [197], addressed the control of liquation cracking during laser-based additive manufacturing of Inconel 718. When the heat input increased the cracking susceptibility of the as-built parts also increased. This is in good agreement with the welding knowledge for Inconel alloys: high input lead to low cooling rates, which promote a more significant diffusion of elements, especially Nb. As a result, Laves phase forms, which greatly impacts the liquation cracking of the material. The same analysis applies to materials with alloying elements that form intermetallic compounds.

An example of how the adjustment of the operating procedure, in this case by controlling the heat input, can be used to modify the microstructure of the as-built parts during wire and arc additive manufacturing was exemplified by Li et al. in [198]. By increasing the wire feedstock temperature, via resistive heating, it was possible to decrease the heat input to promote melting and subsequent deposition. As a result of this lower heat input, a decrease in the columnar grains size was observed together with some equiaxed grains. The reported microstructural evolution is related to the different solidification conditions, thermal gradient and cooling rate, which can be drastically changed when the heat input is varied, thus, promoting different solidification microstructures.

In another work on wire and arc additive manufacturing of a high strength low alloy steel, Rodrigues et al. [199] showed that the heat input can be used not only to control the waviness of thin walls, but also the existing phases and grain size. In fact, higher heat input resulted in a lower surface waviness due to the good wettability during deposition. Additionally, the high heat input lead to the development of a large grain size microstructure and the hardness throughout the part height was seen to be less uniform than when

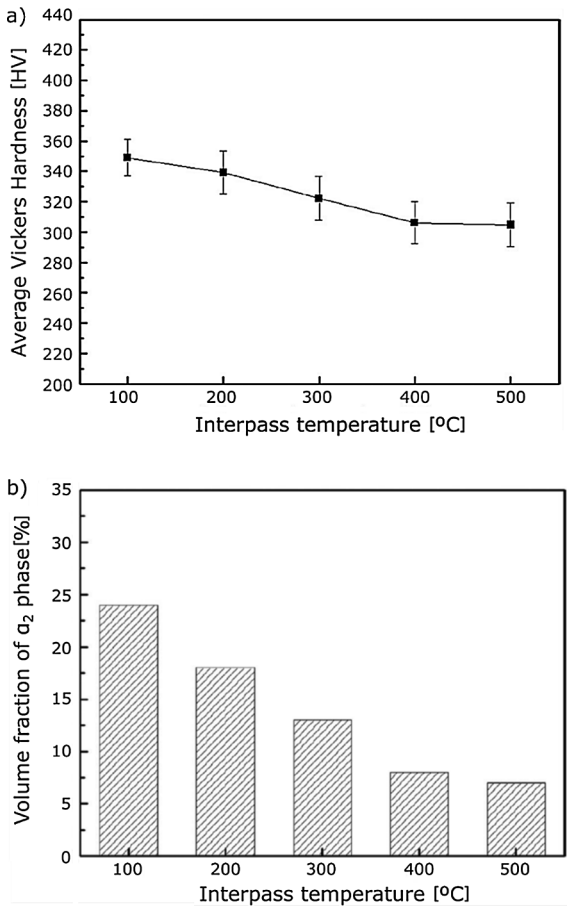

Fig. 13. Change in hardness (a) and volume fraction of α_2 phase (b) as a function of interlayer temperature during wire and arc additive manufacturing of a γ-TiAl alloy (adapted from [202]).

low heat input is used.

Other works have shown that the difference in heat input during wire and arc additive manufacturing do not drastically change the microstructure or mechanical properties of the deposited material. Such as been exemplified for aluminum alloys in [200,201]. However, the existence of reheat cracking in the as-built parts of [200] suggests that there is still need for improvements, namely by acting on the heat input.

The control of the interpass temperature during arc-based additive manufacturing can drastically modify the thermal cycle and microstructural evolution in the as-built parts, similar to what was previously described for arc welding. Ma et al. showed that during wire and arc additive manufacturing of a γ-TiAl alloy control of the interlayer temperature is critical to allow in-situ precipitation α_2 phase [202]. By varying the interlayer temperature during the process, the authors were able to control the α_2 phase fraction and the resulting hardness. The tested interlayer temperatures ranged between 100 and 500 °C, which yielded different microstructures and mechanical properties, as evidenced in Fig. 13. Control of the volume fraction of α_2 is critical in γ-TiAl alloys, since only small fractions of this phase are beneficial to the material mechanical properties. This is related to the fact that α_2 has low ductility, hence the need to properly balance the γ/α_2 ratio [203].

The interpass temperature can also be varied throughout the deposition to locally modify the microstructure of the parts. Such as been exemplified during wire and arc additive manufacturing of Ti-6Al-4V in [204]. Though the production of functionally graded parts appeared not to be the aim of the researchers of [204], they showed that localized shielding gas during deposition could control differently the thermal cycles at distinct locations of the part, thus resulting in different microstructural and mechanical features. If the aim is to increase productivity, it is not practical to let the previously deposited layer to reach room temperature. In this case, forced intercooling [205] can be used to decrease the elapsed time between two consecutive layer depositions increasing the process productivity. If post-process heat treatments are to be applied to refine the microstructure, then, forced cooling can be used with the purpose of reducing the time between deposited layers, controlling the interpass temperature, but avoiding oxidation of the part [206]. Finally, management of the interlayer temperature can be used to control residual stresses and distortion during fusion-based additive manufacturing [207].

The effect of shielding gases during fusion-based additive manufacturing is not yet attracting significant attention. This can be justified by the fact that the most used additive manufacturing process is selective laser melting where inert gases, as Ar or He, are used with the sole objective to prevent or decrease material oxidation. Aside from preventing oxidation, shielding gas during powder-bed additive manufacturing with laser as the heat source, can be used to remove undesired effects, such as fumes or spatter [208].

Some authors [208–210] have started to address this topic in [209]. They observed that the shielding gas flow direction influences spatter generation during selective laser melting: when the laser scanning direction is that of the gas flow a decrease in the spattered power was observed. Additionally, the shielding gas flow should be optimized as reported in [208], where it was observed that low gas flow does not effectively remove spatter or generated fumes, which can then interact with the laser beam and redeposit as unwanted byproducts. Moreover, the uniformity of the gas flow through the working envelop during selective laser melting should be homogenous to decrease the potential formation of pores in the as-built structures [210].

For arc-based additive manufacturing the currently available literature on the effect of shielding gases is scarcer, with few works addressing the effect shielding gases. In [211], the authors used Ar, Ar-CO_2, Ar-H_2 and Ar-He-H_2 during wire and arc additive manufacturing of Inconel 625 and observed that the presence of CO_2 in the shielding gas resulted in higher hardness through the as-built parts, though the waviness of the external walls was significantly larger than for the other shielding gas mixtures. Additionally, samples produced with Ar-CO_2 shielding gas had the higher tensile strength ($\approx$750 MPa), which was approximately 50 MPa above that obtained with other three shielding gas mixtures. The significance of these results, though not specified by the authors, arises from the fact that for some material systems, obtaining defect free and high performing parts does not require fully inert, and more expensive, shielding gases as He or Ar. As demonstrated in [211], it is possible to decrease the shielding gas purity through the introduction of CO_2, and therefore decrease the costs associated with the process, and still achieve high quality parts. Since typically all parts created by wire and arc additive manufacturing are to be used as structural parts, post-machining processes are required to remove the surface waviness. Therefore, the increased waviness observed when CO_2 was added to the Ar as shielding gas may not be highly detrimental.

The effect of shielding gases during wire and arc additive manufacturing is quite important since, depending on the shielding gas selection, it can consume or add energy to the arc and thus affect the deposited depth and width, as well as, its chemistry due to liquid/gas reactions in the melt pool.

Though only inert gases are used during powder bead additive manufacturing, active shielding gases, such as O_2 or CO_2, can greatly assist the additive manufacturing processes based on electric arc for alloys systems that do not require fully inert gases such as low alloy and stainless steels. As described before, the use of active gases during arc welding can help to control the melt pool depth and width, as well as promote better arc stability and modify the transfer mode and, subsequently, the process productivity. So far, to the best of the author's knowledge, aside from the recent work of Jurić et al. [211] described above, there are no comprehensive reports addressing the effect of active shielding gases during arc-based additive manufacturing.

4.3. Use of grain refiners or filler materials to control the microstructure and chemical composition

4.3.1. In welding

The use of grain refiners is widely used in both welding and casting technologies to decrease the grain size of the solidified metals and/or to promote the columnar to equiaxed transition. Typically, in fusion-based welding, the introduction of alloying elements to control the grain structure is done by incorporate them in the filler material. These alloying elements may have two distinct functions:

(i) act as solid nuclei ahead of the solidification front; (ii) change the molten pool chemical composition.

According to the homogenous nucleation theory, there are two main contributions to the free energy change during solidification. The first contribution is related to the free volume energy, which is the difference between the liquid and solid phases and has a negative value, if the temperature is below the equilibrium solidification temperature. The second contribution arises from the formation of a liquid/solid boundary and has a positive contribution to the total free energy change of the system. Upon solidification, embryos are formed, and these can growth into nuclei when they reach a minimum critical radius above which these nuclei are stable. That is, when the free energy change of the system decreases, the contribution of the free energy volume is higher than that of the liquid/solid boundary. As a result of this dependence with the free energy volume, the modification of the composition of the melt pool can be such that this term gains more importance than the liquid/solid surface energy. If that is the case, the critical nuclei radius will be smaller, and nucleation occurs more readily. In fact, it can be demonstrated that this critical radius is dependent on the melting point of the material, latent heat of fusion, surface free energy and transformation temperature [212]. Though homogenous nucleation does not occur in fusion welding, it is a good starting point to explain the mechanisms which promotes the formation of new grains in the melt pool: heterogeneous nucleation.

The existence of solid particles in the melt pool favors nucleation of new grains since the surface free energy is lowered, thus contributing to a decrease in the volume free energy. In heterogenous nucleation, the critical radius depends on the solid/liquid surface tension and the volume free energy. It must be noticed that for a given material, the critical radius for nucleation is the same for both homogenous and heterogeneous nucleation. However, the activation barrier for the latter is lower, thus favoring this type of nucleation.

During autogenous fusion welding the composition of both base material and liquid metal are similar. As such, the initial grain growth occurs by epitaxy [213]. In this case, spontaneous solidification can occur below the *liquidus* temperature. In opposition, during non-autogenous fusion welding, the use of a filler material with a composition different from that of the base material can lead to a different type of heterogeneous nucleation, which is facilitated by the presence of chemical inhomogeneities. Nonetheless, growth by epitaxy is still possible.

The use of inoculants to promote grain refinement during fusion welding has been widely studied in the last decades [126,214,215]. These inoculants, if are not dissolved by the liquid metal are favorable nucleation sites which can assist in the refinement process. The efficiency of these inoculant particles will depend on parameters such as surface roughness and chemical affinity between the particle and the solid which is to be formed [213].

As described before, solidification of the weld pool can occur with very small undercooling at the fusion boundary, and by epitaxy typically large columnar grains are obtained. The need to obtain equiaxed grains in the fusion zone drove the welding community to understand and modify the solidification conditions so that the columnar to equiaxed transition could occur during fusion welding.

There are multiple mechanisms to achieve the columnar to equiaxed transition including grain detachment, dendrite fragmentation and heterogenous nucleation. The former two can be induced by the fluid flow and temperature gradients across the melt pool, as previously described. The latter concerns the use of dedicated filler materials that can add solid particles to the melt pool to act as nucleation sites during solidification, or by inducing chemical composition changes that can facilitate in the heterogenous nucleation process. It must be noticed that there are other options to insert inoculants in the melt pool. However, as illustrated in [215] these approaches require machining of the base metal, which will then be filled with the desired inoculant. Though such solution can also be effective to decrease the grain size and promote equiaxed grains, it is technically challenging and time-consuming. For this reason, the use of dedicated filler materials is the first choice in both arc- and hybrid-based welding.

Filler materials typically have different composition of that of the base material(s) to be joined and are used to control the composition of the fusion zone. The use of filler materials is especially important during dissimilar welding of alloys which do not exhibit good thermo-physical compatibility. For example, fusion welding of ferritic to austenitic steels for the petrochemical industry is problematic due to the significantly different thermal stresses arising from the fact that both alloys exhibit distinct coefficients of thermal expansion [216]. Additionally, carbon migration from the ferritic steel to the austenitic one may occur, which can accelerate the occurrence of creep at the ferritic steel fusion boundary. To overcome these problems, Ni-based filler materials are used [217–220]. Because Ni-based filler materials have a coefficient of thermal expansion that lies between the two base materials, the thermal stresses across the joint are not so severe. Additionally, Ni-based filler materials can retard carbon migration due to the low diffusivity of this element in Ni-based alloys.

Joining of Aluminum to steel by fusion-based methods is problematic not only due to the difference in the coefficient of thermal expansion, but also due to the formation of Fe-Al brittle intermetallic compounds [221]. Dong et al. showed that for this dissimilar combination proper selection of the filler material during arc-based welding is fundamental: while the use of Al-Si filler was effective in restricting the thickness of the intermetallic compounds, the opposite behavior was observed for the Al-Cu filler resulting in diminished mechanical properties [222].

The use of filler material during laser welding is less frequent than in arc or hybrid welding. However, Weigl et al. successfully joined Aluminum to Copper using Al12Si (at.%) and Cu3Si (at.%) fillers [223]. It was observed that the Al12Si filler enhanced the fluidity of the molten pool, resulting in a more uniform mixture of the base materials when compared to the Cu3Si filler. Due to the more uniform mixing within the fusion zone when the Al12Si filler was used, a significant improve in ductility was obtained.

Ni-based superalloys are a specific class of advanced engineering alloys which are known for their weldability problems [224]. As a result of their high alloying content and need for specific precipitates to be present at high operating temperatures, appropriate welding procedures have to be developed. In fact, the combined effect of Aluminum and Titanium in Ni-based superalloys are known to decrease the material weldability. As a result, multiple defects such as solidification cracking, grain boundary liquation cracking, strain age cracking and ductility dip cracking may occur. Aside from grain boundary liquation cracking, which occurs in the heat

affected zone, all other defects occur in the fusion zone and multiple filler materials can be used to mitigate their appearance [218,219].

Most Aluminum alloys series (1XXX, 3XXX, 5XXX and 6XXX series) exhibit good weldability when fusion-based methods are used. However, 2XXX and 7XXX series are prone to liquation and solidification cracking as a result of the high content of alloying elements [225]. Since 7XXX Aluminum alloys have very good mechanical properties, solving their weldability issues is critical [226,227]. The 7XXX series are difficult to weld without porosities due to the presence of Zn. Another important problem is the reaction with O_2. So, besides the use of an inert gas, filler materials with Si are a good solution, since Si is a known deoxidant agent. To solve such weldability problems, researchers developed and used dedicated filler materials to control the chemical composition and microstructure of the fusion zone.

For example, Soysal et al. [228] found that during gas tungsten arc welding of AA 2024, the use of a nonmatching filler material, AA 4145, greatly reduced cracking susceptibility of the base material. Here, the use of a filler material with a different composition from that of the original base material promotes a new solidification path that is less susceptible to cracking thus improving the joint mechanical properties.

For both 2XXX and 7XXX Aluminum alloys series, the introduction of Sc promotes exceptional grain refinement and the solidification microstructure changes from dendritic to equiaxed. Because Sc is very expensive and small amounts of this element have a significant impact on the grain refinement, researchers focused on the development of Sc-based filler materials that can increase the weldability of 2XXX and 7XXX Aluminum alloys series [229]. The work of Norman et al. [229] clearly showed that only above a certain Sc concentration, which depends on the base material to be welded, grain refinement occurs. When the Sc concentration surpasses the minimum required for the refinement effect to arise, formation of Al_3Sc particles occurs in the melt pool which then act as nucleation sites upon solidification of the surrounding liquid.

Other researchers further extended the scope of [229] and developed filler materials containing both Sc and/or Zr [230], which resulted in grain refinement due to the formation of nanometric Al_3(Sc, Zr) particles. The grain refinement was more significant when Sc and Zr were simultaneously used in the same filler material since Zr is known to reduce coarsening of Al_3Sc particles.

Though most research works use filler materials to control the microstructure and composition of the fusion zone, there are some examples where the introduction of inoculant particles can be performed without any filler material. Such as been recently demonstrated by Ma et al. [231]. By using Al_2O_3 and SiC nanoparticles during laser melting of pure Ni, the authors found that it was possible to increase the fusion zone depth by 68%, while decreasing the heat affected zone width by a similar amount. Though not fully explained yet, the reasons for such unusual behavior are attributed to the fact that the selected nanoparticles are effective in reducing the heat dissipation, thus promoting a deeper weld pool, while at the same time effectively restricting the grain coarsening and decreasing the extent of the heat affected zone.

As evidenced by the examples provided above, for a given alloy system, key specific grain refiners must be selected to achieve an effective refinement effect. Table 3 depicts some of the most common elements as filler materials and their effects when welding several engineering alloys.

As comprehensively described above, the effect of filler materials and grain refiners to control the grain structure and/or composition during fusion welding is well established and the same principles can be applied during fusion-based additive manufacturing.

Table 3
Effect of different filler materials in fusion welding of engineering alloys.

Alloy system(s)	Element used	Effect	Reference
9Cr–1Mo to 316LN stainless steel	Inconel 182	Improvement of mechanical properties and thermal stability	[216]
304 austenitic stainless steel to 409 ferritic stainless steel	310 austenitic stainless steel	Formation of ferrite and austenite in the fusion zone	[232]
304 austenitic stainless steel to 409 ferritic stainless steel	316L austenitic stainless steel	Formation of ferrite and austenite in the fusion zone	[232]
304 austenitic stainless steel to 409 ferritic stainless steel	310 austenitic stainless steel	Formation of martensite which induced cracking in the fusion zone	[232]
AA5456	AA5356	Decrease cracking susceptibility	[19]
AA5754 to AZ31	ZnAl	Decrease the formation of brittle compounds	[233]
AA60616 to GXES steel	Zn-15Al (wt.%)	Improve the joint microstructure	[234]
AA6016 to DP600 steel	Zn-15Al (wt.%)	Improve the joint microstructure	[235]
Cu to 304 stainless steel	Cu	Avoid formation of cracks	[236]
Cu to 304 stainless steel	66.5Ni-30Cu-4Fe-0.5C (wt. %)	Detrimental to the joint microstructure, forming cracks	[236]
Inconel 617 to 310 austenitic stainless steel	Inconel 617	Improved the joint mechanical properties	
Inconel 617 to 310 austenitic stainless steel	310 austenitic stainless steel	Formation of low melting point precipitates which promoted cracking	
Inconel 657 to 310 stainless steel	Inconel A	Improved ductility and strength of the joint	[237]
Inconel 657 to 310 stainless steel	Inconel 617	Increase in dendrite grain size	[237]
Inconel 657 to 310 stainless steel	310 stainless steel	Improved ductility of the joint	[237]
Inconel 718 to 316L stainless steel			
Pearlitic ductile cast iron	Ni	Decrease the martensite content in the fusion zone	[238]
Pearlitic ductile cast iron	7018 Mild Steel	Decrease the martensite content in the fusion zone	[238]
Ti-6Al-4V	Ti grade 3	Decrease of hardness in the fusion zone	[239]

In fact, multiple works in the field of additive manufacturing have been using the approach of using dedicated grain refiners or inoculants and filler materials to optimize the microstructure and mechanical properties in the as-build parts. These will be discussed next.

4.3.2. In additive manufacturing

The discussion about the mechanisms in which the use of grain refiners or filler materials can be used in fusion-based additive manufacturing follows the same reasoning as previously detailed for fusion welding.

Research on both powder-bed and wire-feed additive manufacturing techniques have used either inoculants or dedicated wires.

A class of materials where the addition of grain refiners may have a very high impact are in Ni-based superalloys, used for high temperature applications. The existent of the γ' phase is known to increase the alloy high temperature mechanical properties [240] and the volume fraction of γ' can be increased with additions of Ti and Al. However, the susceptibility for defect generation upon solidification increases, via strain age cracking phenomena. In fact, when the combined sum of Ti, Al and Nb is above 4 at.% the material is considered unweldable, thus preventing its manufacturing by additive manufacturing techniques. One potential approach to overcome the manufacturability problems of high alloyed Ni-based alloys is using a dilute alloy such as Inconel 625, and then add particles to the melt pool that contribute to an increase in the high temperature resistance of the as-built part.

Copper et al. [241] comprehensively studied the effects on the microstructure and hardness of Inconel 625 during powder-bed laser additive manufacturing. The authors separately used SiC, TiC and Al_2O_3 dispersed with the Inconel 625 raw powder. They reported that SiC and TiC are melted during the laser scanning, but upon solidification they precipitate with a smaller grain size. Additions of Al_2O_3 are not effective since reprecipitation does not occur. It must be pointed out that complete melting of the SiC and TiC particles and their subsequent resolidification into a small size is debatable. We believe that the reduced grain size of these particles occurs due to insipient melting along their grain boundaries, which leads to a decrease in grain size. This is further corroborated by the fact that the same behavior has not been reported for Al_2O_3 and this must be related to the significantly different melting points of the compound. For Al_2O_3, SiC and TiC the corresponding melting points are of 2072, 2730 and 3160 °C, respectively. The high temperature of the molten pool during selective laser melting can effectively promote complete melting of the Al_2O_3 particles but not of the SiC and TiC ones. Nonetheless, the existence of refined SiC and TiC particles in the as-built parts increases the hardness. The improvement on the mechanical properties in powder-bed laser additive manufacturing of Inconel 625 using dispersed TiC particles was corroborated in [242], where an ultimate tensile strength above 1 GPa and elongation to fracture of more than 20% were obtained.

The use of TiB_2 nanosized particles mixed with the raw Inconel 625 powder was also reported in [243] using a laser as the heat source. The TiB_2 particles were found at the grain boundaries of the as-solidified microstructure and a significant strengthening effect by pinning of the grain boundary movement was observed: while the ultimate tensile strength and fracture strain of the TiB_2-free parts were of about 840 MPa and 16%, respectively, the presence of the nanoparticles increased these values to approximately 1020 MPa and 19%.

Ho et al. [244] used WC-W_2C inoculants during powder-bed laser additive manufacturing of Inconel 718, a highly alloyed Ni-based alloy. Though there was no assessment of the mechanical properties, the presence of eutectic WC-W_2C provided extra

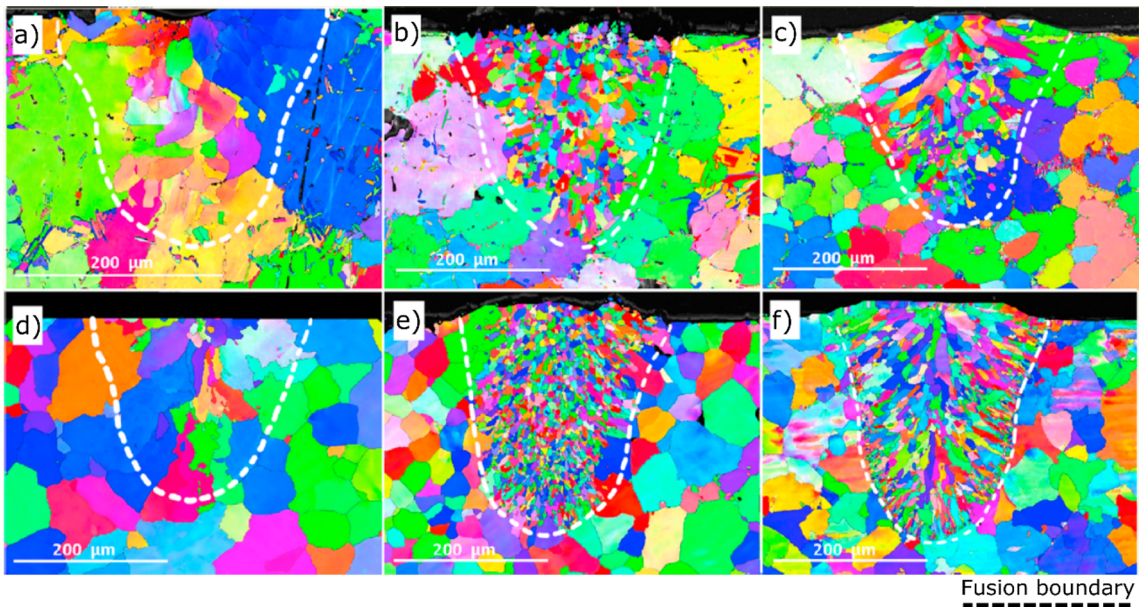

Fig. 14. EBSD maps for two Aluminum alloys processed by selective laser melting: (a) Al-7Si without grain refiners; (b) Al-7Si with 0.33 wt.% Tibor; (c) Al-7Si with 0.4 wt.% Sc; (d) Al 6061 without grain refiners; (e) AA 6061 with 0.33 wt.% Tibor; (f) AA 6061 with 0.4 wt.% Sc (from [246]).

nucleation sites for Inconel 718 resulting in a decrease in grain size. However, precipitation of a Nb-rich phase occurred along the grain boundaries, suggesting that there may exist a decrease in mechanical properties of the as-built alloys. More studies are required to understand if the grain refinement effect induced by the WC-W_2C particles is endangered by the precipitation of the Nb-rich phase.

The use of grain refiners during powder-bed additive manufacturing of Aluminum alloys is also expanding. High strength Al-Cu-Mg alloys can be processed using powder-bed additive manufacturing techniques provided that a low travel speed of the heat source is used, otherwise hot cracking occurs [245]. As described before, microalloying is an effective way to decrease cracking susceptibility and increase the mechanical properties of Aluminum alloys. Nie et al. [192] demonstrated the importance to precise control Zr microalloying addition during selective laser melting of Al-Cu-Mg: when the amount of Zr increased up to 2 wt.%, the yield and ultimate tensile strength always increased; above 2 wt.% a decrease in mechanical properties was observed. The controlled addition of Zr, via the introduction of Al_3Zr and ZrO particles, acted as heterogenous nucleation sites, promoting grain refinement, hence justifying the increase in the mechanical properties of the as-built parts. Additionally, Zr-based precipitates were observed, which also contributed to an increase in mechanical properties.

TiB_2 particles can be used not only to promote grain refinement in Ni-based superalloys, as previously described, but also to achieve the same effect in Aluminum alloys [246]. In [246], the authors tested the use of Tibor, a commercial titanium-boron grain refiner with a chemical composition, in wt.%, of Al5Ti1B, and Sc to act as grain refiners during selective laser melting of two Aluminum alloys, Al-7Si and 6061. They observed that both particles are effective in promoting a grain refinement effect, similarly to what was described for fusion-based welding before, though the effect in the Al-7Si alloy was less evident due to poison mechanism induced by Si [247]. Despite both Al5Ti1B and Sc promote grain refinement, the former has a stronger effect as evidenced by the EBSD maps depicted in Fig. 14.

Martin et al. [13] used ZrH_2 to process AA 7075 by selective laser melting, which is considered a non-weldabled alloy. The introduction of ZrH_2 particles promoted an equiaxed grain growth. Since an equiaxed grain morphology can more easily accommodate strain in the semi-solid state, solidification cracking was avoided. Without the introduction of these particles, the typical columnar grain structures developed, and cracking was observed.

More recently, Xie et al. [248] studied the effect of TiB_2 during selective laser melting of Al-12Si. The remarkable efficiently of TiB_2 to refine the microstructure is evident in Fig. 15. Furthermore, the crystallographic texture drastically changes upon the addition the TiB_2, with the development of a random crystallographic orientation. A result of these microstructural changes an improvement in the mechanical properties, tested under compression, was obtained.

Titanium alloys are probably the class of engineering alloys which have the most potent and effective grain refiners. This is exemplified in the work of Mantri et al. [249], and will more evident when focus is given (below) to the use of grain refiners during wire and arc additive manufacturing. In [249], the addition of only 0.5 wt.% B decreased the grain size by nearly 40 times in a Ti-20V alloy, and up to 100 times in a Ti-12Mo alloy, as depicted in Fig. 16. Furthermore, the introduction of B was seen to modify the morphology of the as-solidified microstructure from lath-like to near equiaxed. It must be noticed that currently, there are no reports on the effect of B on the mechanical properties of the as-built alloys.

Some recent examples for the use of grain refiners during powder-bed additive manufacturing of stainless steels have also been reported [250,251]. The authors used TiC nanoparticles during selective laser melting of 316L stainless steel. In principle, the use of

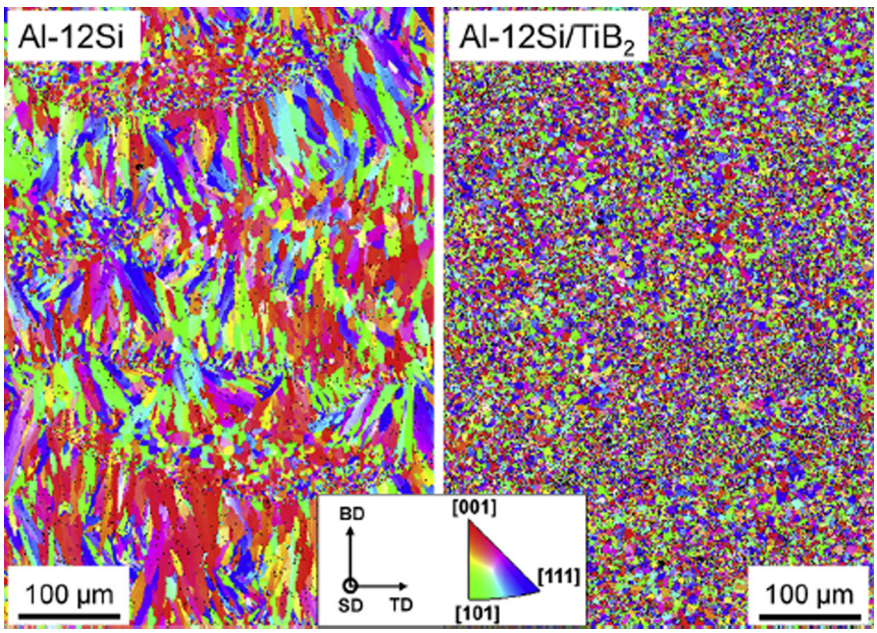

Fig. 15. Microstructure in after selective laser melting of Al-12Si alloy: (a) without TiB_2; (b) with TiB (from [248]).

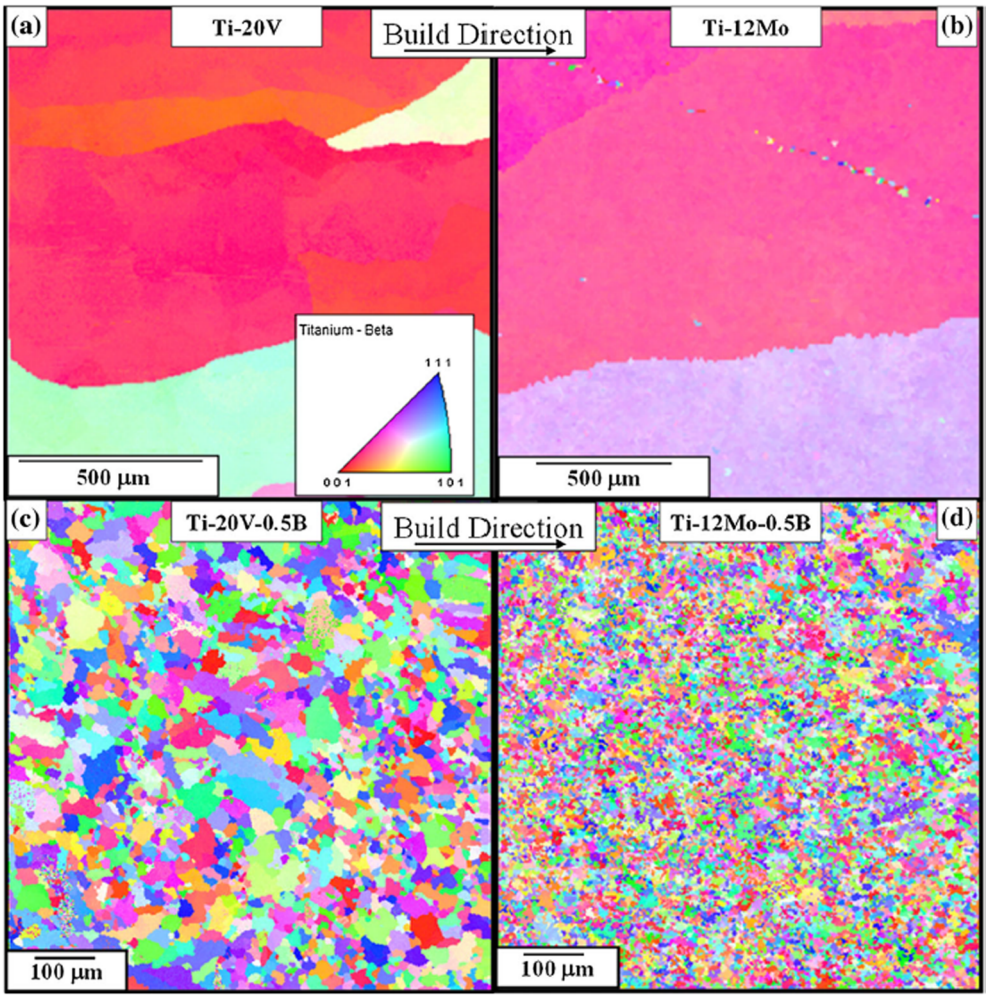

Fig. 16. Effect of B additions during laser additive manufacturing of Ti-based alloys: (a) Ti-20V parts; (b) Ti-12Mo parts; (c) Ti-20V-0.5B parts; (d) Ti-12Mo-0.5B (from [249]).

any high hardness ceramic particle, with good wettability in the molten surrounding alloy, thermodynamic stability and high melting point can be used as a reinforcement during fusion-based additive manufacturing. For 316L stainless steels, TiC particles have all the above-mentioned properties, making these ideal candidates to improve the mechanical resistance of the as-built parts. In fact, the introduction of TiC nanoparticles drastically increased the room temperature yield strength from 600 to 800 MPa. It must be noticed that complete melting of the TiC particles did not occur, though some agglomeration due to insipient surface melting was observed. If complete melting of the TiC particles occurred, it was not expected such high mechanical resistance of the produced parts, since TiC is effective in restricting crack propagation and once dissolved in the liquid hardly there would be reprecipitation upon cooling.

Currently, most of the research on fusion-based additive manufacturing has been focused on powder-bed additive manufacturing. Consequently, less research works can be found on the use of grain refiners during wire and arc additive manufacturing. In the case of arc-based additive manufacturing with a wire as feedstock material, the grain refiners are typically introduced directly into the wire. As it will be shown, this area has a significant growing potential since production of dedicated wires is common process as wires have been used as welding consumables for decades now.

Bermingham et al. [252] clearly exemplified how the modification of the wire feedstock during wire and arc additive manufacturing can drastically change the microstructure of the as-deposited material. Fig. 17 depicts a cross-sectional view of as-built parts. Letters (a) to (c) refers to the conventional Ti-6Al-4V wire, (d) to (f) to a modified Ti-3Al-8V-6Cr-4Mo-4Zr and (g) to (i) to Ti-3Al-8V-6Cr-4Mo-4Zr + La_2O_3 wire. While the introduction of Cr, Mo and Zr into the master Ti-Al-V alloy act as growth restricting solute and promotes some degree of grain refinement it does not promote the columnar to equiaxed transition, though the width of the columnar grains is significantly reduced. However, when, to the growth restricting solute elements, La_2O_3 is added a significant grain refinement of the microstructure occurs and the columnar to equiaxed transition is clearly observed. Though no mechanical testing was performed on these samples, it is expected that improved mechanical properties are achieved when both the grain refinement and the columnar to equiaxed transition exist in the as-built material sample.

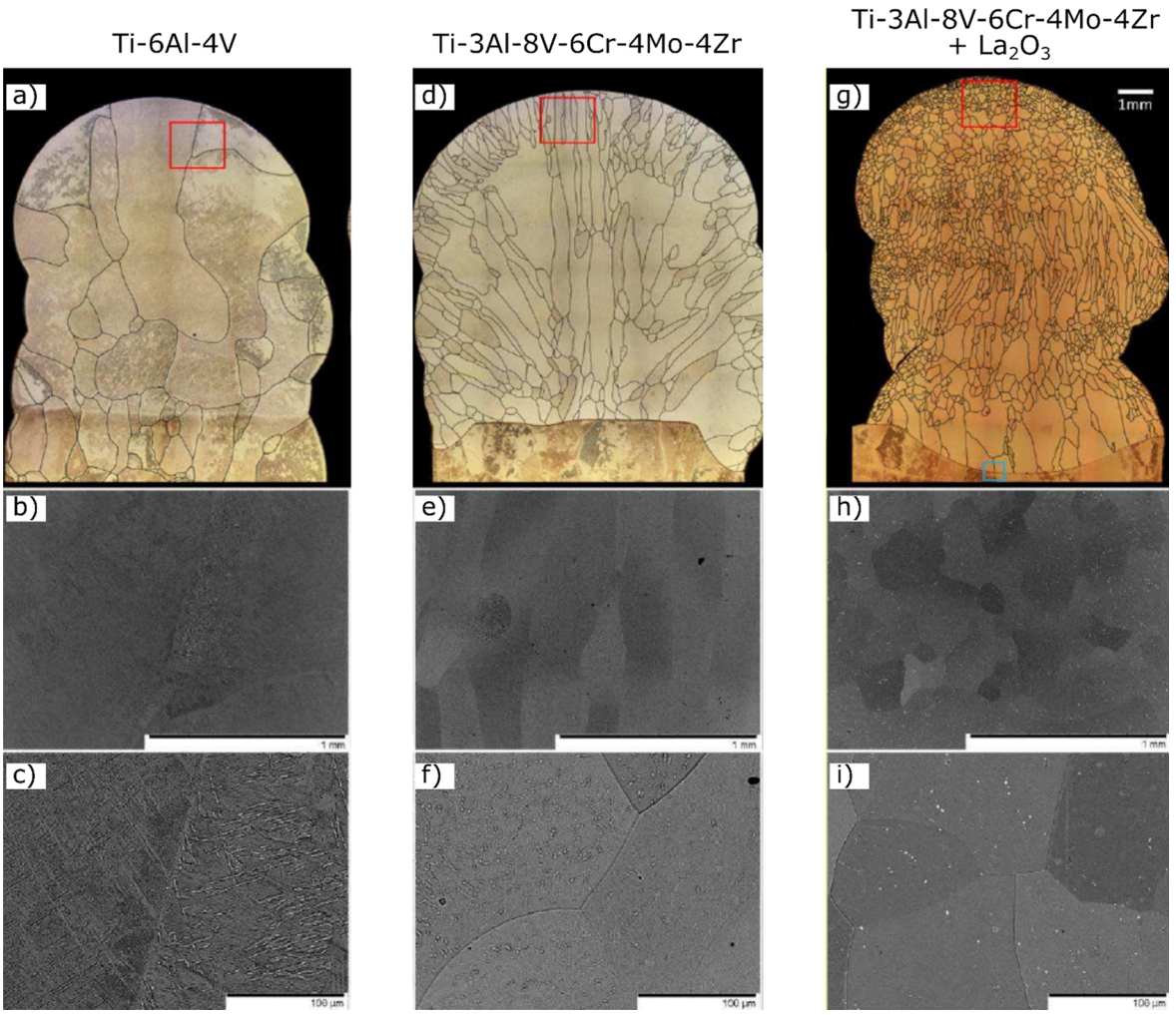

Fig. 17. Macro and microstructures of: (a–c) Ti-6Al-4V; (d–f) Ti-3Al-8V-6Cr-4Mo-4Zr; (g–i) Ti-3Al-8V-6Cr-4Mo-4Zr + La_2O_3. The red squares on the top row represent the regions analysed by scanning electron microscopy depicted in the middle and bottom rows (adapted from [252]).

The effect of B on the microstructure and mechanical properties of Ti-6Al-4V parts produced by wire and arc additive manufacturing was also studied in [253]. In this case, introduction of B into the melt pool was achieved by painting each deposited layer with a B-based paint. With this approach, B (or any other element/compound) is deposited on the material and when the next layer is deposited, B will be incorporated into the melt pool. B was selected as a grain refiner since it has been shown that this element effectively promotes grain refinement in Ti-based alloys [254]. With the introduction of B into the as-built parts, several microstructural changes occurred: the existence of B as solute promoted enough constitutional supercooling to restrict lateral columnar growth, thus resulting in a grain refinement effect; TiB needles finely dispersed in the as-built parts promoted the nucleation of higher volume fraction and more isotropic morphology of α phase; despite no significant differences in the mechanical properties were observed in the as-built parts, after heat treatment the B-added parts greatly improved their mechanical strength.

The strategy to deposit a grain refiner by painting each deposited layer was again followed by the same authors but using LaB_6 instead [255]. Similarly to previous work with B, a very small amount of LaB_6 (less than 0.1 wt.%) was used. The reason to select grain refiners which are actually effectively in such small concentration is related to an ASMT standard for additive manufacturing of Ti-6Al-4V [256], which allows a maximum addition of 0.1 wt.% of any element other than Ti, Al and V up to a maximum of 0.4 wt.%. La, alongside with B, Be and C, is an element which can produce a significant grain refinement effect in such small concentration. Additionally, rare earth elements such as La can reduce the oxygen concentration in Titanium alloys. As such, the introduction of LaB_6 can potentially act as a grain refiner while at the same time promote oxygen pick up and decrease oxidation, for example. Interesting changes in the weld pool morphology and microstructure were reported upon the introduction of LaB_6: introduction of La was seen to reverse the direction of the Marangoni flow of the melt pool, resulting in narrower deposited beads; when in the melt pool, LaB_6 decomposes to La_2O_3 and TiB and this microstructural changes result in an increase of the tensile strength, though ductility is reduced; the decomposed TiB drastically increase the part anisotropy owing to the highly directional growth of this phase.

As in can be inferred from the results presented in [253,255], B and LaB_6 can effectively decrease the grain size and improve the

mechanical properties in Ti-6Al-4V parts. However, is must be noticed that the introduction of B, or any other element, by painting each deposited layer is a rather time consuming and technically challenging task. We hypothesize that such approach is due to the difficulty to control the B level (below 0.13 wt.%) that must exist in a dedicated Ti-6Al-4V-based wire to be used during wire and arc additive manufacturing. It is expected that with the increasingly interest in arc-based additive manufacturing for the creation of large Ti-6Al-4V components with short delivery times, more efforts will be devoted to the production of dedicated wires which can incorporate some of the most potent grain refiners for this class of alloys.

Other authors have recently used the same strategy of painting each deposited layer of Ti-6Al-4V but using CaF_2 [257]. During activated tungsten inert gas of these alloys, CaF_2 is used as a flux to alter the melt pool dimensions, namely decrease of its width. For wire and arc additive manufacturing, this capability is of special interest, since the resolution obtained using this technique is rather poor when compared to electron beam and laser power-based techniques [258,259]. The use of the CaF_2 was effective in decreasing, by nearly 30%, the width of the molten pool, which was attributed to a change in the Marangoni convention movement, similar to what occurred when LaB_6 was used [255]. Additionally, the introduction of CaF_2 was also seen to affect the microstructure of the as-built parts by increasing the content of β phase. Despite the higher volume fraction of β phase in the as-built parts, a decrease in the mechanical strength and decrease in ductility was reported, though the opposite was expected since typically for Titanium alloys the β phase is more ductile while α has higher mechanical strength. Further detailed studies are necessary to understand how these microstructural induced changes modified the mechanical properties of the produced parts after the introduction of CaF_2.

Though Ti-6Al-4V is the most common Ti alloys used in industry, additive manufacturing of other Ti alloys is also increasing. Meredy et al. [260] used Si during wire and arc additive manufacturing of commercially pure Ti. Similarly, to [253,255,257] the grain refiner was introduced using a Si-based paint. The effect of small amounts of Si is clearly evidenced in the cross sections of the as-built walls depicted in Fig. 18. By increasing the Si content, a significant decrease in the prior β grain size was observed, showing that Si can effectively refine the width of the columnar grains. However, no columnar to equiaxed transition occurred suggesting that the as-built parts still present a relatively high anisotropy in their mechanical properties.

Table 4 lists the effect of several alloying elements during fusion-based additive manufacturing of metallic parts, in a similar methodology as adopted for designing Table 3.

4.4. Control of the microstructure using external stimuli

4.4.1. Electromagnetic stimuli in welding and additive manufacturing

During arc-based welding, the presence of an external magnetic field influences both the arc and weld pool behavior due to the Lorentz force, $\vec{F}$. This force is governed by the current density, $\vec{j}$, and the magnetic induction, $\vec{B}$, and is defined as $\vec{F} = \vec{j} \times \vec{B}$. Electromagnetic stirring can occur when the applied external magnetic field is parallel to welding arc axis, resulting in a Lorentz force perpendicular to both the magnetic field and the radial component of the diverging current through the arc and weld pool. This results in the rotation of the arc accompanied by an annular flow of the liquid metal in the fusion zone. In the center and edge of the molten pool the resulting annular flow is null. The use of electromagnetic stirring during arc-based welding can modify the weld bead shape and appearance, alter the solidification microstructure of the fusion zone and refine it, decrease porosity and promote the redistribution of solute in the molten pool [263]. Redistribution of solute during solidification is of special interest to decrease elemental segregation, which of major importance to decrease hot-cracking susceptibility.

One of the critical issues during fusion-based additive manufacturing is the formation of pores. Pore formation is more likely to occur in powder-bed systems than in wire-feed ones, since in the former the existence of gases in between the powder particles make it more prone for the development of porosity during the process. Powder-bed additive manufacturing using laser or electron beam sources is similar to laser and electron beam welding, respectively [107]. During laser or electron beam welding, the high energy

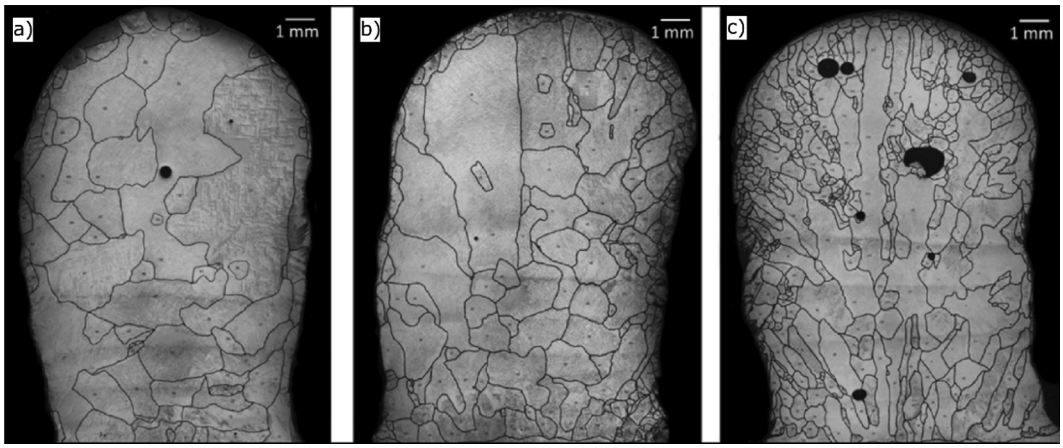

Fig. 18. Effect of Si addition during wire and arc additive manufacturing of commercially pure Ti: (a) 0.04 wt.% Si; (b) 0.19 wt.%; (c) 0.75 wt.% (from [260]).

Table 4
Effect of different elements during fusion-based additive manufacturing of several engineering alloys.

Alloy system	Element used	Effect	Reference
316L stainless steel	TiC	Grain refinement	[250,251]
Al-12Si (wt.%)	TiB_2	Grain refinement	[248]
AA 2024	Zr	Columnar to equiaxed transition; change in the thermal conductivity	[192]
AA 5083	Ti	Grain refinement; Columnar to equiaxed transition	[261]
AA 6061	AlTi5Bi1 (wt.%)	Grain refinement	[246]
AA 6061	AlSc2 (wt.%)	Grain refinement	[246]
AA 7075	ZrH_2	Grain refinement; columnar to equiaxed transition	[13]
Inconel 625	SiC	Hardness increase	[241]
Inconel 625	TiC	Hardness increase	[241]
Inconel 625	Al_2O_3	Decreased structural integrity of the part	[241]
Inconel 625	TiB_2	Grain refinement; increase of mechanical properties	[243]
Inconel 718	WC-W_2C	Grain refinement	[244]
Ti	Si	Grain refinement	[257]
Ti-6Al-4V	B	Grain refinement	[253]
Ti-6Al-4V	C	Grain refinement	[262]
Ti-6Al-4V	CaF_2	Increase the volume fraction of β phase	[257]
Ti-6Al-4V	Cr-Mo-Zr	Grain refinement; Columnar to equiaxed transition	[252]
Ti-6Al-4V	Cr-Mo-Zr + La_2O_3	Grain refinement; Columnar to equiaxed transition	[252]
Ti-6Al-4V	LaB_6	Grain refinement	[255]
Ti20V	B	Grain refinement	[249]
Ti12Mo	B	Grain refinement	[249]

density of the process can actively contribute to increase the likelihood of pore formation. As previously described, Aluminum alloys are probably the class of engineering alloys more prone to pore formation during fusion-based welding [264]. Several factors contribute to porosity formation during fusion-based welding, such as: absorption of the gases (N, O and/or H) by the weld pool that are not released upon solidification; and dissolution of hydrides typically found in as-cast Al parts; instability and keyhole collapse.

One of the most effective way to reduce porosity during laser or electron beam welding of Al alloys is through the use of electromagnetic stirring. In [265], the authors showed that with electromagnetic stirring it was possible to significantly decrease pore density, though this was not eliminated completely. Zhou et al. [266], showed that the use of electromagnetic forces during pulsed laser welding can be used to control the back-filling speed of the weld pool. Control of the back-filling speed during weld solidification is critical since two competing factors, solidification rate and back-filling speed, will dictate pore formation. In pulsed laser welding, after each pulse, the liquid metal at the top of the keyhole will start filling the keyhole. Simultaneously, at the top of the keyhole the liquid will start to solidify and may prevent complete filling of the keyhole generating porosity in the material. Therefore, it is critical to delay the solidification process by control of the pulse shape [267] or, as in the case of [266], by the imposition of external electromagnetic forces. A more comprehensive approach to decrease porosity during laser welding encompasses the use of both control of the laser pulse and electromagnetic forces.

Despite electromagnetic stirring is not yet used in fusion-based additive manufacturing to control pore formation, recent works have exploited this procedure to control the microstructure and therefore the mechanical properties of the as-built parts. Liu et al. [268] have shown that imposing an external magnetic field during laser processing Inconel 718, it was observed a more uniform residual stress distribution, a decrease in Laves phase formation, and broke the large columnar grains observed in additive manufacturing. The decrease in Laves formation in Inconel 718, which is known to be detrimental to the part mechanical properties [269], is attributed to the redistribution of solute promoted by the stirring effect caused by the applied magnetic field. Nb, Ti and Al are all alloying elements that then to be segregation during solidification of Inconel, promoting Laves formation. As a result of the stirring in the melt pool, these elements are redistributed into the melt pool moving from the solid/liquid interface. As a result, Laves formation significantly decreases, which results in optimized mechanical properties when compared to the parts produced without an external magnetic field. The more uniform and lower residual stresses in the parts built with an external magnetic field were attributed to the temperature field variation as a results of the stirring in the melt pool: with the aid of the magnetic field, stirring of the liquid metal decreases the temperature gradient and decreases solidification speed, hence the lower residual stresses in comparison to samples fabricated without an magnetic external field. One very important point raised by the work of Liu et al. [268] is the fact that electromagnetic stirring can be used to effectively increase the mechanical properties of the as-built parts without the need for post-processing heat treatment. Such is especially relevant for repair operations, where additive manufacturing technologies are starting to become more relevant [258,259].

Though the use of magnetic external field has not been reported in arc-based additive manufacturing, its potential advantages are significant. In arc-based additive manufacturing it is possible to obtain very high deposition rates, in opposition to those possible for powder-bed systems. However, this high deposition rate comes at the expense of loss in dimensional accuracy. As result, arc-based additively manufactured parts often need to be machined to remove irregularities in the external surfaces. These superficial irregularities arise from the evolution of the melt pool boundary conditions during the process. In traditional arc-based welding, that is, without superimposition of an external magnetic field, an unstable flow, also called self-flow, of the liquid metal occurs, and random changes in the width and penetration depth of the melt pool can occur. Different mechanisms act synergistically to create this

unstable fluid flow: variations in the surface tension and density with temperature, or the so-called Marangoni effect; buoyance effects enhanced by the significant different in temperature along the melt pool; electromagnetic forces arising from the divergence of the electric current within the melt pool; and shear forces resulting from the arc plasma along the surface of the melt pool. The variation in the width and depth of the melt pool during arc-based welding can be directly transposed to arc-based additive manufactured due to the fundamental similarities between both processes. Therefore, the techniques used to mitigate such deleterious effects can be effectively used by the additive manufacturing community.

As described in [263], the imposition of an external magnetic field during arc-welding can promote the annular flow to dominate the self-flow resulting in weld beads with more regular shape and with predictable width and depth. When applied to arc-based additive manufacturing it the aim of obtaining more stable weld beads, it is expected to obtain parts with increased dimensional tolerance, reducing the need for post-processing machining making this technique more competitive in comparison with powder-bed ones.

Another potential application for the use of external magnetic fields during fusion-based additive manufacturing is to promote grain refinement, similar to what is already well-established in welding. Numerous works have addressed the effect of external magnetic fields to promote grain refinement in the fusion zone of welded joints [270–272]. Several mechanisms can act to achieve this refinement effect. One is dendrite fragment whose mechanism has been previously detailed. Another mechanism that can account for the refinement effect is the decrease of the temperature gradient in the melt pool as a result of the externally imposed electromagnetic stimuli. The more thorough mixing of the liquid metal in combination with the decrease in the temperature gradient when a magnetic field is used increases the constitutional supercooling, which, in turn, enhances nucleation. It must also be noted that both the magnetic field strength and frequency have distinct effects on grain refinement: higher strength and/or low frequency promote more effectively grain refinement in the fusion zone. The detrimental effect of increasing the frequency for grain refinement is attributed to the mobility of the liquid metal which decreases, due to inertia. As pointed out by [270], that the effectiveness of electromagnetic forces for grain refinement will depend on the alloys to be processed. In fact, for alloy with larger solidification range, the refinement effect is more notorious since the fragmented particles will have more time to effectively stir within the melt pool.

To the best of the author's knowledge, so far, only one work has used an external electromagnetic stimulus to control the grain size in fusion-based additive manufacturing. In [273], the authors were able to use an external magnetic field during plasma arc additive manufacturing. When the magnetic field was employed, the stronger stirring effect within the melt pool changed the solidification microstructure from columnar dendritic to near-spheroidal, thus resulting in a more refined grain structure. The induced Lorentz force was able to create a strong rotation of the liquid metal which promoted breaking of the dendritic tips. The existence of dendritic fragments, alongside with the reduction of the temperature gradient in the melt pool, effectively refined the grain in throughout the part. The texture and grain morphology in the electromagnetic assisted parts were seen to be more uniform than when no magnetic field is imposed, which resulted in higher strength and wear resistance.

Alongside with helping with the fluid flow during the welding or additive manufacturing process, electromagnetic stimuli can be used to control the droplet transfer, as widely exemplified for arc welding [274]. The transfer modes during welding are known to affect the shape and dimension of the molten pool, spatter and fumes formation, microstructure and mechanical properties and, more importantly, production rates. There are currently more than 20 transfer modes in welding [275] and these depend on a series of complex interaction between the type of filler wire (feedstock material in arc-based additive manufacturing), polarity of the electrode, current and voltage, and shielding gas [187].

From an application point of view, the use of external magnetic fields is easier to implement for welding than for additive manufacturing. However, as illustrated in [268,273], with proper adaption, the use of this external stimuli can be of extreme importance to tune and enhance the microstructure and mechanical properties of fusion-based additively manufactured parts.

4.4.2. Ultrasonic stimuli in welding and additive manufacturing

Another way to control the grain structure and obtain grain refinement during welding by mechanical means can be achieved by ultrasonic vibration. Some works [130,161,276] have addressed the use of ultrasonic vibration during fusion-based welding.

In [130,276] ultrasonic vibration of the workpiece was used. However, such approach may be difficult if it is necessary for a tight clamping of the materials to be welded. If that is the case, ultrasonic vibration can be induced by the attachment of the sonotrode to the filler material, which, when in contact with the weld pool, will transmit the ultrasonic vibration to the weld pool as exemplified by Yuan et al. in [161].

Dai [130] during gas tungsten arc welding of AA 7075 and Cui et al. [276] for shielded metal arc welding of an AL-6XN supermartensitic stainless steel, used ultrasonic vibration of the base material with different purposes.

In Dai's work [130] ultrasonic vibration was used to refine the grain structure of the fusion zone and decrease solidification cracking susceptibility. As a result of the interaction of the ultrasonic waves with the melt pool, higher cooling rates were obtained, which lead to a decrease in grain size ranging between 30 and 40% when compared to the welds made without ultrasonic vibration. As a result of this grain size decrease a superior hardness in the fusion zone was obtained.

Cui et al. [276], aimed to promote a thorough mixing in the fusion zone. Often, in arc welding using a filler material, there exists the formation of unmixed regions. These heterogenous structures can be detrimental to the joint properties, since the effect of the filler material is negligible in those regions. The effect of the ultrasonic waves in the melt pool results in a strong mixing of liquid completely avoiding the formation of unmixed regions. The use of ultrasonic stimuli during fusion welding can, therefore, improve grain refinement but also to homogenize the chemical composition throughout the fusion zone which is typically beneficial for the material.

More recently, Yuan et al. used ultrasonic stimuli to refine the fusion zone microstructure of two Mg alloys, AZ31 and AZ91 [161]. In this case, the authors studied the position of the ultrasonic probe relatively to the arc and its influence in the grain refinement. With the variation of the offset distance between the arc and the ultrasonic probe it was observed that the area fraction of refined grains first increased, and then decreased. This is related to the fact that if the ultrasonic probe is between the arc and the mushy zone then dendrite fragmentation is more likely to occur and therefore promote grain refinement. If the probe was placed in the mushy zone, the grain refinement effect was only visible in the center of the welded joint. An example of the microstructures obtained during welding of AZ31 with and without ultrasonic are depicted in Fig. 19. In can be observed that the degree of grain refinement throughout the fusion zone depends on the existence or not of ultrasonic stirring but also on the relative position of the ultrasonic probe.

Currently, there are not reports on the use of ultrasonic stimuli during fusion-based additive manufacturing. However, the advantages in terms of microstructural controls are significant and may trigger the interest of the additive manufacturing community to invest in this different approach to obtain grain refinement and a more evenly distributed composition in the as-built parts.

4.5. Summary and future expectations regarding the microstructural control during additive manufacturing

There is a series of actions in arc welding that can be used to improve the microstructure of the melted region, refining the grain size, controlling its chemical composition and, thus, its mechanical properties. Additionally, there is a multitude of potential alloys systems that can be used in additive manufacturing. Some works [13] report that more than 5500 different alloys are currently available for additive manufacturing, though only few such as Inconel, Ti-6Al-4V and AlSi10Mg, for example, can actually be produced with appropriate microstructures and defect-free. The same effect was previously observed during welding, where a vast range

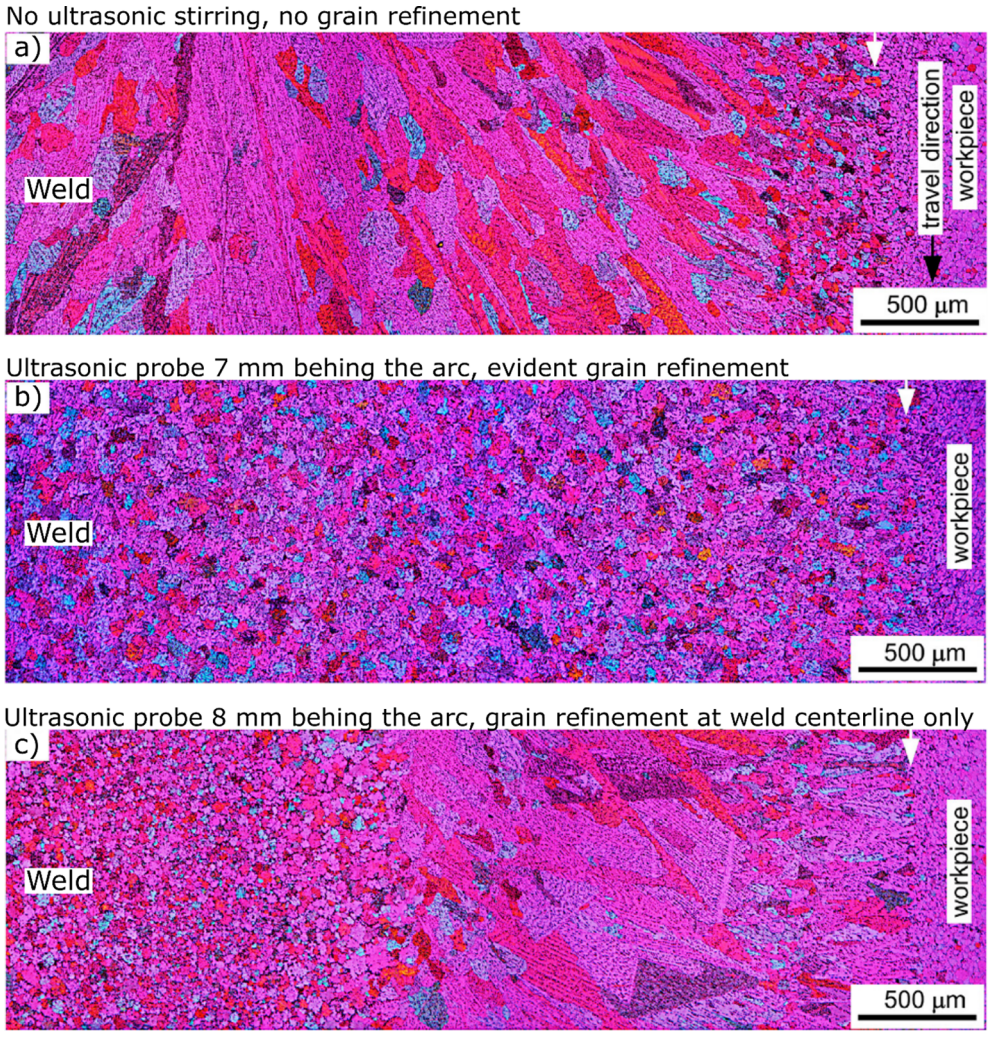

Fig. 19. Microstructure in the fusion zone of AZ31 welds: (a) without ultrasonic stirring; (b) with ultrasonic stirring and the ultrasonic probe located between the arc and the mushy zone; (c) with ultrasonic stirring and the ultrasonic probe located in the mushy zone. Adapted from [161].

of alloys were considered “unweldable”. However, these “unweldable” alloys turned out to be weldable provided that appropriate processes and procedures were developed. These, as described in this section, encompass the modulation of the heat source, use grain refiners or adjust operating procedures. Some key examples from both welding can additive manufacturing were selected and discussed to highlight the multiple similarities between processes and microstructural evolution.

It is expected that with the growing research in the fundamental aspects of non-equilibrium solidification of fusion-based additive manufacturing and with the support of knowledge generated by welding community, most of the available alloys for additive manufacturing can in fact be produced with optimized microstructures and adequate mechanical properties for functional and structural applications.

5. Process parameter optimization criteria for additive manufacturing

A critical issue in additive manufacturing is to optimize the process parameters to obtain defect-free parts. Typically, in both laser and electron beam additive manufacturing research works, process parameters as power, travel speed and hatch distance are varied to obtain fully dense. However, a literature survey shows that there is a wide range of process parameters combinations capable of obtaining defect-free parts, or defective ones, even when the energy density is the same.

Additionally, in additive manufacturing, it is critical to determine the hatch distance that, for a given set of power, travel speed and layer thickness, can be used to produce parts free of porosities or lack of fusion without sacrificing productivity.

The hatch distance selection should be performed to ensure that one deposited track is fully joined to the previous one avoiding detrimental production defects, such as lack of fusion and/or pores. In powder-bed systems the heat conduction is not as effective as in wire feed systems, owing to potential irregularities in the powder distribution that may prevent optimum heat flow during the interaction between the heat source and the material. For that reason, often it is possible to observe regions where the powder did not completely melt resulting in an internal defect that may compromise the integrity of the structure. To guarantee that all powder is completely melted during production and to avoid the presence of lack of fusion defects and pores, it is understandable that the hatch distance should be as small as possible. However, this approach is not feasible for two main reasons: (1) productivity would decrease drastically if the hatch distance was significantly reduced; (2) the complex thermal cycles that the already deposited layers would experience could induce further non-desirable phase transformations (depending on the material used).

The hatch distance is, in fact, the lateral displacement of the heat source between two adjacent layers and there are no theoretical considerations that allow its determination, that is, the hatch distance is set experimentally. Thus, one objective of this work is to establish criteria to determine the best hatch distance for any given set of process parameters. For this, three distinct criteria (geometric, energetic and thermal) are proposed for the optimization of this parameter. The simplifications used ensure that the obtained hatch distance establishes an upper bound value, thus providing a good starting point for process optimization.

5.1. Geometric criterion to determine the hatch distance, h

Consider, for simplicity, that the fusion zone created in a given deposited track is a semi-circle, as schematically depicted in Fig. 20. Such simplification is valid owing to the conduction mode model derived by Eagar et al. [277], which predicts this type of geometry when conduction mode is observed and was experimentally validated for fusion-based additive manufacturing in [149]. To avoid lack of fusion between a deposited layer and the one deposited underneath, it is necessary to remelt part of the latter. The thickness of remelted material is defined as $Z_{remelted}$. Therefore, for a layer thickness defined by Z_{powder}, the heat source needs to create a semi-circular fusion zone with a melted radius, R_m, defined according to Eq. (19):

$$R_m = Z_{powder} + Z_{remelted}, \tag{19}$$

It is important to notice that it is assumed that the energy used to melt the material is the same whether the material is in powder or solid.

Since the geometric profile created by a given set of power, travel speed and layer thickness is known, it is possible to select the

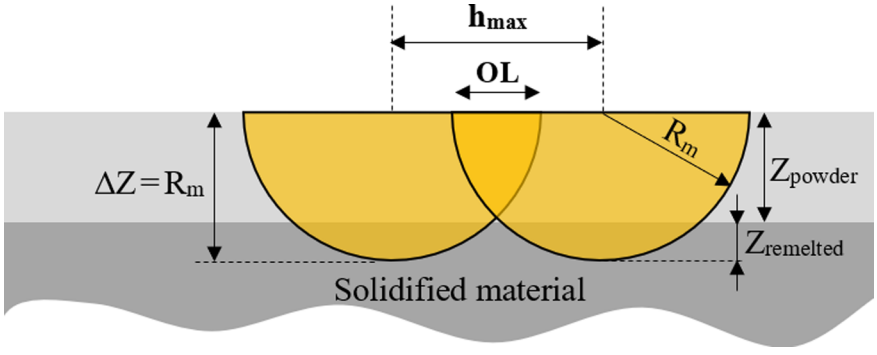

Fig. 20. Geometrical profile created by two consecutive melted tracks in additive manufacturing where melting of the powder and partial remelting of part of the previously deposited layer occurs.

maximum hatch distance, h_{max}, that will ensure that the second deposited track will fully melt the deposited powder and part of the solid substrate, without leaving non-melted powder between the two adjacent tracks. As a consequence of selecting a given hatch distance, the overlap between the two tracks will be defined by the overlap distance, OL, as depicted in Fig. 20. The overlap distance, OL, between two consecutive tracks is given by:

$$OL = 2R_m - h_{max}, \tag{20}$$

However, it must be noticed that increasing the overlap distance, decreases the hatch distance below a maximum value, h_{max}, schematically presented in Fig. 20. If the hatch spacing is lower than h_{max}, a higher amount of previously solidified material will melt and solidify again. In opposition, if the selected hatch distance is higher than h_{max}, then there will be an amount of powder that will not be melted by the following deposited track (Fig. 21).

Thus, the amount of non-melted powder increases when increasing the hatch distance above h_{max}. The relation between the Z_{powder}, R_m and h_{max} is given by Eq. (21):

$$Z_{powder} = \frac{1}{2}\sqrt{4R_m^2 - h_{max}^2}, \tag{21}$$

So, the hatch distance, h, should be equal or lower than:

$$h \leq h_{max} = 2\sqrt{R_m^2 - Z_{powder}^2}, \tag{22}$$

Expressing in terms of $Z_{remelted}$ and Z_{powder} (Eq. (19)), the hatch distance should be equal or below h_{max}, so that:

$$h \leq h_{max} = 2\sqrt{Z_{remelted}^2 + 2Z_{powder}Z_{remelted}}, \tag{23}$$

Experimentally, it is rather expedite to determine both values of $Z_{remelted}$ and Z_{powder} (which is, in fact, the thickness of deposited powder before processing) as it is just necessary to deposit a few tracks of material using different values of power, travel speed (and eventually layer thickness) and, by analyzing the cross section of those melted deposits, determine the necessary values to obtain the maximum hatch distance that can ensure complete melting. However, other defects, such as pores, may occur for certain sets of processing parameters and this reasoning is only valid for situations where keyhole is not observed in additive manufacturing, which may not be always the case [149].

The above-mentioned criterion allows to determine an optimum hatch spacing simply based on geometric relationships between consecutive deposited tracks considering that the process parameters (power, P, and travel speed, v) are adequate to generate an approximate semi-circular region of melted material with a radius of R_m. This geometric criterion does not address the issue of which process parameters are needed to generate a melted region with a radius R_m. Thus, two additional criteria can be used to determine the theoretical value of the melted radius, R_m, and thus determine an upper bound value for the hatch distance parameter based on Eq. (22).

5.2. Energy criterion to determine the melted radius, R_m

This criterion assumes, for simplicity, an adiabatic system and that all the introduced energy is used to raise the material temperature above its melting temperature but below the vaporization point. Under these conditions, the fundamental equation of calorimetry can be used to determine the process energy (E) as follows:

$$E = m\ C_{p\ solid}\ \Delta T_{solid} + m\ Heat_{fusion} + m\ C_{p\ liquid}\ \Delta T_{liquid}, \tag{24}$$

where m is the mass of material [kg]; $C_{p\ solid}$ and $C_{p\ liquid}$ are the heat capacity [J kg^{-1} K^{-1}] of the solid and liquid material,

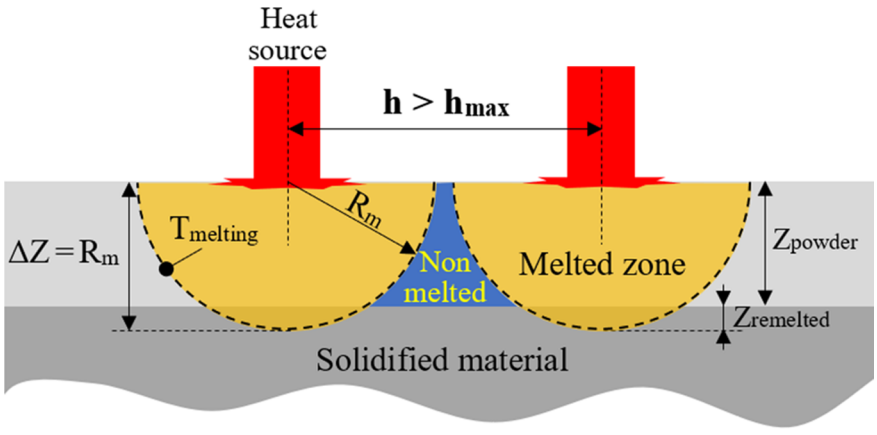

Fig. 21. Schematic representation of a non-melted region if the hatch distance, h, is higher than the maximum allowed hatch distance, h_{max}.

respectively; $Heat_{fusion}$ is the latent heat of fusion [J kg^{-1}]; ΔT_{solid} and ΔT_{liquid} are, respectively, the temperature increase (in [K]) in both the solid and liquid phases owing to the energy introduced in the control volume. It is assumed that evaporation is negligible, so the latent heat of evaporation is not considered.

Considering that the beads created during the additive manufacturing process can be approximated to a semi-circular shape, as schematically depicted in Fig. 22, the volume of the melted region is given by:

$$V = \frac{1}{2}\pi\ R_m^2\ \Delta y, \tag{25}$$

Since V = m/ρ

and $E = P{\cdot}t = P\frac{\Delta y}{v}$

the energy defined in Eq. (24) is equivalent to:

$$P\frac{\Delta y}{v} = \rho\frac{1}{2}\pi\ R_m^2\ \Delta y(C_{p\ solid}\ \Delta T_{solid} + Heat_{fusion} + C_{p\ liquid}\ \Delta T_{liquid}), \tag{26}$$

Solving for R_m:

$$R_m = \sqrt{\frac{2}{\pi}\frac{P}{v}\frac{1}{\rho\ (C_{p\ solid}\ \Delta T_{solid} + Heat_{fusion} + C_{p\ liquid}\ \Delta T_{liquid})}}, \tag{27}$$

From Eq. (27) it is possible to determine the theoretical radius of melted material R_m (layer thickness plus a part of the previously deposited track). Owing to the simplifications assumed to determine R_m, this value is higher than in actual practical conditions, thus acting as an upper bound limit. That is, this is the maximum radius of melted pool created for a given set of processing parameters. After R_m is known it is possible to determine the upper bound value for the hatch distance using Eq. (22).

5.3. Thermal criterion to determine the melted radius, R_m

The third proposed criterion to determine the R_m value is based on the Rosenthal equation, which is widely used to estimate the thermal cycle experienced in conduction welding mode.

The solution of the Rosenthal equation in the case of three-dimensional heat flow was previously presented in Eq. (2) as:

$$T - T_0 = \frac{P}{2\ \pi\ K\ R}e^{-\frac{v(R-x)}{2\alpha}}, \tag{2}$$

Analyzing the temperature distribution at x = 0, where the temperature is maximum, a simplified equation (Eq. (28)) allows to determine the temperature T at a distance R from the heat source:

$$T = T_0 + \frac{P}{2\ \pi\ K\ R}e^{\left(-\frac{vR}{2\alpha}\right)}, \tag{28}$$

In this criterion, similarly to previous based on energy considerations, it is assumed that part of the melted material incorporates the thickness of the powder layer, as well as, a fraction of the previously deposited layer to ensure complete joining between two consecutive layers. The thermal diffusivity (α) and the thermal conductivity (K) are related to the powder. An efficiency parameter, η, needs to be coupled to account for the power losses, such as radiation to air, convection in the molten pool or conduction to adjacent material.

Calculating the radius R corresponding to the *liquidus* temperature of the material, it is possible to determine the corresponding R_m value. Though Eq. (28) cannot be explicit in terms of the radius R, it is possible to obtain the pair of numerical values

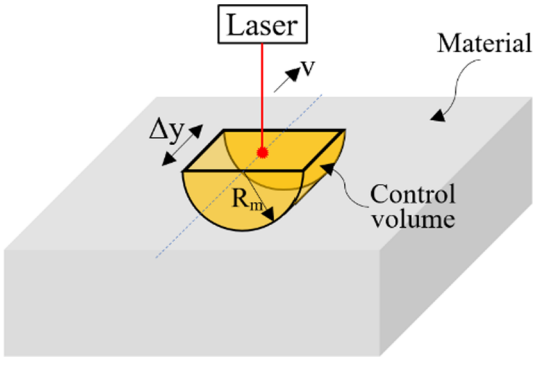

Fig. 22. Schematic representation of the control volume assuming (for simplification) a semi-circular melt pool used for the determination of the energy introduced during the process.

(temperature; radius) based on a given power introduced in the material and its thermophysical properties. Therefore, the solution of interest is the pair (*liquidus* temperature; R_m). With the theoretical value of R_m calculated, the maximum hatch distance can be computed using Eq. (22).

5.4. Effectiveness of the proposed criteria

It is important to emphasize that all the proposed criteria consider some simplifications, namely: it is assumed that the thermophysical properties of the powder and of the as-deposited material are the same, disregarding the effects of porosity and grain boundaries between individual powder grains.

Other process variables, such as layer thickness and powder grain size are important to ensure that parts are fully dense and free of defects. If the layer thickness is larger than half of the beam diameter, the probability to have regions with incomplete fusion gradually increases with increasing hatching distance. Additionally, it is not possible to obtain powders with a tight control of grain size distribution, without compromising powder production costs. Therefore, it is important to take into consideration the powder size distribution. If the powder distribution is slightly skewed towards high grain sizes (above half of the beam diameter), the probability for lack of fusion to occur is more significant. Furthermore, the use of irregular shaped powders [146] or reused powders [278] may impair heat conduction and the process parameters will need adjustments to ensure complete melting during the build.

To test the effectiveness of the proposed criteria, the maximum theoretical hatch distance was computed based on the energetic and thermal criteria. No calculations were performed for the geometric criterion since these are based on cross section measurements of single tracks.

For the energetic criterion, data from [148] was selected. In [148], the authors have comprehensively studied the influence of hatch distance on the production of compact parts in AISI 316L stainless steel by laser additive manufacturing. From Fig. 23, it can be observed that there is a point where the hatch distance used in [148] is higher than the theoretical computed value. In fact, in [148], it was observed that after this point the as-build parts start to have a lower density as a result of the porosity created, which is in good agreement with the fact that the selected hatch distance is higher than the one calculated by the energy criterion. Nevertheless, it must be mentioned that the porosity of the samples produced in [148] is lower than 1%.

For the thermal criteria, the experimental parameters selected were those used in the production of Ti-6Al-4V parts by laser additive manufacturing reported in [279]. In that study, the hatch distance was kept constant at 50 μm, varying both the laser power and the travel speed. The maximum calculated hatch distance for the different processing parameters is depicted in Fig. 24.

As it can be observed, typically, the maximum theoretical hatch distance is higher than the value used in [279], but this is still a good approach for a first screening to determine the hatch distance for a given set of processing parameters. Furthermore, these results suggest that in the case of Ref. [279], for some experimental conditions, the hatch distance could be increased thus increasing productivity.

Schematically, the methodology to determine the maximum theoretical hatch distance for the three proposed criteria can be schematically presented in Fig. 25.

From these three distinct criteria, it is possible to obtain a good reference for the hatch distance for a given set of power and travel speed of the heat source, despite the assumptions made, the major ones being: all the energy is transferred into the material and the heat source diameter was taken as a point. From a practical perspective, the geometric criterion is the simplest to use to determine the optimum hatch distance.

In order for other researchers to be able to use the aforementioned criteria and obtain the theoretical values of both R_m and hatch distance, an Excel file with those equations is permanently available at https://drive.google.com/drive/folders/1ZPVqNRFlxv7fYbeslL7Ppw6NlQYodSN4?usp=sharing.

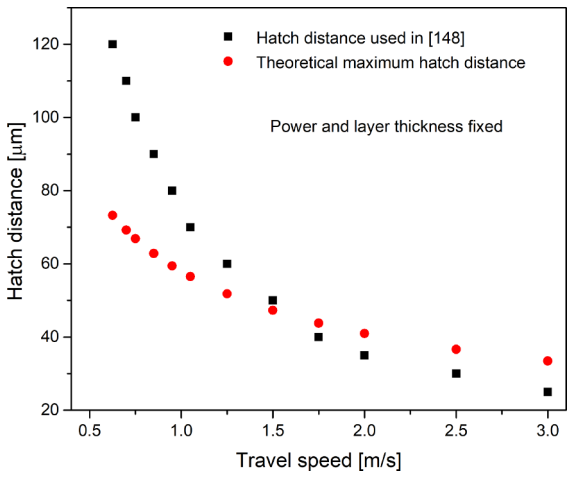

Fig. 23. Comparison between calculated hatch distance based on energetic criterion and the one used in [148] (power and layer thickness were kept constant and the velocity varied) with maximum theoretical hatch distance determined based on Eq. (22).

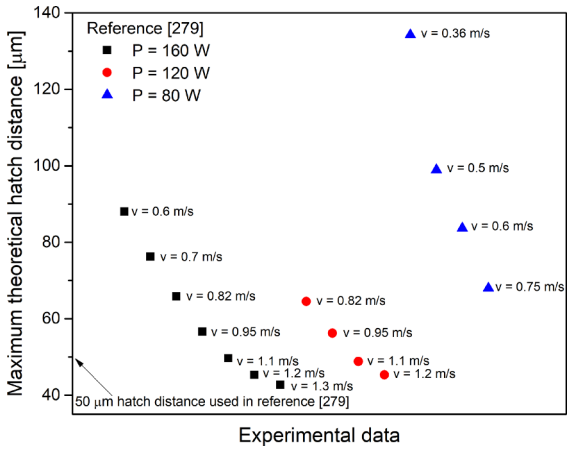

Fig. 24. Use of the thermal criterion to evaluate the hatch distance: comparison between hatch distance used in [279] (for process parameters were the layer thickness was kept constant, while the power and the travel speed were varied) with maximum theoretical hatch distance determined based on Eq. (22). The hatch distance used in all experimental conditions of [279] was of 50 μm.

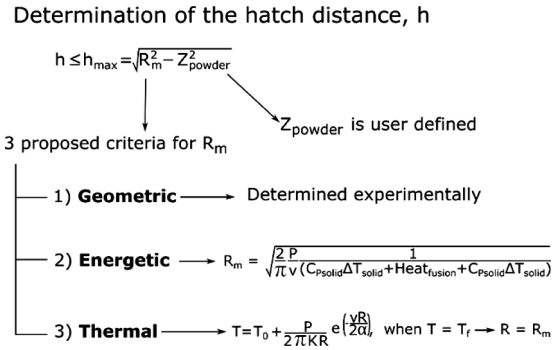

Fig. 25. Schematic representation of the methodology used to determine the maximum theoretical hatch distance for the three proposed criteria.

6. A dimensionless parameter for energy density calculations in additive manufacturing

As referred before, there is no universal equation to determine the energy input or energy density in additive manufacturing. Additionally, from the analysis previously presented, two parameters were not considered, and these were the diameter of the heat source and the powder grain size.

Thus, it is necessary to develop a more generic definition of the energy or power input during additive manufacturing that considers both the heat source diameter and the size of the powder particles or the diameter of raw wires, for powder-bed and wire fed systems, respectively. Such would greatly help to replicate experiments and could potentially benefit the additive manufacturing community so that the influence of different process parameters could be fully understood and manipulated to achieve high quality parts. In the course of their research, the authors of the current paper have noticed that several works often do not report, for example, the beam diameter used which is of paramount importance.

One potential explanation for this may be related to the fact that most research laboratories use industrial equipment, and these usually have fixed working parameters (such as beam spot size and defocusing) with no possible adjustment. This is a common procedure in industrial equipment, where the parameters to control are set to a limited range to prevent damages and reduce setup time. Therefore, it is possible to assume that the beam diameter used in those investigations is the one set by the machine manufacturer. However, for academia-related research, additive manufacturing machines have more degrees of freedom and manufacturers tend to allow that process variables can be changed when compared to close-looped machines used in industry.

The considerable number of equations used to describe the energy and/or power put into play during fusion-based additive manufacturing makes it difficult to compare different works and interpret some of the results. Therefore, it is proposed an equation for the energy density during additive manufacturing, defined as:

$$ED = \beta \frac{P}{v\ h\ d}, \tag{29}$$

where β is a dimensionless parameter defined as the ratio between the powder grain size or wire diameter (g_s) and the diameter of the heat source ($d_{HeatSource}$):

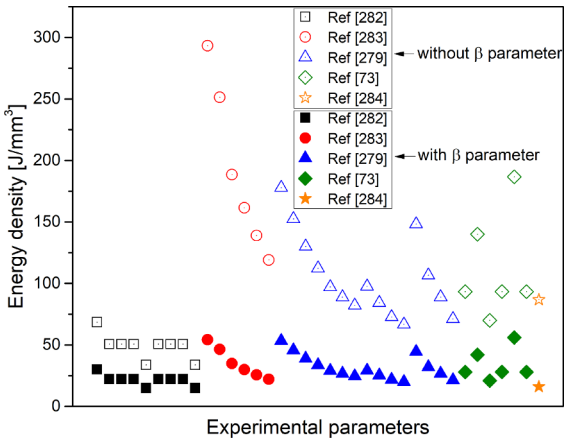

Fig. 26. Comparison of the energy density calculations with (fully colored symbols) and without (open symbols) the dimensionless β parameter, defined by the grain size to beam diameter ratio. References [73,279,282–284] were used for these calculations.

$$\beta = \frac{g_s}{d_{HeatSource}}, \tag{30}$$

With the introduction of the β parameter, it is possible to consider all the main process parameters including the beam diameter, $d_{HeatSource}$, and the average grain size of the powder, g_s, or the diameter of the wire for wire-fed systems. It must be noticed that the use of the β parameter is only valid for additive manufacturing techniques based on laser or electron beam sources, since in arc-based ones it is not possible to accurately quantify the size of the heat source.

The use of dimensionless numbers in additive manufacturing was already used in [280,281] to gain a clearer understanding on the influence of different process parameters on the quality of the produced parts and to correlate process parameters of different research groups, though it was not introduced yet in the energy density equation.

To evaluate the feasibility of using the β parameter to compare the process parameters in powder-bed additive manufacturing, it was computed the energy density values with and without the β parameter based on key reference works of additive manufacturing of Ti-6Al-4V alloy [73,279,282–284], as depicted in Fig. 26.

Note that the selected process parameters were the ones that ensured a dense part (> 99%) after the building process.

Without the use of the β parameter, the energy density to produce a given part by powder-bed laser additive manufacturing, can range from as low as 33 J/mm^3 up to 293 J/mm^3. In opposition, when the energy density calculation is performed using the dimensionless parameter β, the energy density varies in a significantly narrower range, between 20 and 54 J/mm^3. This evidences the need to introduce both the powder grain size and the heat source diameter to effectively compare works performed by different research groups in distinct experimental conditions.

7. Conclusions

This paper evidences the major similarities between fusion-based multipass arc welding and fusion-based additive manufacturing, especially in terms of thermal effects, solidification mechanisms, and chemical reactions within the melted region, as well as, distortion and residual stresses. The major concepts developed in fusion welding were described in detail and applied to different materials that are also being used in additive manufacturing.

Several techniques exist to avoid defects and improve the microstructure of the fusion and heat affected zones that can be directly transferred to both powder-bed and arc-based additive manufacturing.

A critical analysis of additive manufacturing was made in light of welding to optimize processing parameters showing the synergistic relation between both processes.

Three distinct criteria (geometric, energetic and thermal) were used to determine an optimum hatch distance for a given set of process parameters. Evaluation of these criteria was performed using actual data reported in the literature. It was observed that the theoretical values of the hatch distance correspond to an upper bound limit, which can be of assistance for researchers to tune the process parameters (power, travel speed and layer thickness) to obtain defect-free parts without compromising productivity.

However, there are other process parameters, namely the size of the heat source and the grain size of the material to be deposited, that affect the quality of additive manufacturing, besides those contained in the heat input concept. Thus, it is proposed an equation to compute the energy density (ED), or in-volume heat input, that takes into consideration the main process parameters: power (P), travel speed (v), layer thickness (d), hatch distance (h), powder grain size (g_s) and heat source diameter ($d_{HeatSource}$). This equation is defined by:

$$ED = \beta \frac{P}{v\ h\ d}$$

where β is a dimensionless parameter, defined as: $\beta = \frac{g_s}{d_{HeatSource}}$

This allows to compare the energy density used with different equipment and experimental conditions taking in consideration the main process parameters. It was verified that the energy density to obtain defect-free parts by additive manufacturing has significant less scattering, when compared to the same equation without considering the dimensionless parameter β.

8. Future outlook

Ongoing research on additive manufacturing is too much focused on controlling deposition strategies using internet of things and computer-based tools regardless of materials. This is an important field to assess the economic and social aspects of the technology. However, materials and their properties cannot be disregarded as they are the ones determining the performance of manufactured components.

Thus, refocusing on the technology, other areas still need to be addressed:

(1) Thermal analysis combining material thermo-physical properties (e.g. thermal expansion coefficient) and deposition strategies to minimize defects and distortions. Existing work on multipass welding by electric arc and laser welding could be a starting point to further develop and shorten the time needed to industrialize apply additive manufacturing.
(2) Microstructural and mechanical properties of parts closely follow the solidification evolution observed in fusion welding for a wide diversity of materials, including non-ferrous alloys.
(3) Existing knowledge on arc welding technology can be directly incorporated into wire and arc additive manufacturing, namely: heat source manipulation; operating processes, including shielding gases effect; chemical corrections of the molten pool.
(4) Welding metallurgy is, nowadays, a well-established research field where the effect of heat input on cooling rates can be quantified and modified to prevent detrimental effects, such as porosity or formation of precipitation. This knowledge can be directly incorporated into additive manufacturing techniques were fusion occurs.
(5) Other areas not target by this paper but already identified concern the study of impact loading and fatigue resistance of additively manufactured parts.
(6) Finally, the potential of using distinct powder material combinations to produce functional graded parts for high value applications is also a challenge.

Acknowledgements

The authors acknowledge Fundação para a Ciência e Tecnologia (FCT) for its financial support through the project UID/EMS/00667/2019, Fundo Regional para a Ciência e Tecnologia and Projeto de I&DT for companies in copromotion SLM-XL, (Ref 3346), funded by Fundo Europeu de Desenvolvimento Regional (FEDER) through Programa Operacional Regional de Lisboa. The authors acknowledge Dr. Bey Vrancken from Lawrence Livermore National Laboratory and Professor Haijun Gong from Georgia Southern University for providing some of the experimental data used in this work. Helpful discussions with Dr. Julian Escobar and Dr. Camilo Salvador from University of Campinas are gratefully acknowledged.

References

[1] DebRoy T, Wei HLL, Zuback JSS, Mukherjee T, Elmer JWW, Milewski JOO, et al. Additive manufacturing of metallic components – process, structure and properties. Prog Mater Sci 2018;92:112–224. https://doi.org/10.1016/j.pmatsci.2017.10.001.
[2] Bandyopadhyay A, Heer B. Additive manufacturing of multi-material structures. Mater Sci Eng R Reports 2018;129:1–16. https://doi.org/10.1016/j.mser.2018.04.001.
[3] MacDonald E, Wicker R. Multiprocess 3D printing for increasing component functionality. Science (80-) 2016;353. https://doi.org/10.1126/science.aaf2093. aaf2093–aaf2093.
[4] Williams SW, Martina F, Addison AC, Ding J, Pardal G, Colegrove P. Wire + arc additive manufacturing. Mater Sci Technol 2016;32:641–7. https://doi.org/10.1179/1743284715Y.0000000073.
[5] Kirka MM, Nandwana P, Lee Y, Dehoff RR. Solidification and solid-state transformation sciences in metals additive manufacturing. Scr Mater 2017;135:130–4. https://doi.org/10.1016/j.scriptamat.2017.01.005.
[6] Mukherjee T, Manvatkar V, De A, DebRoy T. Mitigation of thermal distortion during additive manufacturing. Scr Mater 2017;127:79–83. https://doi.org/10.1016/j.scriptamat.2016.09.001.
[7] Maekawa A, Serizawa H, Murakawa H. Fast computation based on an iterative substructure method for three-dimensional simulation of multipass welding. J Press Vessel Technol 2015;137:041410. https://doi.org/10.1115/1.4029189.
[8] Murugan S, Rai SK, Kumar P, Jayakumar T, Raj B, Bose MS. Temperature distribution and residual stresses due to multipass welding in type 304 stainless steel and low carbon steel weld pads. Int J Press Vessel Pip 2001;78:307–17. https://doi.org/10.1016/S0308-0161(01)00047-3.
[9] Manurung YHP, Ngendang R, Rahim MR, Zakaria MY, Redza MR, Sulaiman MS, et al. Welding distortion analysis of multipass joint combination with different sequences using 3D FEM and experiment. Int J Press Vessel Pip 2013;111–112:89–98. https://doi.org/10.1016/j.ijpvp.2013.05.002.
[10] Duranton P, Devaux J, Robin V, Gilles P, Bergheau JM. 3D modelling of multipass welding of a 316L stainless steel pipe. J Mater Process Technol 2004;153–154:457–63. https://doi.org/10.1016/j.jmatprotec.2004.04.128.
[11] Sridharan N, Cakmak E, List FA, Ucar H, Constantinides S, Babu SS, et al. Rationalization of solidification mechanism of Nd–Fe–B magnets during laser directed-energy deposition. J Mater Sci 2018;53:8619–26. https://doi.org/10.1007/s10853-018-2178-7.
[12] Kenel C, Grolimund D, Li X, Panepucci E, Samson VA, Sanchez DF, et al. In situ investigation of phase transformations in Ti-6Al-4V under additive manufacturing conditions combining laser melting and high-speed micro-X-ray diffraction. Sci Rep 2017;7:16358. https://doi.org/10.1038/s41598-017-16760-0.
[13] Martin JH, Yahata BD, Hundley JM, Mayer JA, Schaedler TA, Pollock TM. 3D printing of high-strength aluminium alloys. Nature 2017;549:365–9. https://doi.org/10.1038/nature23894.
[14] Kutz M. Mechanical engineers' handbook. 3rd ed. Hoboken: John Wiley & Sons Inc; 2014https://doi.org/10.1002/9781118985960.
[15] Meredith R. Welding Torch. US2274631A; 1942.

[16] Yan J, Gao M, Zeng X. Study on microstructure and mechanical properties of 304 stainless steel joints by TIG, laser and laser-TIG hybrid welding. Opt Lasers Eng 2010;48:512–7. https://doi.org/10.1016/j.optlaseng.2009.08.009.
[17] Oliveira JP, Barbosa D, Fernandes FMB, Miranda RM. Tungsten inert gas (TIG) welding of Ni-rich NiTi plates: functional behavior. Smart Mater Struct 2016;25:03LT01. https://doi.org/10.1088/0964-1726/25/3/03LT01.
[18] Gao X-L, Zhang L-J, Liu J, Zhang J-X. A comparative study of pulsed Nd:YAG laser welding and TIG welding of thin Ti6Al4V titanium alloy plate. Mater Sci Eng A 2013;559:14–21. https://doi.org/10.1016/j.msea.2012.06.016.
[19] Kumar A, Sundarrajan S. Optimization of pulsed TIG welding process parameters on mechanical properties of AA 5456 Aluminum alloy weldments. Mater Des 2009;30:1288–97. https://doi.org/10.1016/j.matdes.2008.06.055.
[20] Iordachescu D, Quintino L, Miranda R, Pimenta G. Influence of shielding gases and process parameters on metal transfer and bead shape in MIG brazed joints of the thin zinc coated steel plates. Mater Des 2006;27:381–90. https://doi.org/10.1016/j.matdes.2004.11.010.
[21] Quintino L, Pimenta G, Iordachescu D, Miranda RM, Pépe NV. MIG brazing of galvanized thin sheet joints for automotive industry. Mater Manuf Process 2006;21:63–73. https://doi.org/10.1081/AMP-200060621.
[22] Kah P, Latifi H, Suoranta R, Martikainen J, Pirinen M. Usability of arc types in industrial welding. Int J Mech Mater Eng 2014;9:1–12. https://doi.org/10.1186/s40712-014-0015-6.
[23] Selvi S, Vishvaksenan A, Rajasekar E. Cold metal transfer (CMT) technology – an overview. Def Technol 2018;14:28–44. https://doi.org/10.1016/j.dt.2017.08.002.
[24] Akman E, Demir A, Canel T, Sinmazçelik T. Laser welding of Ti6Al4V titanium alloys. J Mater Process Technol 2009;209:3705–13. https://doi.org/10.1016/j.jmatprotec.2008.08.026.
[25] Steen WM, Mazumder J. Laser material processing. London: Springer London; 2010https://doi.org/10.1007/978-1-84996-062-5.
[26] Oliveira JP, Fernandes FMB, Miranda RM, Schell N, Ocaña JL. Residual stress analysis in laser welded NiTi sheets using synchrotron X-ray diffraction. Mater. Des. 2016;100:180–7. https://doi.org/10.1016/j.matdes.2016.03.137.
[27] Torkamany MJ, Malek Ghaini F, Poursalehi R, Ghaini FM, Poursalehi R. Dissimilar pulsed Nd : YAG laser welding of pure niobium to Ti–6Al–4V. J Mater 2014;53:915–20. https://doi.org/10.1016/j.matdes.2013.07.094.
[28] Zeng Z, Panton B, Oliveira JP, Han A, Zhou YN. Dissimilar laser welding of NiTi shape memory alloy and copper. Smart Mater Struct 2015;24:125036. https://doi.org/10.1088/0964-1726/24/12/125036.
[29] Oliveira JP, Panton B, Zeng Z, Andrei CM, Zhou Y, Miranda RM, et al. Laser joining of NiTi to Ti6Al4V using a Niobium interlayer. Acta Mater 2016;105:9–15. https://doi.org/10.1016/j.actamat.2015.12.021.
[30] Franchini F, Pierantozzi P. Electron beam welding of dissimilar materials: niobium-base alloy C-103 with titanium-base alloy Ti-6AI-4V ELI. Weld Int 1992;6:792–7. https://doi.org/10.1080/09507119209548287.
[31] Zeng Z, Yang M, Oliveira JP, Song D, Peng B. Laser welding of NiTi shape memory alloy wires and tubes for multi-functional design applications. Smart Mater Struct 2016;25:085001. https://doi.org/10.1088/0964-1726/25/8/085001.
[32] Zeng Z, Oliveira JP, Yang M, Song D, Peng B. Functional fatigue behavior of NiTi-Cu dissimilar laser welds. Mater Des 2017;114:282–7. https://doi.org/10.1016/j.matdes.2016.11.023.
[33] Magnabosco I, Ferro P, Bonollo F, Arnberg L. An investigation of fusion zone microstructures in electron beam welding of copper-stainless steel. Mater Sci Eng A 2006;424:163–73. https://doi.org/10.1016/j.msea.2006.03.096.
[34] Sun Z, Karppi R. The application of electron beam welding for the joining of dissimilar metals: an overiew. J Mater Process Technol 1996;59:257–67. https://doi.org/10.1016/0924-0136(95)02150-7.
[35] Cao X, Jahazi M, Immarigeon JPP, Wallace W. A review of laser welding techniques for magnesium alloys; 2006. https://doi.org/10.1016/j.jmatprotec.2005.06.068.
[36] Oliveira JP, Miranda RM, Braz Fernandes FM. Welding and joining of NiTi shape memory alloys: a review. Prog Mater Sci 2017;88:412–66. https://doi.org/10.1016/j.pmatsci.2017.04.008.
[37] Yunlian Q, Ju D, Quan H, Liying Z. Electron beam welding, laser beam welding and gas tungsten arc welding of titanium sheet. Mater Sci Eng A 2000;280:177–81. https://doi.org/10.1016/S0921-5093(99)00662-0.
[38] Wang T, Zhang BG, Chen GQ, Feng JC, Tang Q. Electron beam welding of Ti-15-3 titanium alloy to 304 stainless steel with copper interlayer sheet. Trans Nonferrous Met Soc China (English Ed) 2010;20:1829–34. https://doi.org/10.1016/S1003-6326(09)60381-2.
[39] Oliveira JP, Zeng Z, Berveiller S, Bouscaud D, Braz Fernandes FM, Miranda RM, et al. Laser welding of Cu-Al-Be shape memory alloys: microstructure and mechanical properties. Mater Des 2018;148:145–52. https://doi.org/10.1016/j.matdes.2018.03.066.
[40] Chen S, Li L, Chen Y, Huang J. Joining mechanism of Ti/Al dissimilar alloys during laser welding-brazing process. J Alloys Compd 2011;509:891–8. https://doi.org/10.1016/j.jallcom.2010.09.125.
[41] Hu Y, He X, Yu G, Ge Z, Zheng C, Ning W. Heat and mass transfer in laser dissimilar welding of stainless steel and nickel. Appl Surf Sci 2012;258:5914–22. https://doi.org/10.1016/j.apsusc.2012.02.143.
[42] Oliveira JP, Zeng Z, Andrei C, Braz Fernandes FM, Miranda RM, Ramirez AJ, et al. Dissimilar laser welding of superelastic NiTi and CuAlMn shape memory alloys. Mater Des 2017;128:166–75. https://doi.org/10.1016/j.matdes.2017.05.011.
[43] Li X, Xie J, Zhou Y. Effects of oxygen contamination in the argon shielding gas in laser welding of commercially pure titanium thin sheet. J Mater Sci 2005;40:3437–43. https://doi.org/10.1007/s10853-005-0447-8.
[44] Quintino L, Miranda RM, Williams S, Kong CJ. Gas shielding in fibre laser welding of high strength pipeline steel. Sci Technol Weld Join 2011;16:399–404. https://doi.org/10.1179/1362171810Y.0000000002.
[45] Wei HL, Elmer JW, DebRoy T. Crystal growth during keyhole mode laser welding. Acta Mater 2017;133:10–20. https://doi.org/10.1016/j.actamat.2017.04.074.
[46] Sibillano T, Ancona A, Berardi V, Schingaro E, Basile G, Lugarà PM. Optical detection of conduction/keyhole mode transition in laser welding. J Mater Process Technol 2007;191:364–7. https://doi.org/10.1016/j.jmatprotec.2007.03.075.
[47] Oliveira JP, Miranda RM, Schell N, Braz Fernandes FM. High strain and long duration cycling behavior of laser welded NiTi sheets. Int J Fatigue 2016;83:195–200. https://doi.org/10.1016/j.ijfatigue.2015.10.013.
[48] Dumovic M, Dunne D, Norrish J, Li H, Monaghan BJ. Effect of cooling rate on microstructural evolution and hardness of self-shielded arc weld deposits containing 1 wt% aluminium. Weld World 2018. https://doi.org/10.1007/s40194-018-0568-8.
[49] Barrick EJ, Jain D, DuPont JN, Seidman DN. Effects of heating and cooling rates on phase transformations in 10 Wt Pct Ni steel and their application to gas tungsten arc welding. Metall Mater Trans A 2017;48:5890–910. https://doi.org/10.1007/s11661-017-4379-0.
[50] Vannod J, Bornert M, Bidaux J-E, Bataillard L, Karimi A, Drezet J-M, et al. Mechanical and microstructural integrity of nickel–titanium and stainless steel laser joined wires. Acta Mater 2011;59:6538–46. https://doi.org/10.1016/j.actamat.2011.06.031.
[51] Lee WB, Bang KS, Jung SB. Effects of intermetallic compound on the electrical and mechanical properties of friction welded Cu/Al bimetallic joints during annealing. J Alloys Compd 2005;390:212–9. https://doi.org/10.1016/j.jallcom.2004.07.057.
[52] Unfried-Silgado J, Ramirez AJ. Modeling and characterization of as-welded microstructure of solid solution strengthened Ni-Cr-Fe alloys resistant to ductility-dip cracking Part II: Microstructure characterization. Met Mater Int 2014;20:307–15. https://doi.org/10.1007/s12540-014-1022-0.
[53] Chatterjee S, Abinandanan TA, Chattopadhyay K. Phase formation in Ti/Ni dissimilar welds. Mater Sci Eng A 2008;490:7–15. https://doi.org/10.1016/j.msea.2007.12.041.
[54] Cui L, Li X, He D, Chen L, Gong S. Effect of Nd:YAG laser welding on microstructure and hardness of an Al-Li based alloy. Mater Charact 2012;71:95–102. https://doi.org/10.1016/j.matchar.2012.06.011.
[55] Elangovan K, Balasubramanian V. Influences of post-weld heat treatment on tensile properties of friction stir-welded AA6061 aluminum alloy joints. Mater Charact 2008;59:1168–77. https://doi.org/10.1016/j.matchar.2007.09.006.

[56] Xiao L, Liu L, Zhou Y, Esmaeili S. Resistance-spot-welded AZ31 magnesium alloys: Part I. Dependence of fusion zone microstructures on second-phase particles. Metall Mater Trans A Phys Metall Mater Sci 2010;41:1511–22. https://doi.org/10.1007/s11661-010-0197-3.
[57] Oliveira JP, Braz Fernandes FM, Miranda RM, Schell N, Ocaña JL. Effect of laser welding parameters on the austenite and martensite phase fractions of NiTi. Mater Charact 2016;119:148–51. https://doi.org/10.1016/j.matchar.2016.08.001.
[58] Oliveira JP, Fernandes FMB, Schell N, Miranda RM. Martensite stabilization during superelastic cycling of laser welded NiTi plates. Mater Lett 2016;171:273–6. https://doi.org/10.1016/j.matlet.2016.02.107.
[59] Song X, Xie M, Hofmann F, Jun TS, Connolley T, Reinhard C, et al. Residual stresses in Linear Friction Welding of aluminium alloys. Mater Des 2013;50:360–9. https://doi.org/10.1016/j.matdes.2013.03.051.
[60] Garzón CM, Ramirez AJ. Growth kinetics of secondary austenite in the welding microstructure of a UNS S32304 duplex stainless steel. Acta Mater 2006;54:3321–31. https://doi.org/10.1016/j.actamat.2006.03.018.
[61] Kou S. Welding metallurgy. 2nd ed. Hoboken: John Wiley & Sons Inc; 2002https://doi.org/10.1002/0471434027.
[62] Benyounis KY, Olabi AG, Hashmi MSJ. Effect of laser welding parameters on the heat input and weld-bead profile. J Mater Process Technol 2005;164–165:978–85. https://doi.org/10.1016/j.jmatprotec.2005.02.060.
[63] DuPont JN, Marder A. Thermal efficiency of arc welding processes. Weld J 1995;74:406–16.
[64] Deng D, Murakawa H. Numerical simulation of temperature field and residual stress in multi-pass welds in stainless steel pipe and comparison with experimental measurements. Comput Mater Sci 2006;37:269–77. https://doi.org/10.1016/j.commatsci.2005.07.007.
[65] Javadi Y, Ashoori M. Sub-surface stress measurement of cross welds in a dissimilar welded pressure vessel. Mater Des 2015;85:82–90. https://doi.org/10.1016/j.matdes.2015.07.012.
[66] Smith DJ, Bouchard PJ, George D. Measurement and prediction of residual stresses in thick-section steel welds. J Strain Anal Eng Des 2000;35:287–305. https://doi.org/10.1243/0309324001514422.
[67] Murugan S, Kumar PV, Raj B, Bose MSC. Temperature distribution during multipass welding of plates. Int J Press Vessel Pip 1998;75:891–905. https://doi.org/10.1016/S0308-0161(98)00094-5.
[68] Liu W, Lu F, Wei Y, Ding Y, Wang P, Tang X. Special zone in multi-layer and multi-pass welded metal and its role in the creep behavior of 9Cr 1Mo welded joint. Mater Des 2016;108:195–206. https://doi.org/10.1016/j.matdes.2016.06.102.
[69] Wong KV, Hernandez A. A review of additive manufacturing. ISRN Mech Eng 2012;2012:1–10. https://doi.org/10.5402/2012/208760.
[70] Miranda RM, Lopes G, Quintino L, Rodrigues JP, Williams S. Rapid prototyping with high power fiber lasers. Mater Des 2008;29:2072–5. https://doi.org/10.1016/j.matdes.2008.03.030.
[71] Islam M, Purtonen T, Piili H, Salminen A, Nyrhilä O. Temperature profile and imaging analysis of laser additive manufacturing of stainless steel. Phy. Proc 2013;41:835–42. https://doi.org/10.1016/j.phpro.2013.03.156.
[72] Matilainen V, Piili H, Salminen A, Syvänen T, Nyrhilä O. Characterization of process efficiency improvement in laser additive manufacturing. Phys Proc 2014;56:317–26. https://doi.org/10.1016/j.phpro.2014.08.177.
[73] Thijs L, Verhaeghe F, Craeghs T, Van Humbeeck J, Kruth JP. A study of the microstructural evolution during selective laser melting of Ti-6Al-4V. Acta Mater 2010;58:3303–12. https://doi.org/10.1016/j.actamat.2010.02.004.
[74] Enneti RK, Morgan R, Atre SV. Effect of process parameters on the Selective Laser Melting (SLM) of tungsten. Int J Refract Met Hard Mater 2018;71:315–9. https://doi.org/10.1016/j.ijrmhm.2017.11.035.
[75] Haberland C, Elahinia M, Walker JM, Meier H, Frenzel J. On the development of high quality NiTi shape memory and pseudoelastic parts by additive manufacturing. Smart Mater Struct 2014;23:104002. https://doi.org/10.1088/0964-1726/23/10/104002.
[76] Wang Z, Palmer TA, Beese AM. Effect of processing parameters on microstructure and tensile properties of austenitic stainless steel 304L made by directed energy deposition additive manufacturing. Acta Mater 2016;110:226–35. https://doi.org/10.1016/j.actamat.2016.03.019.
[77] Mukherjee T, Zhang W, DebRoy T. An improved prediction of residual stresses and distortion in additive manufacturing. Comput Mater Sci 2017;126:360–72. https://doi.org/10.1016/j.commatsci.2016.10.003.
[78] Wang Z, Denlinger E, Michaleris P, Stoica AD, Ma D, Beese AM. Residual stress mapping in Inconel 625 fabricated through additive manufacturing: method for neutron diffraction measurements to validate thermomechanical model predictions. Mater Des 2017;113:169–77. https://doi.org/10.1016/j.matdes.2016.10.003.
[79] Beese AM, Carroll BE. Review of mechanical properties of Ti-6Al-4V made by laser-based additive manufacturing using powder feedstock. JOM 2016;68:724–34. https://doi.org/10.1007/s11837-015-1759-z.
[80] Bobbio LD, Qin S, Dunbar A, Michaleris P, Beese AM. Characterization of the strength of support structures used in powder bed fusion additive manufacturing of Ti-6Al-4V. Addit Manuf 2017;14:60–8. https://doi.org/10.1016/j.addma.2017.01.002.
[81] Farshidianfar MH, Khajepour A, Gerlich AP. Effect of real-time cooling rate on microstructure in Laser Additive Manufacturing. J Mater Process Technol 2016;231:468–78. https://doi.org/10.1016/j.jmatprotec.2016.01.017.
[82] Repossini G, Laguzza V, Grasso M, Colosimo BM. On the use of spatter signature for in-situ monitoring of Laser Powder Bed Fusion. Addit Manuf 2017;16:35–48. https://doi.org/10.1016/j.addma.2017.05.004.
[83] Roehling TT, Wu SSQ, Khairallah SA, Roehling JD, Soezeri SS, Crumb MF, et al. Modulating laser intensity profile ellipticity for microstructural control during metal additive manufacturing. Acta Mater 2017;128:197–206. https://doi.org/10.1016/j.actamat.2017.02.025.
[84] Montecinos S, Cuniberti A. Martensitic transformation and grain size in a Cu-Al-Be alloy. Proc Mater Sci 2012;1:149–55. https://doi.org/10.1016/j.mspro.2012.06.020.
[85] Liu WH, Wu Y, He JY, Nieh TG, Lu ZP. Grain growth and the Hall-Petch relationship in a high-entropy FeCrNiCoMn alloy. Scr Mater 2013;68:526–9. https://doi.org/10.1016/j.scriptamat.2012.12.002.
[86] Taha AS, Hammad FH. Application of the Hall-Petch relation to microhardness measurements on Al, Cu, Al-MD 105, and Al-Cu Alloys. Phys Status Solidi 1990;119:455–62. https://doi.org/10.1002/pssa.2211190207.
[87] Oliveira JP, Zeng Z, Omori T, Zhou N, Miranda RM, Fernandes FMB. Improvement of damping properties in laser processed superelastic Cu-Al-Mn shape memory alloys. Mater Des 2016;98:280–4. https://doi.org/10.1016/j.matdes.2016.03.032.
[88] Oliveira JP, Panton B, Zeng Z, Omori T, Zhou Y, Miranda RM, et al. Laser welded superelastic Cu–Al–Mn shape memory alloy wires. Mater Des 2016;90:122–8. https://doi.org/10.1016/j.matdes.2015.10.125.
[89] Sutou Y, Omori T, Kainuma R, Ishida K. Grain size dependence of pseudoelasticity in polycrystalline Cu-Al-Mn-based shape memory sheets. Acta Mater 2013;61:3842–50. https://doi.org/10.1016/j.actamat.2013.03.022.
[90] Carroll BE, Otis RA, Borgonia JP, Suh JO, Dillon RP, Shapiro AA, et al. Functionally graded material of 304L stainless steel and inconel 625 fabricated by directed energy deposition: characterization and thermodynamic modeling. Acta Mater 2016;108:46–54. https://doi.org/10.1016/j.actamat.2016.02.019.
[91] Tammas-Williams S, Todd I. Design for additive manufacturing with site-specific properties in metals and alloys. Scr Mater 2017;135:105–10. https://doi.org/10.1016/j.scriptamat.2016.10.030.
[92] Bobbio LD, Bocklund B, Otis R, Borgonia JP, Dillon RP, Shapiro AA, et al. Characterization of a functionally graded material of Ti-6Al-4V to 304L stainless steel with an intermediate V section. J Alloys Compd 2018. https://doi.org/10.1016/j.jallcom.2018.01.156.
[93] DuPont JN. Microstructural evolution and high temperature failure of ferritic to austenitic dissimilar welds. Int Mater Rev 2012;57:208–34. https://doi.org/10.1179/1743280412Y.0000000006.
[94] Ng CH, Mok ESH, Man HC. Effect of Ta interlayer on laser welding of NiTi to AISI 316L stainless steel. J Mater Process Technol 2015;226:69–77. https://doi.org/10.1016/j.jmatprotec.2015.06.039.
[95] Miranda RM, Assunção E, Silva RJC, Oliveira JP, Quintino L. Fiber laser welding of NiTi to Ti-6Al-4V. Int J Adv Manuf Technol 2015;81:1533–8. https://doi.org/10.1007/s00170-015-7307-8.
[96] Bobbio LD, Otis RA, Borgonia JP, Dillon RP, Shapiro AA, Liu ZK, et al. Additive manufacturing of a functionally graded material from Ti-6Al-4V to Invar:

experimental characterization and thermodynamic calculations. Acta Mater 2017;127:133–42. https://doi.org/10.1016/j.actamat.2016.12.070.
[97] Niendorf T, Leuders S, Riemer A, Brenne F, Tröster T, Richard HA, et al. Functionally graded alloys obtained by additive manufacturing. Adv Eng Mater 2014;16:857–61. https://doi.org/10.1002/adem.201300579.
[98] Raghavan N, Dehoff R, Pannala S, Simunovic S, Kirka M, Turner J, et al. Numerical modeling of heat-transfer and the influence of process parameters on tailoring the grain morphology of IN718 in electron beam additive manufacturing. Acta Mater 2016;112:303–14. https://doi.org/10.1016/j.actamat.2016.03.063.
[99] Raghavan N, Simunovic S, Dehoff R, Plotkowski A, Turner J, Kirka M, et al. Localized melt-scan strategy for site specific control of grain size and primary dendrite arm spacing in electron beam additive manufacturing. Acta Mater 2017;140:375–87. https://doi.org/10.1016/j.actamat.2017.08.038.
[100] Parthasarathy J, Starly B, Raman S. A design for the additive manufacture of functionally graded porous structures with tailored mechanical properties for biomedical applications. J Manuf Process 2011;13:160–70. https://doi.org/10.1016/j.jmapro.2011.01.004.
[101] Pyka G, Burakowski A, Kerckhofs G, Moesen M, Van Bael S, Schrooten J, et al. Surface modification of Ti6Al4V open porous structures produced by additive manufacturing. Adv Eng Mater 2012;14:363–70. https://doi.org/10.1002/adem.201100344.
[102] Slotwinski JA, Garboczi EJ, Hebenstreit KM. Porosity measurements and analysis for metal additive manufacturing process control. J Res Natl Inst Stand Technol 2014;119:494. https://doi.org/10.6028/jres.119.019.
[103] Gong X, Anderson T, Chou K. Review on powder-based electron beam additive manufacturing technology. In: ASME/ISCIE 2012 Int. Symp. Flex. Autom.; 2012. p. 507. https://doi.org/10.1115/ISFA2012-7256.
[104] Campbell I, Bourell D, Gibson I. Additive manufacturing: rapid prototyping comes of age. Rapid Prototyp J 2012;18:255–8. https://doi.org/10.1108/13552541211231563.
[105] Dutta B, Froes FH (Sam). The Additive Manufacturing (AM) of titanium alloys. Met Powder Rep 2017;72:96–106. https://doi.org/10.1016/j.mprp.2016.12.062.
[106] Matsunawa A, Seto N, Kim J, Mizutani M, Katayama S. Dynamics of keyhole and molten pool in high-power CO2 laser welding. In: Chen X, Fujioka T, Matsunawa A, editors. Library (Lond); 2000. p. 34. https://doi.org/10.1117/12.377006.
[107] Oliveira JP, Cavaleiro AJ, Schell N, Stark A, Miranda RM, Ocana JL, et al. Effects of laser processing on the transformation characteristics of NiTi: a contribute to additive manufacturing. Scr Mater 2018;152:122–6. https://doi.org/10.1016/j.scriptamat.2018.04.024.
[108] Zäh MF, Lutzmann S. Modelling and simulation of electron beam melting. Prod Eng 2010;4:15–23. https://doi.org/10.1007/s11740-009-0197-6.
[109] Vastola G, Zhang G, Pei QXX, Zhang Y-WW. Controlling of residual stress in additive manufacturing of Ti6Al4V by finite element modeling. Addit Manuf 2016;12:231–9. https://doi.org/10.1016/j.addma.2016.05.010.
[110] Wang Z, Stoica AD, Ma D, Beese AM. Stress relaxation in a nickel-base superalloy at elevated temperatures with in situ neutron diffraction characterization: application to additive manufacturing. Mater Sci Eng A 2018;714:75–83. https://doi.org/10.1016/j.msea.2017.12.058.
[111] Harrison NJ, Todd I, Mumtaz K. Reduction of micro-cracking in nickel superalloys processed by Selective Laser Melting: a fundamental alloy design approach. Acta Mater 2015;94:59–68. https://doi.org/10.1016/j.actamat.2015.04.035.
[112] Carter LN, Martin C, Withers PJ, Attallah MM. The influence of the laser scan strategy on grain structure and cracking behaviour in SLM powder-bed fabricated nickel superalloy. J Alloys Compd 2014;615:338–47. https://doi.org/10.1016/j.jallcom.2014.06.172.
[113] Catchpole-Smith S, Aboulkhair N, Parry L, Tuck C, Ashcroft IA, Clare A. Fractal scan strategies for selective laser melting of 'unweldable' nickel superalloys. Addit Manuf 2017;15:113–22. https://doi.org/10.1016/j.addma.2017.02.002.
[114] Cloots M, Uggowitzer PJ, Wegener K. Investigations on the microstructure and crack formation of IN738LC samples processed by selective laser melting using Gaussian and doughnut profiles. Mater Des 2016;89:770–84. https://doi.org/10.1016/j.matdes.2015.10.027.
[115] Chauvet E, Kontis P, Jägle EA, Gault B, Raabe D, Tassin C, et al. Hot cracking mechanism affecting a non-weldable Ni-based superalloy produced by selective electron Beam Melting. Acta Mater 2018;142:82–94. https://doi.org/10.1016/j.actamat.2017.09.047.
[116] Everton SK, Hirsch M, Stravroulakis P, Leach RK, Clare AT. Review of in-situ process monitoring and in-situ metrology for metal additive manufacturing. Mater Des 2016;95:431–45. https://doi.org/10.1016/j.matdes.2016.01.099.
[117] Lopez A, Bacelar R, Pires I, Santos TG, Sousa JP, Quintino L. Non-destructive testing application of radiography and ultrasound for wire and arc additive manufacturing. Addit Manuf 2018;21:298–306. https://doi.org/10.1016/j.addma.2018.03.020.
[118] Hirsch M, Patel R, Li W, Guan G, Leach RK, Sharples SD, et al. Assessing the capability of in-situ nondestructive analysis during layer based additive manufacture. Addit Manuf 2017;13:135–42. https://doi.org/10.1016/j.addma.2016.10.004.
[119] Santos TG, VilaCca P, Quintino L, Dos Santos J, Miranda RM. Application of Eddy current techniques to inspect friction spot welds in aluminium alloy Aa2024 and a composite material. Weld World 2011;55:12–8. https://doi.org/10.1007/BF03321315.
[120] Santos TG, Vilaça P, Miranda RM. Electrical conductivity field analysis for evaluation of FSW joints in AA6013 and AA7075 alloys. J Mater Process Technol 2011;211:174–80. https://doi.org/10.1016/j.jmatprotec.2010.08.030.
[121] Muthupandi V, Bala Srinivasan P, Seshadri SK, Sundaresan S. Effect of weld metal chemistry and heat input on the structure and properties of duplex stainless steel welds. Mater Sci Eng A 2003;358:9–16. https://doi.org/10.1016/S0921-5093(03)00077-7.
[122] Yuan T, Luo Z, Kou S. Mechanism of grain refining in AZ91 Mg welds by arc oscillation. Sci Technol Weld Join 2017;22:97–103. https://doi.org/10.1080/13621718.2016.1199127.
[123] Zong R, Chen J, Wu C, Padhy GK. Influence of shielding gas on undercutting formation in gas metal arc welding. J Mater Process Technol 2016;234:169–76. https://doi.org/10.1016/j.jmatprotec.2016.03.020.
[124] Rao SRK, Reddy GM, Kamaraj M, Rao KP. Grain refinement through arc manipulation techniques in Al-Cu alloy GTA welds. Mater Sci Eng A 2005;404:227–34. https://doi.org/10.1016/j.msea.2005.05.080.
[125] Kou S, Le Y. Grain structure and solidification cracking in oscillated arc welds of 5052 aluminum alloy. Metall Trans A 1985;16:1345–52. https://doi.org/10.1007/BF02670338.
[126] Villaret V, Deschaux-Beaume F, Bordreuil C. A solidification model for the columnar to equiaxed transition in welding of a Cr-Mo ferritic stainless steel with Ti as inoculant. J Mater Process Technol 2016;233:115–24. https://doi.org/10.1016/j.jmatprotec.2016.02.017.
[127] Torbati AM, Miranda RM, Quintino L, Williams S, Yapp D. Optimization procedures for GMAW of bimetal pipes. J Mater Process Technol 2011;211:1112–6. https://doi.org/10.1016/j.jmatprotec.2011.01.013.
[128] Yao Q, Luo Z, Li Y, Yan FY, Duan R. Effect of electromagnetic stirring on the microstructures and mechanical properties of magnesium alloy resistance spot weld. Mater Des 2014;63:200–7. https://doi.org/10.1016/j.matdes.2014.06.004.
[129] Li Y, Zhang Y, Bi J, Luo Z. Impact of electromagnetic stirring upon weld quality of Al/Ti dissimilar materials resistance spot welding. Mater Des 2015;83:577–86. https://doi.org/10.1016/j.matdes.2015.06.042.
[130] Dai W-LL. Effects of high-intensity ultrasonic-wave emission on the weldability of aluminum alloy 7075–T6. Mater Lett 2003;57:2447–54. https://doi.org/10.1016/S0167-577X(02)01262-4.
[131] Dos Santos EBF, Pistor R, Gerlich AP. High frequency pulsed gas metal arc welding (GMAW-P): the metal beam process. Manuf Lett 2017;11:1–4. https://doi.org/10.1016/j.mfglet.2017.01.001.
[132] Praveen P, Yarlagadda PKDV, Kang MJ. Advancements in pulse gas metal arc welding. J Mater Process Technol 2005;164–165:1113–9. https://doi.org/10.1016/j.jmatprotec.2005.02.100.
[133] Krampit AK. Welding with double modulation of the main welding parameters. Weld Int 2012;26:867–9. https://doi.org/10.1080/09507116.2011.653171.
[134] Sundaresan S, Janaki Ram GD, Madhusudhan Reddy G. Microstructural refinement of weld fusion zones in α–β titanium alloys using pulsed current welding. Mater Sci Eng A 1999;262:88–100. https://doi.org/10.1016/S0921-5093(98)01010-7.
[135] Alipooramirabad H, Ghomashchi R, Paradowska A, Reid M. Residual stress- microstructure- mechanical property interrelationships in multipass HSLA steel welds. J Mater Process Technol 2016;231:456–67. https://doi.org/10.1016/j.jmatprotec.2016.01.020.
[136] Lan L, Kong X, Qiu C, Zhao D. Influence of microstructural aspects on impact toughness of multi-pass submerged arc welded HSLA steel joints. Mater Des

2016;90:488–98. https://doi.org/10.1016/j.matdes.2015.10.158.
[137] Balasubramanian V, Ravisankar V, Reddy GM. Effect of pulsed current and post weld aging treatment on tensile properties of argon arc welded high strength aluminium alloy. Mater Sci Eng A 2007;459:19–34. https://doi.org/10.1016/j.msea.2006.12.125.
[138] Liu A, Tang X, Lu F. Arc profile characteristics of Al alloy in double-pulsed GMAW. Int J Adv Manuf Technol 2013;65:1–7. https://doi.org/10.1007/s00170-012-4141-0.
[139] Çam G, İpekoğlu G. Recent developments in joining of aluminum alloys. Int J Adv Manuf Technol 2017;91:1851–66. https://doi.org/10.1007/s00170-016-9861-0.
[140] Lin J, Lv Y, Liu Y, Sun Z, Wang K, Li Z, et al. Microstructural evolution and mechanical property of Ti-6Al-4V wall deposited by continuous plasma arc additive manufacturing without post heat treatment. J Mech Behav Biomed Mater 2017;69:19–29. https://doi.org/10.1016/j.jmbbm.2016.12.015.
[141] Lin JJ, Lv YH, Liu YX, Xu BS, Sun Z, Li ZG, et al. Microstructural evolution and mechanical properties of Ti-6Al-4V wall deposited by pulsed plasma arc additive manufacturing. Mater Des 2016;102:30–40. https://doi.org/10.1016/j.matdes.2016.04.018.
[142] Guo J, Zhou Y, Liu C, Wu Q, Chen X, Lu J. Wire arc additive manufacturing of AZ31 magnesium alloy: grain refinement by adjusting pulse frequency. Materials (Basel) 2016;9. https://doi.org/10.3390/ma9100823.
[143] Janaki Ram GD, Venugopal Reddy A, Prasad Rao K, Reddy GM, Sarin Sundar JK. Microstructure and tensile properties of Inconel 718 pulsed Nd-YAG laser welds. J Mater Process Technol 2005;167:73–82. https://doi.org/10.1016/j.jmatprotec.2004.09.081.
[144] Mousavi SAAA, Niknejad ST. Study on the microstructure and mechanical properties of Nd:YAG pulsed laser beam weld of UNS-C17200 copper beryllium alloy. J Mater Process Technol 2010;210:1472–81. https://doi.org/10.1016/j.jmatprotec.2010.04.005.
[145] Tsukamoto S, Kawaguchi I, Arakane G, Honda H. Suppression of porosity using pulse modulation of laser power in 20 kW CO2 laser welding. In: Int. Congr. Appl. Lasers Electro-Optics, Laser Institute of America; 2001. p. 400–408. https://doi.org/10.2351/1.5059890.
[146] Aboulkhair NT, Everitt NM, Ashcroft I, Tuck C. Reducing porosity in AlSi10Mg parts processed by selective laser melting. Addit Manuf 2014;1:77–86. https://doi.org/10.1016/j.addma.2014.08.001.
[147] Slotwinski JA, Garboczi EJ. Porosity of additive manufacturing parts for process monitoring. AIP Conf Proc 2014;1581(33):1197–204. https://doi.org/10.1063/1.4864957.
[148] Sun Z, Tan X, Tor SB, Yeong WY. Selective laser melting of stainless steel 316L with low porosity and high build rates. Mater Des 2016;104:197–204. https://doi.org/10.1016/j.matdes.2016.05.035.
[149] King WE, Barth HD, Castillo VM, Gallegos GF, Gibbs JW, Hahn DE, et al. Observation of keyhole-mode laser melting in laser powder-bed fusion additive manufacturing. J Mater Process Technol 2014;214:2915–25. https://doi.org/10.1016/j.jmatprotec.2014.06.005.
[150] Qi T, Zhu H, Zhang H, Yin J, Ke L, Zeng X. Selective laser melting of Al7050 powder: melting mode transition and comparison of the characteristics between the keyhole and conduction mode. Mater Des 2017;135:257–66. https://doi.org/10.1016/j.matdes.2017.09.014.
[151] Dai D, Gu D. Effect of metal vaporization behavior on keyhole-mode surface morphology of selective laser melted composites using different protective atmospheres. Appl Surf Sci 2015;355:310–9. https://doi.org/10.1016/j.apsusc.2015.07.044.
[152] Dinda GP, Dasgupta AK, Mazumder J. Laser aided direct metal deposition of Inconel 625 superalloy: microstructural evolution and thermal stability. Mater Sci Eng A. 2009;509:98–104. https://doi.org/10.1016/j.msea.2009.01.009.
[153] Yadroitsev I, Gusarov A, Yadroitsava I, Smurov I. Single track formation in selective laser melting of metal powders. J Mater Process Technol 2010;210:1624–31. https://doi.org/10.1016/j.jmatprotec.2010.05.010.
[154] Mostafa A, Picazo Rubio I, Brailovski V, Jahazi M, Medraj M. Structure, texture and phases in 3D printed IN718 alloy subjected to homogenization and HIP treatments. Metals (Basel) 2017;7:196. https://doi.org/10.3390/met7060196.
[155] Lee YS, Zhang W. Modeling of heat transfer, fluid flow and solidification microstructure of nickel-base superalloy fabricated by laser powder bed fusion. Addit Manuf 2016;12:178–88. https://doi.org/10.1016/j.addma.2016.05.003.
[156] Xiao H, Li S, Han X, Mazumder J, Song L. Laves phase control of Inconel 718 alloy using quasi-continuous-wave laser additive manufacturing. Mater Des 2017;122:330–9. https://doi.org/10.1016/j.matdes.2017.03.004.
[157] Sochalski-Kolbus LM, Payzant EA, Cornwell PA, Watkins TR, Babu SS, Dehoff RR, et al. Comparison of residual stresses in Inconel 718 simple parts made by electron beam melting and direct laser metal sintering. Metall Mater Trans A Phys Metall Mater Sci 2015;46:1419–32. https://doi.org/10.1007/s11661-014-2722-2.
[158] Sames WJ, Unocic KA, Helmreich GW, Kirka MM, Medina F, Dehoff RR, et al. Feasibility of in situ controlled heat treatment (ISHT) of Inconel 718 during electron beam melting additive manufacturing. Addit Manuf 2017;13:156–65. https://doi.org/10.1016/j.addma.2016.09.001.
[159] Lee YS, Kirka MM, Dinwiddie RB, Raghavan N, Turner J, Dehoff RR, et al. Role of scan strategies on thermal gradient and solidification rate in electron beam powder bed fusion. Addit Manuf 2018;22:516–27. https://doi.org/10.1016/j.addma.2018.04.038.
[160] Dehoff RR, Kirka MM, Sames WJ, Bilheux H, Tremsin AS, Lowe LE, et al. Site specific control of crystallographic grain orientation through electron beam additive manufacturing. Mater Sci Technol 2014;31:931–8. https://doi.org/10.1179/1743284714y.0000000734.
[161] Yuan T, Kou S, Luo Z. Grain refining by ultrasonic stirring of the weld pool. Acta Mater 2016;106:144–54. https://doi.org/10.1016/j.actamat.2016.01.016.
[162] Biradar NS, Raman R. Grain refinement in Al-Mg-Si alloy TIG welds using transverse mechanical arc oscillation. J Mater Eng Perform 2012;21:2495–502. https://doi.org/10.1007/s11665-012-0207-2.
[163] Gery D, Long H, Maropoulos P. Effects of welding speed, energy input and heat source distribution on temperature variations in butt joint welding. J Mater Process Technol 2005;167:393–401. https://doi.org/10.1016/j.jmatprotec.2005.06.018.
[164] Akbari D, Sattari-Far I. Effect of the welding heat input on residual stresses in butt-welds of dissimilar pipe joints. Int J Press Vessel Pip 2009;86:769–76. https://doi.org/10.1016/j.ijpvp.2009.07.005.
[165] Xia M, Biro E, Tian Z, Zhou YN. Effects of heat input and martensite on HAZ softening in laser welding of dual phase steels. ISIJ Int 2008;48:809–14. https://doi.org/10.2355/isijinternational.48.809.
[166] OdabaşI A, Ünlü N, Göller G, Eruslu MN. A study on laser beam welding (LBW) technique: effect of heat input on the microstructural evolution of superalloy inconel 718. Metal. Mater Trans A Phys Metall Mater Sci 2010;41:2357–65. https://doi.org/10.1007/s11661-010-0319-y.
[167] Osoba LO, Ojo OA. Influence of laser welding heat input on HAZ cracking in newly developed Haynes 282 superalloy. Mater Sci Technol 2012;28:431–6. https://doi.org/10.1179/1743284711y.0000000078.
[168] Peng D, Shen J, Tang Q, Wu CP, Zhou YB. Effects of aging treatment and heat input on the microstructures and mechanical properties of TIG-welded 6061–T6 alloy joints. Int J Miner Metall Mater 2013;20:259–65. https://doi.org/10.1007/s12613-013-0721-8.
[169] Wang F, Williams S, Rush M. Morphology investigation on direct current pulsed gas tungsten arc welded additive layer manufactured Ti6Al4V alloy. Int J Adv Manuf Technol 2011;57:597–603. https://doi.org/10.1007/s00170-011-3299-1.
[170] Ravisankar A, Velaga SK, Rajput G, Venugopal S. Influence of welding speed and power on residual stress during gas tungsten arc welding (GTAW) of thin sections with constant heat input: a study using numerical simulation and experimental validation. J Manuf Process 2014;16:200–11. https://doi.org/10.1016/j.jmapro.2013.11.002.
[171] Kumar S, Shahi ASS. Effect of heat input on the microstructure and mechanical properties of gas tungsten arc welded AISI 304 stainless steel joints. Mater Des 2011;32:3617–23. https://doi.org/10.1016/j.matdes.2011.02.017.
[172] Unnikrishnan R, Idury KSNS, Ismail TP, Bhadauria A, Shekhawat SK, Khatirkar RK, et al. Effect of heat input on the microstructure, residual stresses and corrosion resistance of 304l austenitic stainless steel weldments. Mater Charact 2014;93:10–23. https://doi.org/10.1016/j.matchar.2014.03.013.
[173] Akbari Mousavi SAA, Miresmaeili R. Experimental and numerical analyses of residual stress distributions in TIG welding process for 304L stainless steel. J Mater Process Technol 2008;208:383–94. https://doi.org/10.1016/j.jmatprotec.2008.01.015.
[174] Kou S. Solidification and liquation cracking issues in welding. JOM 2003;55:37–42. https://doi.org/10.1007/s11837-003-0137-4.
[175] Min D, Shen J, Lai S, Chen J, Xu N, Liu H. Effects of heat input on the low power Nd:YAG pulse laser conduction weldability of magnesium alloy AZ61. Opt Lasers Eng 2011;49:89–96. https://doi.org/10.1016/j.optlaseng.2010.08.010.

[176] Aloraier AS, Ibrahim RN, Ghojel J. Eliminating post-weld heat treatment in repair welding by temper bead technique: role bead sequence in metallurgical changes. J Mater Process Technol 2004;153–154:392–400. https://doi.org/10.1016/j.jmatprotec.2004.04.383.

[177] Aloraier A, Ibrahim R, Thomson P. FCAW process to avoid the use of post weld heat treatment. Int J Press Vessel Pip 2006;83:394–8. https://doi.org/10.1016/j.ijpvp.2006.02.028.

[178] Aloraier A, Al-Mazrouee A, Price JWH, Shehata T. Weld repair practices without post weld heat treatment for ferritic alloys and their consequences on residual stresses: a review. Int J Press Vessel Pip 2010;87:127–33. https://doi.org/10.1016/j.ijpvp.2010.02.001.

[179] Ramjaun T, Stone HJ, Karlsson L, Kelleher J, Moat RJ, Kornmeier JR, et al. Effect of interpass temperature on residual stresses in multipass welds produced using low transformation temperature filler alloy. Sci Technol Weld Join 2013;19:44–51. https://doi.org/10.1179/1362171813y.0000000162.

[180] Jang C, Lee J, Sung Kim J, Eun Jin T. Mechanical property variation within Inconel 82/182 dissimilar metal weld between low alloy steel and 316 stainless steel. Int J Press Vessel Pip 2008;85:635–46. https://doi.org/10.1016/j.ijpvp.2007.08.004.

[181] Dehmolaei R, Shamanian M, Kermanpur A. Microstructural characterization of dissimilar welds between alloy 800 and HP heat-resistant steel. Mater Charact 2008;59:1447–54. https://doi.org/10.1016/j.matchar.2008.01.013.

[182] Maya-Johnson S, Santa JF, Mejía OL, Aristizábal S, Ospina S, Cortés PA, et al. Effect of the number of welding repairs with GTAW on the mechanical behavior of AA7020 aluminum alloy welded joints. Metall Mater Trans B Process Metall Mater Process Sci 2015;46:2332–9. https://doi.org/10.1007/s11663-015-0416-9.

[183] Grevey D, Sallamand P, Cicala E, Ignat S. Gas protection optimization during Nd:YAG laser welding. Opt Laser Technol 2005;37:647–51. https://doi.org/10.1016/j.optlastec.2004.08.015.

[184] Chung BG, Rhee S, Lee CH. The effect of shielding gas types on CO2 laser tailored blank weldability of low carbon automotive galvanized steel. Mater Sci Eng A 1999;272:357–62. https://doi.org/10.1016/S0921-5093(99)00499-2.

[185] Reisgen U, Schleser M, Mokrov O, Ahmed E. Shielding gas influences on laser weldability of tailored blanks of advanced automotive steels. Appl Surf Sci 2010;257:1401–6. https://doi.org/10.1016/j.apsusc.2010.08.042.

[186] Zhao Y, Shi X, Yan K, Wang G, Jia Z, He Y. Effect of shielding gas on the metal transfer and weld morphology in pulsed current MAG welding of carbon steel. J Mater Process Technol 2018;262:382–91. https://doi.org/10.1016/j.jmatprotec.2018.07.003.

[187] Pires I, Quintino L, Miranda RM. Analysis of the influence of shielding gas mixtures on the gas metal arc welding metal transfer modes and fume formation rate. Mater Des 2007;28:1623–31. https://doi.org/10.1016/j.matdes.2006.02.012.

[188] Materials H, Enneti RK, Morgan R, Atre SV. Effect of process parameters on the Selective Laser Melting (SLM) of tungsten. Int J Refract Metals Hard Mater 2018;71:315–9. https://doi.org/10.1016/j.ijrmhm.2017.11.035.

[189] Yan W, Ge W, Qian Y, Lin S, Zhou B, Liu WK, et al. Multi-physics modeling of single/multiple-track defect mechanisms in electron beam selective melting. Acta Mater 2017;134:324–33. https://doi.org/10.1016/j.actamat.2017.05.061.

[190] Mercelis P, Kruth J-P. Residual stresses in selective laser sintering and selective laser melting. Rapid Prototyp J 2006;12:254–65. https://doi.org/10.1108/13552540610707013.

[191] Parry L, Ashcroft IA, Wildman RD. Understanding the effect of laser scan strategy on residual stress in selective laser melting through thermo-mechanical simulation. Addit Manuf 2016;12:1–15. https://doi.org/10.1016/j.addma.2016.05.014.

[192] Nie X, Zhang H, Zhu H, Hu Z, Ke L, Zeng X. Effect of Zr content on formability, microstructure and mechanical properties of selective laser melted Zr modified Al-4.24Cu-1.97Mg-0.56Mn alloys. J Alloys Compd 2018;764:977–86. https://doi.org/10.1016/j.jallcom.2018.06.032.

[193] Bi G, Sun C-N, Chen H, Ng FL, Ma CCK. Microstructure and tensile properties of superalloy IN100 fabricated by micro-laser aided additive manufacturing. Mater Des 2014;60:401–8. https://doi.org/10.1016/j.matdes.2014.04.020.

[194] Bi G, Gasser A. Restoration of nickel-base turbine blade knife-edges with controlled laser aided additive manufacturing. Phys Proc 2011;12:402–9. https://doi.org/10.1016/j.phpro.2011.03.051.

[195] Tang HP, Yang GY, Jia WP, He WW, Lu SL, Qian M. Additive manufacturing of a high niobium-containing titanium aluminide alloy by selective electron beam melting. Mater Sci Eng A 2015;636:103–7. https://doi.org/10.1016/j.msea.2015.03.079.

[196] Chen Y, Lu F, Zhang K, Nie P, Elmi Hosseini SR, Feng K, et al. Investigation of dendritic growth and liquation cracking in laser melting deposited Inconel 718 at different laser input angles. Mater Des 2016;105:133–41. https://doi.org/10.1016/j.matdes.2016.05.034.

[197] Chen Y, Zhang K, Huang J, Hosseini SRE, Li Z. Characterization of heat affected zone liquation cracking in laser additive manufacturing of Inconel 718. Mater Des 2016;90:586–94. https://doi.org/10.1016/j.matdes.2015.10.155.

[198] Li Z, Liu C, Xu T, Ji L, Wang D, Lu J, et al. Reducing arc heat input and obtaining equiaxed grains by hot-wire method during arc additive manufacturing titanium alloy. Mater Sci Eng A 2019;742:287–94. https://doi.org/10.1016/j.msea.2018.11.022.

[199] Rodrigues TA, Duarte V, Avila JA, Santos TG, Miranda R, Oliveira J. Wire and arc additive manufacturing of HSLA steel: effect of thermal cycles on microstructure and mechanical properties. Addit Manuf 2019;27:440–50. https://doi.org/10.1016/j.addma.2019.03.029.

[200] Horgar A, Fostervoll H, Nyhus B, Ren X, Eriksson M, Akselsen OM. Additive manufacturing using WAAM with AA5183 wire. J Mater Process Technol 2018;259:68–74. https://doi.org/10.1016/j.jmatprotec.2018.04.014.

[201] Ayarkwa KF, Williams SW, Ding J. Assessing the effect of TIG alternating current time cycle on aluminium wire + arc additive manufacture. Addit Manuf 2017;18:186–93. https://doi.org/10.1016/j.addma.2017.10.005.

[202] Ma Y, Cuiuri D, Shen C, Li H, Pan Z. Effect of interpass temperature on in-situ alloying and additive manufacturing of titanium aluminides using gas tungsten arc welding. Addit Manuf 2015;8:71–7. https://doi.org/10.1016/j.addma.2015.08.001.

[203] Kothari K, Radhakrishnan R, Wereley NM. Advances in gamma titanium aluminides and their manufacturing techniques. Prog Aerosp Sci 2012;55:1–16. https://doi.org/10.1016/j.paerosci.2012.04.001.

[204] Wu B, Pan Z, Ding D, Cuiuri D, Li H. Effects of heat accumulation on microstructure and mechanical properties of Ti6Al4V alloy deposited by wire arc additive manufacturing. Addit Manuf 2018;23:151–60. https://doi.org/10.1016/j.addma.2018.08.004.

[205] Wu B, Pan Z, Ding D, Cuiuri D, Li H, Fei Z. The effects of forced interpass cooling on the material properties of wire arc additively manufactured Ti6Al4V alloy. J Mater Process Technol 2018;258:97–105. https://doi.org/10.1016/j.jmatprotec.2018.03.024.

[206] Montevecchi F, Venturini G, Grossi N, Scippa A, Campatelli G. Idle time selection for wire-arc additive manufacturing: a finite element-based technique. Addit Manuf 2018;21:479–86. https://doi.org/10.1016/j.addma.2018.01.007.

[207] Denlinger ER, Heigel JC, Michaleris P, Palmer TA. Effect of inter-layer dwell time on distortion and residual stress in additive manufacturing of titanium and nickel alloys. J Mater Process Technol 2015;215:123–31. https://doi.org/10.1016/j.jmatprotec.2014.07.030.

[208] Ladewig A, Schlick G, Fisser M, Schulze V, Glatzel U. Influence of the shielding gas flow on the removal of process by-products in the selective laser melting process. Addit Manuf 2016;10:1–9. https://doi.org/10.1016/j.addma.2016.01.004.

[209] Bin Anwar A, Pham QC. Selective laser melting of AlSi10Mg: effects of scan direction, part placement and inert gas flow velocity on tensile strength. J Mater Process Technol 2017;240:388–96. https://doi.org/10.1016/j.jmatprotec.2016.10.015.

[210] Ferrar B, Mullen L, Jones E, Stamp R, Sutcliffe CJ. Gas flow effects on selective laser melting (SLM) manufacturing performance. J Mater Process Technol 2012;212:355–64. https://doi.org/10.1016/j.jmatprotec.2011.09.020.

[211] Jurić I, Garašić I, Bušić M, Kožuh Z. Influence of shielding gas composition on structure and mechanical properties of wire and arc additive manufactured Inconel 625. JOM. 2019;71:703–8. https://doi.org/10.1007/s11837-018-3151-2.

[212] Callister W, Rethwisch D. Materials science and engineering – an introduction. 9th ed. United States of America: Wiley; 2014.

[213] David SA, Vitek JM. Correlation between solidification parameters and weld microstructures. Int Mater Rev 2014;34:213–45. https://doi.org/10.1179/imr.1989.34.1.213.

[214] Janaki Ram G, Mitra T, Raju M, Sundaresan S. Use of inoculants to refine weld solidification structure and improve weldability in type 2090 Al-Li alloy. Mater Sci Eng A 2000;276:48–57. https://doi.org/10.1016/S0921-5093(99)00515-8.

[215] Tang Z, Seefeld T, Vollertsen F. Grain refinement by laser welding of AA 5083 with addition of Ti/B. Phys Proc 2011;12:123–33. https://doi.org/10.1016/j.phpro.2011.03.016.

[216] Sireesha M, Albert SK, Shankar V, Sundaresan S. A comparative evaluation of welding consumables for dissimilar welds between 316LN austenitic stainless steel and Alloy 800. J Nucl Mater 2000;279:65–76. https://doi.org/10.1016/S0022-3115(99)00275-5.
[217] Alexandrov BT, Hope AT, Sowards JW, Lippold JC, McCracken S. Weldability studies of high-Cr, Ni-Base filler metals for power generation applications. Weld World 2011;55:65–76. https://doi.org/10.1007/BF03321288.
[218] Collins MG, Ramirez AJ, Lippold JC. An investigation of ductility-dip cracking in nickel-based weld metals – Part III. Weld J 2004;83:39S–49S.
[219] Ramirez AJ, Lippold JC. High temperature behavior of Ni-base weld metal Part I. Ductility and microstructural characterization. Mater Sci Eng A 2004;380:259–71. https://doi.org/10.1016/j.msea.2004.03.074.
[220] Ramirez AJ, Sowards JW, Lippold JC. Improving the ductility-dip cracking resistance of Ni-base alloys. J Mater Process Technol 2006;179:212–8. https://doi.org/10.1016/j.jmatprotec.2006.03.095.
[221] Oliveira JP, Ponder K, Brizes E, Abke T, Ramirez AJ. Combining resistance spot welding and friction element welding for dissimilar joining of aluminum to high strength steels. J Mater Process Technol 2019. https://doi.org/10.1016/j.jmatprotec.2019.04.018.
[222] Dong H, Hu W, Duan Y, Wang X, Dong C. Dissimilar metal joining of aluminum alloy to galvanized steel with Al–Si, Al–Cu, Al–Si–Cu and Zn–Al filler wires. J Mater Process Technol 2012;212:458–64. https://doi.org/10.1016/j.jmatprotec.2011.10.009.
[223] Weigl M, Albert F, Schmidt M. Enhancing the ductility of laser-welded copper-aluminum connections by using adapted filler materials. Phys Proc 2011;12:332–8. https://doi.org/10.1016/j.phpro.2011.03.141.
[224] Henderson MB, Arrell D, Larsson R, Heobel M, Marchant G. Nickel based superalloy welding practices for industrial gas turbine applications. Sci Technol Weld Join 2004;9:13–21. https://doi.org/10.1179/136217104225017099.
[225] Sutton M, Yang B, Reynolds A, Taylor R. Microstructural studies of friction stir welds in 2024–T3 aluminum. Mater Sci Eng A 2002;323:160–6. https://doi.org/10.1016/S0921-5093(01)01358-2.
[226] Norman AF, Drazhner V, Prangnell PB. Effect of welding parameters on the solidification microstructure of autogenous TIG welds in an Al–Cu–Mg–Mn alloy. Mater Sci Eng A 1999;259:53–64. https://doi.org/10.1016/S0921-5093(98)00873-9.
[227] Owen R. Neutron and synchrotron measurements of residual strain in TIG welded aluminium alloy 2024. Mater Sci Eng A 2003;346:159–67. https://doi.org/10.1016/S0921-5093(02)00547-6.
[228] Soysal T, Kou S. Effect of filler metals on solidification cracking susceptibility of Al alloys 2024 and 6061. J Mater Process Technol 2019;266:421–8. https://doi.org/10.1016/j.jmatprotec.2018.11.022.
[229] Norman AF, Birley SS, Prangnell PB. Development of new high strength Al – Sc filler wires for fusion welding 7000 series aluminium aerospace alloys. Sci Technol Weld Join 2003;8:235–45. https://doi.org/10.1179/136217103225010989.
[230] Seshagiri PC, Nair BS, Reddy GM, Rao KS, Bhattacharya SS, Rao KP. Improvement of mechanical properties of aluminium–copper alloy (AA2219) GTA welds by Sc addition. Sci Technol Weld Join 2008;13:146–58. https://doi.org/10.1179/174329308X283866.
[231] Ma C, Chen L, Cao C, Li X. Nanoparticle-induced unusual melting and solidification behaviours of metals. Nat Commun 2017;8:14178. https://doi.org/10.1038/ncomms14178.
[232] Shojaati M, Beidokhti B. Characterization of AISI 304/AISI 409 stainless steel joints using different filler materials. Constr Build Mater 2017;147:608–15. https://doi.org/10.1016/j.conbuildmat.2017.04.185.
[233] Scherm F, Bezold J, Glatzel U. Laser welding of Mg alloy MgAl3Zn1 (AZ31) to Al alloy AlMg3 (AA5754) using ZnAl filler material. Sci Technol Weld Join 2012;17:364–7. https://doi.org/10.1179/136217112X13333824902080.
[234] Mathieu A, Shabadi R, Deschamps A, Suery M, Matteï S, Grevey D, et al. Dissimilar material joining using laser (aluminum to steel using zinc-based filler wire). Opt Laser Technol 2007;39:652–61. https://doi.org/10.1016/j.optlastec.2005.08.014.
[235] Dharmendra C, Rao KP, Wilden J, Reich S. Study on laser welding–brazing of zinc coated steel to aluminum alloy with a zinc based filler. Mater Sci Eng A 2011;528:1497–503. https://doi.org/10.1016/j.msea.2010.10.050.
[236] Shiri SG, Nazarzadeh M, Sharifitabar M, Afarani MS. Gas tungsten arc welding of CP-copper to 304 stainless steel using different filler materials. Trans Nonferrous Met Soc China 2012;22:2937–42. https://doi.org/10.1016/S1003-6326(11)61553-7.
[237] Naffakh H, Shamanian M, Ashrafizadeh F. Dissimilar welding of AISI 310 austenitic stainless steel to nickel-based alloy Inconel 657. J Mater Process Technol 2009;209:3628–39. https://doi.org/10.1016/j.jmatprotec.2008.08.019.
[238] El-Banna E, Nageda M, Abo El-Saadat M. Study of restoration by welding of pearlitic ductile cast iron. Mater Lett 2000;42:311–20. https://doi.org/10.1016/S0167-577X(99)00204-9.
[239] Barreda J, Santamaría F, Azpiroz X, Irisarri A, Varona J. Electron beam welded high thickness Ti6Al4V plates using filler metal of similar and different composition to the base plate. Vacuum 2001;62:143–50. https://doi.org/10.1016/S0042-207X(00)00454-1.
[240] Costa AMS, Oliveira JP, Salgado MV, Nunes CA, Lopes ESN, Mogili NVV, et al. Effect of Ta and Nb additions in arc-melted Co-Ni-based superalloys: microstructural and mechanical properties. Mater Sci Eng A 2018;730:66–72. https://doi.org/10.1016/j.msea.2018.05.078.
[241] Cooper DE, Blundell N, Maggs S, Gibbons GJ. Additive layer manufacture of Inconel 625 metal matrix composites, reinforcement material evaluation. J Mater Process Technol 2013;213:2191–200. https://doi.org/10.1016/j.jmatprotec.2013.06.021.
[242] Hong C, Gu D, Dai D, Alkhayat M, Urban W, Yuan P, et al. Laser additive manufacturing of ultrafine TiC particle reinforced Inconel 625 based composite parts: tailored microstructures and enhanced performance. Mater Sci Eng A 2015;635:118–28. https://doi.org/10.1016/j.msea.2015.03.043.
[243] Zhang B, Bi G, Wang P, Bai J, Chew Y, Nai MS. Microstructure and mechanical properties of Inconel 625/nano-TiB2 composite fabricated by LAAM. Mater Des 2016;111:70–9. https://doi.org/10.1016/j.matdes.2016.08.078.
[244] Ho IT, Chen YT, Yeh AC, Chen CP, Jen KK. Microstructure evolution induced by inoculants during the selective laser melting of IN718. Addit Manuf 2018;21:465–71. https://doi.org/10.1016/j.addma.2018.02.018.
[245] Zhang H, Zhu H, Qi T, Hu Z, Zeng X. Selective laser melting of high strength Al-Cu-Mg alloys: processing, microstructure and mechanical properties. Mater Sci Eng A 2016;656:47–54. https://doi.org/10.1016/j.msea.2015.12.101.
[246] Carluccio D, Bermingham MJ, Zhang Y, StJohn DH, Yang K, Rometsch PA, et al. Grain refinement of laser remelted Al-7Si and 6061 aluminium alloys with Tibor ® and scandium additions. J Manuf Process 2018;35:715–20. https://doi.org/10.1016/j.jmapro.2018.08.030.
[247] Qiu D, Taylor JA, Zhang M-X, Kelly PM. A mechanism for the poisoning effect of silicon on the grain refinement of Al–Si alloys. Acta Mater 2007;55:1447–56. https://doi.org/10.1016/j.actamat.2006.09.046.
[248] Xi L, Wang P, Prashanth KG, Li H, Prykhodko HV, Scudino S, et al. Effect of TiB2 particles on microstructure and crystallographic texture of Al-12Si fabricated by selective laser melting. J Alloys Compd 2019;786:551–6. https://doi.org/10.1016/j.jallcom.2019.01.327.
[249] Mantri SA, Alam T, Choudhuri D, Yannetta CJ, Mikler CV, Collins PC, et al. The effect of boron on the grain size and texture in additively manufactured β-Ti alloys. J Mater Sci 2017;52:12455–66. https://doi.org/10.1007/s10853-017-1371-4.
[250] AlMangour B, Grzesiak D. Jenn-MingYang, Selective laser melting of TiC reinforced 316L stainless steel matrix nanocomposites: influence of starting TiC particle size and volume content. Mater Des 2016;104:141–51. https://doi.org/10.1016/j.matdes.2016.05.018.
[251] Almangour B, Baek M, Grzesiak D, Lee K. Strengthening of stainless steel by titanium carbide addition and grain refinement during selective laser melting. Mater Sci Eng A 2018;712:812–8. https://doi.org/10.1016/j.msea.2017.11.126.
[252] Bermingham MJ, StJohn DH, Krynen J, Tedman-Jones S, Dargusch MS. Promoting the columnar to equiaxed transition and grain refinement of titanium alloys during additive manufacturing. Acta Mater 2019;168:261–74. https://doi.org/10.1016/j.actamat.2019.02.020.
[253] Bermingham MJJ, Kent D, Zhan H, StJohn DHH, Dargusch MSS. Controlling the microstructure and properties of wire arc additive manufactured Ti–6Al–4V with trace boron additions. Acta Mater 2015;91:289–303. https://doi.org/10.1016/j.actamat.2015.03.035.
[254] Srinivasan R, Miracle D, Tamirisakandala S. Direct rolling of as-cast Ti–6Al–4V modified with trace additions of boron. Mater Sci Eng A 2008;487:541–51. https://doi.org/10.1016/j.msea.2007.10.053.
[255] Bermingham MJ, McDonald SD, Dargusch MS. Effect of trace lanthanum hexaboride and boron additions on microstructure, tensile properties and anisotropy of Ti-6Al-4V produced by additive manufacturing. Mater Sci Eng A 2018;719:1–11. https://doi.org/10.1016/j.msea.2018.02.012.

[256] ASTM F2924-14. Standard Specification for Additive Manufacturing Titanium-6 Aluminum-4 Vanadium with Powder Bed Fusion. West Conshohocken (PA): ASTM International; 2014. https://doi.org/10.1520/F2924-14.
[257] Yin B, Ma H, Wang J, Fang K, Zhao H, Liu Y. Effect of CaF2 addition on macro/microstructures and mechanical properties of wire and arc additive manufactured Ti-6Al-4V components. Mater Lett 2017;190:64–6. https://doi.org/10.1016/j.matlet.2016.12.128.
[258] Rodrigues TA, Duarte V, Miranda RM, Santos TG, Oliveira JP. Current status and perspectives on Wire and Arc Additive Manufacturing (WAAM). Materials (Basel) 2019;12:1121. https://doi.org/10.3390/ma12071121.
[259] Cunningham CR, Flynn JM, Shokrani A, Dhokia V, Newman ST. Invited review article: strategies and processes for high quality wire arc additive manufacturing. Addit Manuf 2018;22:672–86. https://doi.org/10.1016/j.addma.2018.06.020.
[260] Mereddy S, Bermingham MJ, StJohn DH, Dargusch MS. Grain refinement of wire arc additively manufactured titanium by the addition of silicon. J Alloys Compd 2017;695:2097–103. https://doi.org/10.1016/j.jallcom.2016.11.049.
[261] Wang L, Suo Y, Liang Z, Wang D, Wang Q. Effect of titanium powder on microstructure and mechanical properties of wire + arc additively manufactured Al-Mg alloy. Mater Lett 2019;241:231–4. https://doi.org/10.1016/j.matlet.2019.01.117.
[262] Mereddy S, Bermingham MJ, Kent D, Dehghan-Manshadi A, StJohn DH, Dargusch MS. Trace carbon addition to refine microstructure and enhance properties of additive-manufactured Ti-6Al-4V. JOM 2018;70:1670–6. https://doi.org/10.1007/s11837-018-2994-x.
[263] Malinowski-Brodnicka M, Den Ouden G, Vink WJP. Effect of Electromagnetic Stirring on GTA Welds in Austenitic Stainless Steel Application of an axial magnetic field during welding has a significant influence on the shape and solidification of the weld. Weld J 1990(February):52–9.
[264] Zhao H, White DR, DebRoy T. Current issues and problems in laser welding of automotive aluminium alloys. Int Mater Rev 1999;44:238–66. https://doi.org/10.1179/095066099101528298.
[265] Fritzsche A, Hilgenberg K, Teichmann F, Pries H, Dilger K, Rethmeier M. Improved degassing in laser beam welding of aluminum die casting by an electromagnetic field. J Mater Process Technol 2018;253:51–6. https://doi.org/10.1016/j.jmatprotec.2017.10.021.
[266] Zhou J, Tsai HL. Effects of electromagnetic force on melt flow and porosity prevention in pulsed laser keyhole welding. Int J Heat Mass Transf 2007;50:2217–35. https://doi.org/10.1016/j.ijheatmasstransfer.2006.10.040.
[267] Zhou J, Tsai H-L. Porosity formation and prevention in pulsed laser welding. J Heat Transfer 2007;129:1014. https://doi.org/10.1115/1.2724846.
[268] Liu F, Cheng H, Yu X, Yang G, Huang C, Lin X, et al. Control of microstructure and mechanical properties of laser solid formed Inconel 718 superalloy by electromagnetic stirring. Opt Laser Technol 2018;99:342–50. https://doi.org/10.1016/j.optlastec.2017.09.022.
[269] Janaki Ram GD, Venugopal Reddy A, Prasad Rao K, Madhusudhan Reddy G. Control of Laves phase in Inconel 718 GTA welds with current pulsing. Sci Technol Weld Join 2004;9:390–8. https://doi.org/10.1179/136217104225021788.
[270] Mousavi MG, Hermans MJM, Richardson IM, den Ouden G. Grain refinement due to grain detachment in electromagnetically stirred AA7020 welds. Sci Technol Weld Join 2003;8:309–12. https://doi.org/10.1179/136217103225005462.
[271] Watanabe T, Nakamura H, Ei K. Grain refinement by TIG welding with electromagnetic stirring – a study of solidification control of austenitic stainless steel weld metal. Weld Int 1989;3:312–7. https://doi.org/10.1080/09507118909447649.
[272] Lim YC, Yu X, Cho JH, Sosa J, Farson DF, Babu SS, et al. Effect of magnetic stirring on grain structure refinement: Part 2 – Nickel alloy weld overlays. Sci Technol Weld Join 2010;15:400–6. https://doi.org/10.1179/136217110X12720264008231.
[273] Lu B, Cui X, Jiang L, Liu E, Zhang D, Feng X, et al. Influence of electromagnetic stirring on microstructure and wear resistance of plasma arc deposited shape memory alloy. Surf Coat Technol 2019;359:125–31. https://doi.org/10.1016/j.surfcoat.2018.12.044.
[274] Wu H, Chang Y, Lu L, Bai J. Review on magnetically controlled arc welding process. Int J Adv Manuf Technol 2017;91:4263–73. https://doi.org/10.1007/s00170-017-0068-9.
[275] Scotti A, Ponomarev V, Lucas W. A scientific application oriented classification for metal transfer modes in GMA welding. J Mater Process Technol 2012;212:1406–13. https://doi.org/10.1016/j.jmatprotec.2012.01.021.
[276] Cui Y, Xu C, Han Q. Effect of ultrasonic vibration on unmixed zone formation. Scr Mater 2006;55:975–8. https://doi.org/10.1016/j.scriptamat.2006.08.035.
[277] Eagar TW, Tsai NS. Temperature fields produced by traveling distributed heat sources. Weld J 1983;62:346–55.
[278] Tang HP, Qian M, Liu N, Zhang XZ, Yang GY, Wang J. Effect of powder reuse times on additive manufacturing of Ti-6Al-4V by selective electron beam melting. JOM 2015;67:555–63. https://doi.org/10.1007/s11837-015-1300-4.
[279] Gong H, Rafi K, Gu H, Starr T, Stucker B. Analysis of defect generation in Ti – 6Al – 4V parts made using powder bed fusion additive manufacturing processes. Addit Manuf 2014;1–4:87–98. https://doi.org/10.1016/j.addma.2014.08.002.
[280] Mukherjee T, Manvatkar V, De A, DebRoy T. Dimensionless numbers in additive manufacturing. J Appl Phys 2017;121:1–10. https://doi.org/10.1063/1.4976006.
[281] Rubenchik AM, King WE, Wu S. Scaling laws for the additive manufacturing. J Mater Process Technol 2018;257:234–43. https://doi.org/10.1016/j.jmatprotec.2018.02.034.
[282] Xu W, Brandt M, Sun S, Elambasseril J, Liu Q, Latham K, et al. Additive manufacturing of strong and ductile Ti-6Al-4V by selective laser melting via in situ martensite decomposition. Acta Mater 2015;85:74–84. https://doi.org/10.1016/j.actamat.2014.11.028.
[283] Vandenbroucke B, Kruth J. Selective laser melting of biocompatible metals for rapid manufacturing of medical parts. Rapid Prototyp J 2007;13:196–203. https://doi.org/10.1108/13552540710776142.
[284] Vrancken B, Thijs L, Kruth J-P, Van Humbeeck J. Heat treatment of Ti6Al4V produced by Selective Laser Melting: microstructure and mechanical properties. J Alloys Compd 2012;541:177–85. https://doi.org/10.1016/j.jallcom.2012.07.022.

J.P. Oliveira is PhD in Materials Science and Engineering (since 2016) and Assistant Professor at the Department of Mechanical and Industrial Engineering (DEMI), NOVA School of Science and Technology of NOVA University of Lisbon (FCT NOVA) and a researcher at UNIDEMI. Dr. Oliveira's main expertise encompasses the use of advance characterization techniques to correlate the microstructure of welded joints and additive manufacturing parts with their functional and mechanical behavior. Optimization of manufacturing techniques for non-conventional alloys, such as shape memory alloys and high entropy alloys, is also a major part of his research work. He has lead several industrial and fundamental research projects in the areas of welding and additive manufacturing. He has more than 50 papers in peer-reviewed journal and an h-index of 16 (https://scholar.google.pt/citations?user=xAd2_3oAAAAJ&hl=pt-PT). Prior to his currently position at FCT NOVA he held positions at The Ohio State University and University of Waterloo.

Telmo G. Santos is PhD in Mechanical Engineering and Associate Professor at the Department of Mechanical and Industrial Engineering (DEMI), NOVA School of Science and Technology of NOVA University of Lisbon (FCT NOVA) and a researcher at UNIDEMI. His main expertise is Non-Destructive Testing (NDT), Friction Stir Welding and Processing (FSW/FSP), Additive Manufacturing (AM) and hybrid manufacturing processes. Since 2011 he coordinated several research and industrial projects, and created the NDTLab at FCT NOVA (http://sites.fct.unl.pt/labndt-demi/). He has more than 50 papers indexed in SCOPUS and an h-index of 17 (https://scholar.google.pt/citations?user=jhGMP44AAAAJ&hl=pt-PT).

Rosa M. Miranda got her Engineering degree in Metallurgical Engineering at Instituto Superior Técnico, Lisbon Technical University in 1981 and her PhD degree at the same University in 1996. In 2009 got her Habilitation at Faculdade de Ciências e Tecnologia, at Nova University of Lisbon. She is currently Associate Professor with Habilitation in Mechanical Engineering. Her major scientific interests are in the areas of Welding and Joining Technologies (Laser Welding, Friction Stir Welding, Processing and Surfacing Materials), Welding Metallurgy, Materials Processing and Characterization.Professor Miranda has a h-index of 29 (https://scholar.google.pt/citations?user=dgg54dkAAAAJ&hl=pt-PT).